TAMPEREEN TEKNILLINEN YLIOPISTO
TAMPERE UNIVERSITY OF TECHNOLOGY
Julkaisu 807 • Publication 807

Petri Österberg

Wood Quality and Geometry Measurements Based on Cross Section Images

Tampere 2009

Tampereen teknillinen yliopisto. Julkaisu 807
Tampere University of Technology. Publication 807

Petri Österberg

Wood Quality and Geometry Measurements Based on Cross Section Images

Thesis for the degree of Doctor of Technology to be presented with due permission for public examination and criticism in Sähkötalo Building, Auditorium S3, at Tampere University of Technology, on the 9th of June 2009, at 12 noon.

Tampereen teknillinen yliopisto - Tampere University of Technology
Tampere 2009

ISBN 978-952-15-2151-5 (printed)
ISBN 978-952-15-2606-0 (PDF)
ISSN 1459-2045

Abstract

This thesis discusses the application of the image analysis methods for the cross section surface images of wood pieces, such as disc and block samples or logs and boards. The analysis methods have been developed in the laboratory environment for the measurement of wood geometry and quality properties. The focus has been in annual ring analyses, and the algorithms were based on texture analysis methods in order to obtain high robustness. Main algorithms are automatic. The texture based methods work quite well in varying imaging conditions, with chain-saw cut surfaces and moderate defects. In addition, a few geometry and color based algorithms were developed, but they are more sensitive to lighting variations, defects and roughness of wood cross section surface, when automated. The thesis discusses wood properties, the present wood measurement techniques and image based measurement application. Based on the review, technology gaps that can be covered with image based measurements are identified. The required calibration and implementation of algorithms, such as local annual ring width and orientation measurement, counting annual rings, pith locating and defect detection are described. Uncertainties affecting the measurement methods are analyzed. The purpose of the thesis is to create the basis for the development of wood cross section image based measurements for industrial applications.

Preface

The work presented in this thesis has been carried out at the department of Automation Science and Engineering at Tampere University of Technology in 2003-2008.

I would like to thank my patient supervisor professor Risto Ritala for his essential help, support and feedback during the writing process. Laboratory Engineer Heimo Ihalainen's solution proposals helped me through major problems during algorithm implementation. I would like to thank the reviewers professor Heikki Kälviäinen and professor Leena Paavilainen for their valuable comments. I am also thankful for the comments in several discussions with my colleagues. I am deeply grateful to my employer for the possibility to make doctoral studies within research and development projects.

Significant funding and support for the research projects related to the thesis has been obtained from Metsämiesten Säätiö Foundation, Finnish Funding Agency for Technology and Innovation (TEKES), Ministry of Agriculture and Forestry, and large Finnish forest industry companies such as Stora-Enso Oyj, UPM-Kymmene Oyj and Metsäliitto Group. The research has been carried out in close co-operation with Finnish Forest Research Institute, Helsinki University of Technology and University of Joensuu. Finnish Forest Research Institution has delivered and prepared a large amount of wood samples for the research and also collaborated with sample imaging and sample preparation in the early phase of the research. Significance of the expertise in these organizations has been notable for my understanding as an automation engineer about forestry and related application requirements. In application phase both financial support and close research co-operation has been with Finnish forestry equipment manufacturers such as John-Deere Forestry Oy (former Timberjack Oy), Komatsu Forest Oy (former Valmet Oy), Ponsse Oyj, Logset Oy, Vansco Elctronics Oy and in the sawmill-sector with FinScan Oy. Smaller companies have funded application projects related to their products. Contribution of all these organizations is gratefully appreciated.

Finally, I would like to thank my family for the patience during this long-lasting process. Sure past time was rough for us all. I trust I have more time for you after this work.

Tampere, 20th April, 2009

Petri Österberg

Contents

List of Abbreviations

3D	Three-dimensional
CCD	Charge Coupled Device
CMOS	Complementary Metal-Oxide-Semiconductor
CT	Computed Tomography
DFT	Discrete Fourier Transform
EIT	Electrical Impedance Tomography
EM	Expectation-Maximization algorithm
FFT	Fast Fourier Transform
GMM	Gaussian Mixture Models
GNP	Gross National Product
HSV	Hue, Saturation, Value
HSI	Hue, Saturation, Intensity
IR	Infrared
LED	Light-Emitting Diode
MOE	Modulus of Elasticity
MOR	Modulus of Rupture
MRI	Magnetic Resonance Imaging
NIR	Near-Infrared
NMR	Nuclear Magnetic Resonance
PCA	Principal Component Analysis
RF	Radio Frequency
RGB	Red, Green, Blue
SLR	Single-Lens Reflex
SOM	Self-Organizing Map

1 Introduction

Finland is known as a forest nation, in particular in Europe. Approximately 78% of the area of Finland is covered by forests, and thus there exist huge wood resources. This is to be compared with that 10% of the area is waterways and only 12% of the land is being utilized for inhabitation and agriculture. The volume of Finnish wood resources was evaluated in 2006 to be 2189 million cubic meters [112]. The volume of total annual tree growth in Finnish forests has been greater than the utilization of wood since the early seventies. During the past few years the volume of approximately 70% of annual tree growth volume has been utilized [91][112]. Therefore the net volume of Finnish forest resources increases continuously and the utilization of forest resources is sustainable.

1.1 Forestry and Finnish national economy

Forest based industry has a high economic impact for Finland. The forest based industry has generated the basis for the Finnish society during the past decades. It has been and still is an important employer: the forest industry gave work directly for 66700 persons in 2006 [112]. The number of forest industry related workers, such as those working in the forest economy, in the transportation, in the technology sector and in the chemical industry, is evaluated to be about 200 000 persons [2]. Mechanical, electronics (including IT-technology) and forest industry have together provided the majority of the Finnish industrial production value during the last few years. The forest sector has provided about 10% of Finnish Gross National Product for a long time but the share has slightly decreased mainly due to the success of Nokia-led electronics industry as shown in *Figure 1*. The forest industry products contributed approximately 20% of the net exports of Finland in 2006 [112].

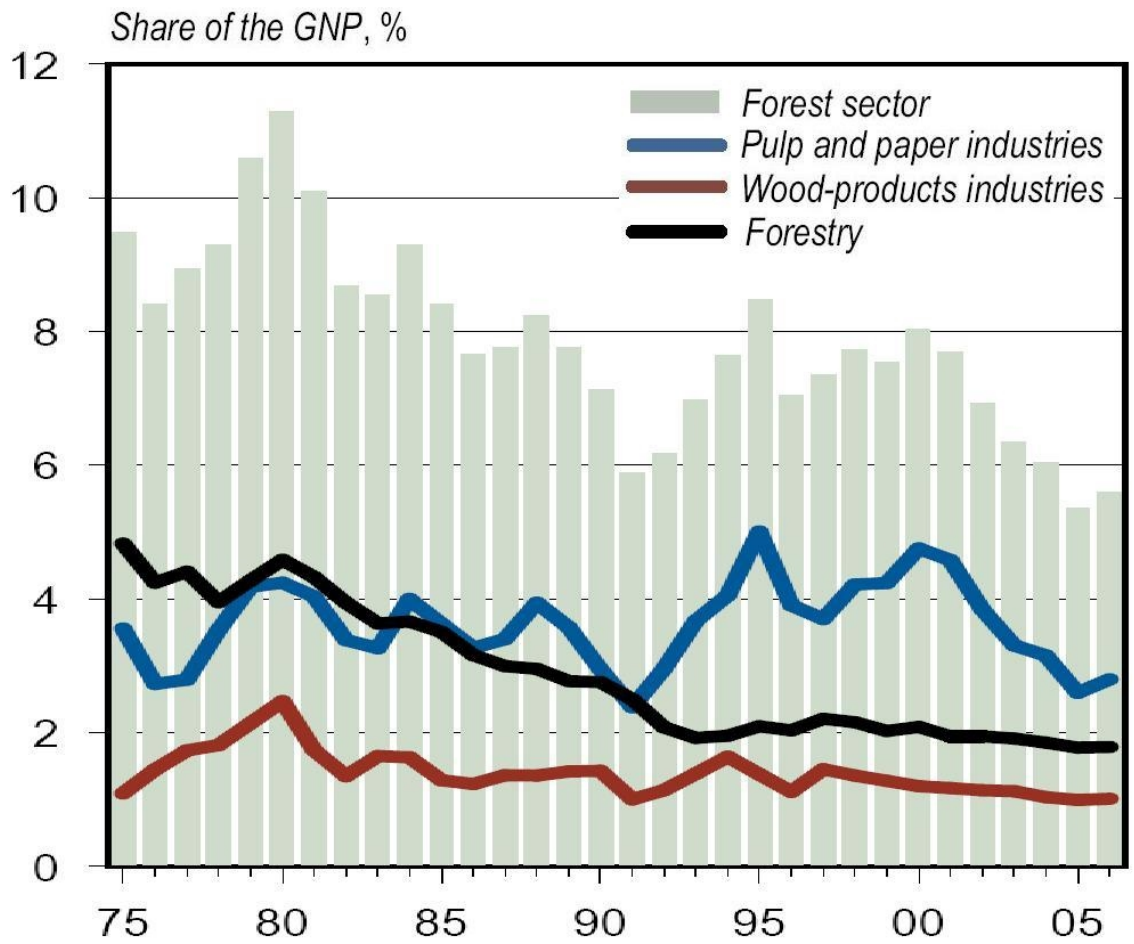

Figure 1. Forest sector percentage share of Finnish GNP in 1975-2006. Annual shares of three main areas within the forest sector are plotted with colors. Image source [112].

Figure 2 presents the total exports of goods from Finland and exports by forest industries over the period 1970-2006: the export of forest industry products has clearly played an important role for Finnish economy for decades. Again the effect of Nokia is noticed as a high increase of the total exports of goods beginning in the early nineties. The total value of forest industry export was 12.5 billion euro in 2006. Due to these facts, it is natural that Finland is particularly at the leading edge of technological development in the forest based industry.

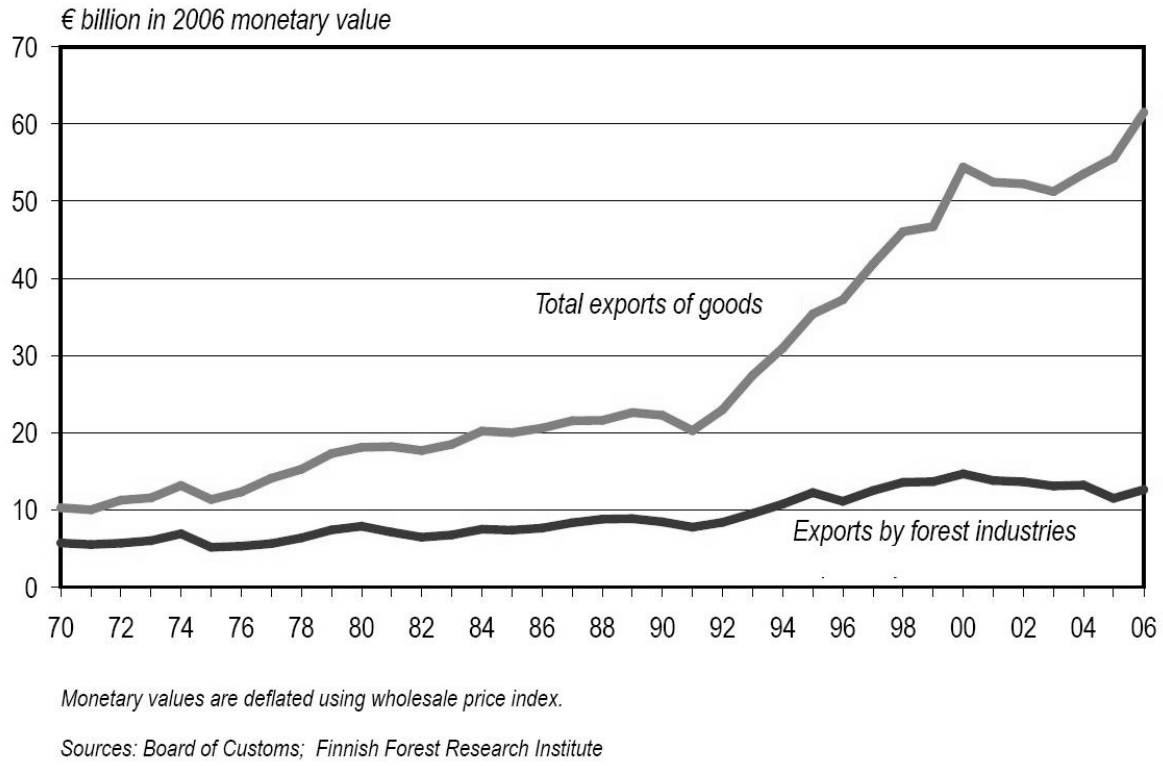

Figure 2. The total export of goods from Finland and exports by forest industries between the years 1970-2006.

Despite that Finland is a rather small country, several Finnish companies operating in the forest based sector are globally significant, in particular in paper making and forestry equipment manufacturing. [2]. *Figure 3* shows, that there are three Finnish companies, Stora Enso, UPM-Kymmene and Metsäliitto, within the ten largest forest industry companies in the world, judged by the annual turnover in 2007. There is also significant sawmill, plywood and house building industry in Finland. Large countries, such as Russia and China, have enormous forest resources. When these countries start to utilize their resources more efficiently, they will be able to compete with the volume of production, in particular in the mechanical forest industry sector. In Finland the possibility to succeed in this competition is to further optimize utilization of wood to develop new high added-value products, and to reduce costs. All these goals are strongly supported by intelligent automation. The major opportunities for the optimization are increasing the quality and thus the value of wood products, and decreasing the amount of waste wood in production. Intelligent wood measurement systems play an important role in the intelligent automation and cost-efficient production. Automation assists in many time-consuming working phases, and it may free the human operator entirely for more important and knowledge-intensive work, thus improving productivity and reducing labor costs. Automation plays also an important role when the

large age groups are approaching the age of retirement and the predicted labor shortage will become reality.

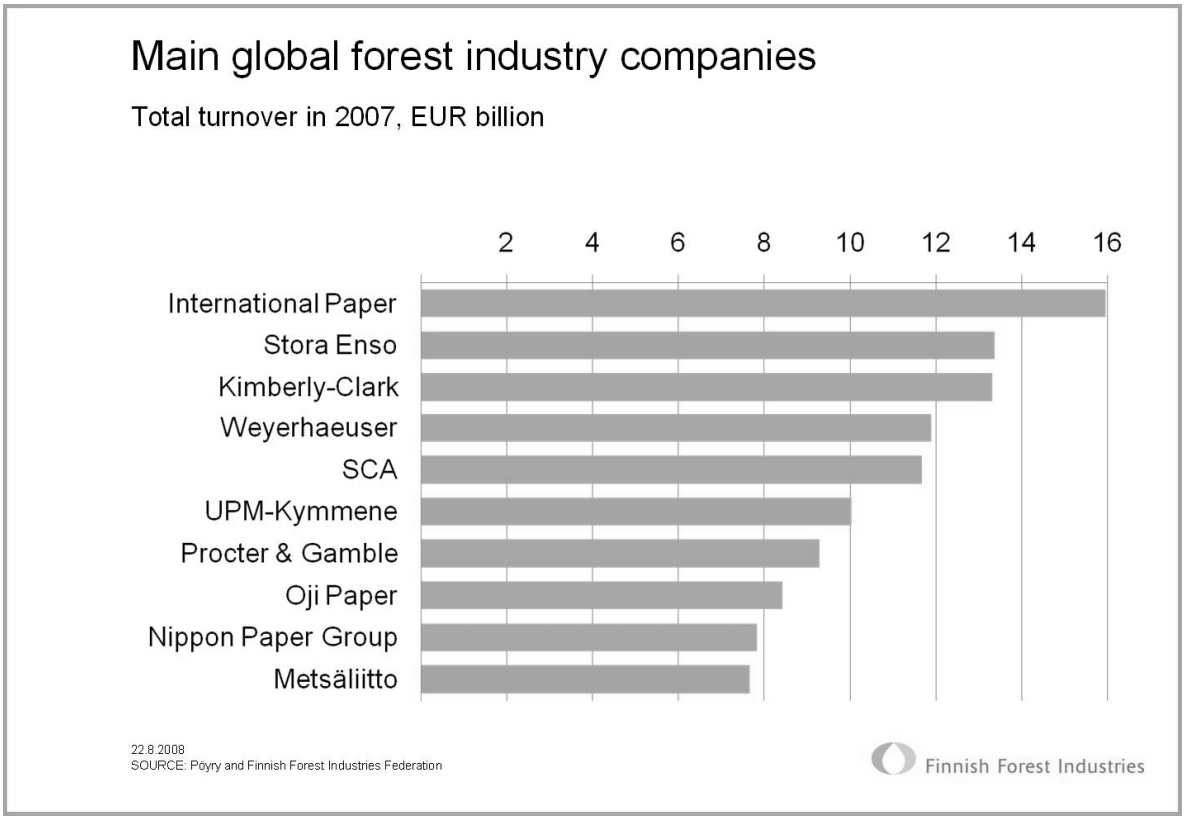

Figure 3. The world's largest forest industry companies judged by the annual turnover in 2007. Image from [39].

The evaluation of the value of wood and the economic transactions in wood trade are based on measurements carried out within the wood supply chain. These wood measurements are mostly about volume, but quality measures of wood are becoming increasingly important. Furthermore, in the wood processing chain there are many measurement positions, at which the information for controlling the processing is generated. Obviously, the development of novel wood measurements methods and devices and improving the existing ones helps to utilize each and every single tree more efficiently in the wood processing chain. Thus the value of the tree can be increased for the benefit of forest based industry, forest owners and the Finnish national economy. In particular, new quality measurements are tools to transform the present supply chain of massive volumes to one in which value creation is maximized with fine grading of the raw material.

In the near future, the image based measurement methods are expected to become increasingly important and will be applied at nearly all branches of the forest based industry. Firstly, such methods may support present measurement systems and make them more effective. Secondly, image based methods will offer completely new solutions in terms of new quality parameters for the forest based industry. The methods will be applied at sawmills or plywood mills, at the measurement stations of pulp and paper mills, or within the forestry equipment, such as harvesters.

1.2 Research problem

The quality measurements of the wood are required throughout the logistic chain of wood from forest to the forestry mills. The automatic measurement of wood quality properties is still in its infancy, and few commercial applications for saw and pulp mills are available, in particular for round wood. In many cases, the wood quality is evaluated by a human observer.

The general research problem to which this thesis contributes is how the hand-made measurements and human evaluations of wood quality and geometry can be replaced or complemented with rapid, reliable and cost-efficient automatic measurements so that the efficiency of the wood logistic chain is improved and the additional value of each tree can be measured and utilized. Some solutions for this research problem have been provided for years by applying several technologies such as X-ray, microwaves and visible light. This work considers the research problem from the viewpoint of wood cross section surface image analysis in the visible light range.

This thesis studies the measurements throughout the supply chain. Today the volume of round wood is automatically measured by the harvester and at the forestry mills, but quality measurements are seldom made automatically, and the few existing quality measurements are based on complicated and thus rather expensive technology, such as X-ray tomography. Quality measurements of sawn wood are made from board face, but annual ring level measurements do not exist. For the harvesters, the quality measurements have been considered almost impossible to develop because of harsh working environment. This thesis is a response to a challenge for finding opportunities for novel, cost-efficient measurement solutions for wood quality and geometry. In recent years, the machine vision systems have

been developing rapidly due to improvement of camera sensor performance and computation power of the processors. At the same time, the cost of camera-based systems has decreased. Therefore imaging is considered in this thesis as the prime candidate technology for automatic wood quality measurement systems providing sufficient measurement accuracy.

1.3 Goals of the work

The goals of this work are divided in two main categories: the analysis of the research problem and case solutions for the research problem based on the analysis. The goals for research problem analysis are to

- review the quality and geometry properties of wood that have economic potential so that their measurement is commercially justified at least at some point of the supply chain

- review the present measurement technology for wood quality and geometry, and identify the technology gaps

The goals related to the solutions for the research problem analysis are to

- innovate methods and algorithms that provide the basis for imaging solutions filling the technology gaps identified in industrial wood measurement applications

- test the algorithms in laboratory environment to prove that the industrial implementation is feasible

- analyze the uncertainties and sources of error in image based wood quality measurements.

The hypothesis of the thesis is that by analyzing cross section surface images of wood taken with color matrix cameras it is possible to develop systems and methods that provide automatically wood quality and geometry information. The hypothesis is tested by developing an imaging system and a set of MATLAB® algorithms for quality and geometry measurement of wood.

The main topic of this research is algorithm development for image-based wood quality and geometry measurements, to be further developed into commercial application for the forest industry. The core of the thesis discusses wood measurement methods developed and the corresponding algorithms based on the digital images of the visible light wavelength. Measurement methods presented in this thesis are developed for digital images of log and board cross section surfaces. The thesis emphasizes the development of methods for the measurement of quality properties, because of the corresponding obvious gap in today's automatic measurement systems at the forest based industry. As the present thesis is algorithmic development for novel quality assessment methods, imaging and analyses during the research is mainly carried out in laboratory environment, but with consideration of eventual industrial applications. Because of parallel research and development activities related to this thesis, some important quality properties of wood measurable from the cross section surface, such as the measurement of rot, were studied only on a rather general level [36]. Furthermore, as the measurements based on images and machine vision are active fields of research, some independent work in parallel with this thesis has been carried out.

The second goal of this thesis work was to review extensively the state-of-art of the wood quality and geometry measurements. The thesis discusses present wood measurement methods, technologies on which commercial and pre-commercial measurement devices are based, and imaging technologies researched for the wood measurement, regardless which technology the imaging device is based on, e.g. visible light, X-ray or microwaves. This analysis suggests which of the present technologies can be replaced or complemented with intelligent image-based solutions, e.g. the acoustic strength measurement of boards.

The thesis discusses aspects significant in future commercial applications of digital image based wood measurement methods of this work: how to meet the speed requirements in real time applications, how to calibrate, how to set up lighting systems, and how to prepare log or board ends so that sufficient image quality required is obtained. The thesis presents the mechanisms causing inaccuracy in the measurements due to optics, hardware, algorithm implementation etc.

1.4 Approach and limitations of the study

This thesis combines wood technology and digital image processing with measurement technology in an interdisciplinary way. Therefore the thesis is image processing oriented, but not comprehensive and theoretical image processing study. Instead the work is to be classified as engineering of techniques to serve as the core of industrial applications of practical relevance. For instance, image analysis methods are not studied very widely to optimize a single given quality measurement value. Rather this study seeks and innovates working solutions to measure a wide spectrum of wood properties, preferably in a manner that can be integrated with existing measurement and machine technology. Thus there may be possibilities for the even more efficient and rapid versions of the presented measurement principle, to be considered in the product development phase.

This research has targeted on measurement of wood properties in two softwood species, the Scots pine and the Norway spruce. These species have been chosen because of they are the most important wood species for the Finnish forest industry according to the annual volume of processed wood species [112].

The thesis discusses methods developed to measure and estimate a set of wood properties from cross section surface, and how the methods are implemented in MATLAB® computation environment. The thesis concentrates on the quality measurements but touches also geometric measurements whenever they can be implemented as components of the quality measurements. However, only few geometry measures are possible to evaluate from cross section surface images. Most quality measurements discussed in this thesis primarily measure dimensions and thus geometric properties such as annual ring width, but the dimensions are required for estimating the quality of wood rather than for managing wood volumes in the supply chain. Thus, these measurements are classified in this thesis as being on quality. The primary approach for developing the automatic wood quality measurement algorithms is local texture analysis. If texture analyses do not offer reasonable results, the color-based algorithms are applied, but typically at the expense of the degree of automation.

Software development for image analysis is not a research area on its own in the thesis, but rather a component in higher level implementation and algorithmic feasibility study. Thus the procedures, algorithms and methods discussed in this thesis can be implemented quite

easily with any programming language. The thesis describes shortly how the methods discussed can be further developed into practical and commercial applications.

The thesis has a weakness in that for many methods either no reference measurements exist or obtaining the reference data is extremely tedious. This is because the quality parameters suggested to be measured are currently evaluated by humans and commonly with classification rather than quantification, or with very time consuming microscopic measurements. As a result the statistical significance of results provided by the methods developed is discussed in this thesis only in broad terms. However, the performance of the main texture analysis method, 2D-Fourier power spectrum, was tested when annual ring width analysis presented in this thesis was compared with other measurement methods to estimate wood strength. In some cases such as pith locating, defect detection or annual ring counting it was possible to recognize intuitively the performance of the method by comparing visually the original image with the measurement result.

The computation time of the algorithms is not optimized in detail within this thesis, and thus some of the algorithms are quite slow, as implemented here. Again, this reflects the proof-of-concept approach to implementation. However, the computation time can be and has been reduced in the application product development stage outside the work of this thesis. Some general aspects related to reducing computation time are discussed in this thesis. Algorithms for several wood quality measurements have been developed during this study, but the result of the development is not a readily commercializable wood quality measurement software package; for example, no graphical user interfaces have been implemented for the algorithms.

The algorithms are developed for the macro-scale cross section surface images of wood that can be obtained with conventional digital cameras. The microscopic images of wood cross sections reveal much more about wood quality, but the cell level measurements are excluded from the scope of the thesis.

1.5 Contributions

The main contributions of the thesis are:

- review of wood properties and current wood measurement technology and the gap analysis based on the review.

- methods for measuring thickness and orientation fields of annual rings, detection of defects, location of pith, detection of orientation and annual ring curvature of board, counting and tracking of annual rings, estimating the shape of wood cross section, thickness of bark and the proportion of latewood, implementation of methods in MATLAB®, and their testing in laboratory environment;

- analysis of sources of uncertainty and error in the measurements developed.

Several algorithms for the automatic wood quality and geometry measurements based on digital cross section surface images are described in this thesis. All wood measurement algorithms presented in Chapter 6 were invented, developed and implemented by the author. The author has tested the functionality of the method with the large set of various wood cross section images. All main methods have been made automatic. However, the degree of automation in the color-based systems is lower than in the texture-based systems: typically in color-based systems thresholding requires that the imaging environment must be constant. The algorithms based on local texture analysis provide reasonable results even for unprepared and slightly decayed cross section surfaces in varying illumination conditions. Pre-existing general image processing algorithms have been used as components to these algorithms. Some of the general algorithms are built-in functions of MATLAB® or available in public MATLAB® toolboxes, such as the image processing toolbox. A pre-existing function particularly important for this study is the 2D Fast Fourier Transform (FFT). Some of the general algorithms are implemented at Tampere University of Technology, Department of Automation Science and Engineering (TUT/ASE) outside the scope of this thesis, for example a MATLAB® implementation for the Welch estimate of two-dimensional power spectrum and implementation of Principal Component Analysis (PCA) of

RGB image. The author has photographed – and prepared, when required – the majority of the wood samples for the research.

The thesis includes a subsection describing a semi-automatic algorithm for color measurement of rot. Author imaged the wood discs, calibrated images and measured the color of rot and produced the calibrated rot color data. This has been omitted from the list of main contributions above, as the approach was suggested to – rather than invented by – the author, and because it is a component of rot penetration model that is being developed in a research work outside the scope of this work.

During the research some intermediate results have been published internationally. Most of the results are published in the proceedings of conferences concerning measurement technology, machine vision and forest research [106][107][108][109]. Widespread cooperation network with governmental institutions as well as commercial companies has been created.

1.6 Structure of the thesis

The thesis consists of nine chapters. Chapter 2 describes the geometric and material properties of wood, which can be perceived as quality properties. The geometric properties are the outer measures and the shape of the logs. The quality properties are properties of green wood and processed wood affecting the wood processing and end use properties of commercial wood products. The properties are discussed mostly from the industrial viewpoint. Chapter 3 is an extensive review of the research and applications of wood measurements. Various non-destructive wood testing technologies are presented. Commercial industrial applications are reviewed with the emphasis on image based methods. Image analysis tools for forest research purposes are also described. Chapter 3 analyzes the gap between present measurement solutions and the industrial needs as outlined in Chapter 2. Chapter 4 describes tools and techniques, which have been used for image based quality analyses in the thesis. The chapter presents generally imaging and lighting devices, imaging set-ups, image types and analysis software. Camera, scale and color calibration methods are described. Chapter 5 offers a short review of the general image analysis methods relevant to this study. The review does not aim to be complete; only the methods chosen for the algorithms developed are covered. The methods have been divided into two categories, color

and texture based methods. Chapter 6 is the core of the thesis. The chapter discusses the analysis methods of cross section surface images developed for wood quality and geometry measurements during this research. The Chapter presents a set of image analysis algorithms, which analyze the cross section surface images of logs and boards and provide measurement information. In particular, quality properties such as local annual ring width, annual ring number and orientation are of central importance. The algorithms are based mostly on texture analysis methods, but also color analyses are discussed. Chapter 7 discusses error and uncertainty sources of the image based wood measurement systems. The errors and uncertainties are divided into ones caused by imaging devices, such as lens distortions, ones caused by imaging arrangements, such as out-of-plane wood surface, ones originating from algorithm implementation, such as thresholding values, and ones caused by operation environment, such as variability in ambient lighting. Chapter 8 considers the relevance of this research to practical wood supply chain management and value creation. Chapter 8 discusses the most prominent application opportunities for the results with remarks on the future of supply chains, the related measurement technology and the role of the methods developed in this thesis. Chapter 8 includes the analysis on how the analysis methods should be developed into real-life applications, and on future needs. The final chapter, Chapter 9, concludes the work.

2 Wood Properties

Humans have utilized many properties of wood for thousands of years. First, humans started burning wood for heating and lighting, in cooking and even in hunting. Then wood was used to build dwellings because of its strength and easy workability. The harder constructions offered a better shield against wild animals and enemies. Even today wood is important construction material and still many houses have a fire place, but in the developed countries it is rather for comfort than for warming. Today the utilization of wood and thus the wood properties of interest are extremely versatile in the developed countries.

A large variety of wood properties are commercially utilized. Economically, the most important industrial utilization of wood can be divided in three sectors:

1. Mechanical wood industry, such as sawmills, plywood mills, carpentry industry and wood based construction.
2. Chemical forest-based industry, such as pulp mills paper and paperboard mills, and the production of wood based chemicals.
3. Energy production using fuel wood, e.g. at thermal power stations.

Obviously, the commercial value of wood is the highest in mechanical wood industry and the lowest as fuel wood. Within mechanical wood processing sector, the raw material value of wood is higher for plywood mills than for sawmills. Fuel wood is often waste wood of sawmills and plywood mills or waste wood produced by a harvester during stem pruning and bucking.

This chapter reviews the properties of timber that are of interest for the forest based industry. The wood properties are divided here in two categories: geometric properties and material properties. Geometric properties are limited here to the outer dimensions of the felled timber, e.g. logs including bark dimensions, or the dimensions of sawn timber, e.g. board. The dimensions of assorted timber piles, such as log pile dimensions, are shortly discussed. The

major part of the wood trade is based on the dimensions of the supplied wood: the length and top diameter of an individual log usually defines the value of the log. Volume is preferred over mass in trade, because the mass depends also on the moisture of the timber. The geometry of the log must be determined in order to determine its volume. Section 2.1 reviews the geometric properties of logs and other pieces of wood.

Section 2.2 describes material properties of wood. The material properties are of high importance for forest industry, because they largely determine the wood processing behavior, and the quality of end products. So far, only a few material and quality properties have been used to determine the economic value of wood. The main reason is that many of the material properties are difficult to determine non-destructively and online within the supply chain.

The borderline between the geometric properties and the material properties is somewhat ambiguous, because many material properties are assessed through geometric properties. In this thesis the dimensions and 3D shape of the logs with and without bark, the dimensions and shape of the sawn wood products, and the dimensions of fuel wood storage and fuel wood pieces, such as chips are considered as geometric properties. All the other properties are classified as material properties.

2.1 Geometric properties of wood

The geometry and material properties of an individual tree depend on genes, habitat, climate conditions during growth and possible damages caused, e.g. by insects, animals, forest equipment, or forest fires. All these affect which wood products can be processed from the tree. In production forests regular forest management, e.g. thinning and fertilization increases the wood growth and hence the wood volume in the forest.

The geometric properties of a tree play an important role both before and after the cut down. The number of saw logs and the amount of pulp wood and their volume depends on the diameter of the trees and their tapering in the forest stand. The diameter of standing trees used as the basis in the wood trade in Finland is measured at the height of 130 cm, i.e. at the breast height. The geometry of trees before falling may indicate the material properties of wood as well. For instance, the boundary of the lowest branches or the height of the lower

boundary of the tree crown correlates with the knottiness of the wood [92][147]. A heavily crooked shape is a problem in processing. When the wood has been sold as standing trees, forest stand parameters such as breast height diameter and crown boundary height are important properties affecting the trade value.

In Finland, 98% of the forests were cut down with harvesters in 2006, and the rest manually by chain saws [112]. Most of the manually cut timber originates from the thinning of small forest areas. In harvesting the most important geometric parameters of a tree are the stem diameter and the length along the stem surface. Both parameters are related to tapering. Geometric defects, such as crooks, reduce the value of the stem. Bent trunks, scars and knot enlargements on the log are highly indicative for the processing problems. After the falling of the tree, bucking determines the geometric properties of saw logs and pulp wood, so that the number of saw logs is optimized. In addition to the length and diameter of the stem, the volume of the logs must be known. Bucking decisions are made based on stem dimensions [147]. The decision on cutting locations is a complex one whenever the stems are curved or crooked, and needs human involvement. Bucking determines how many and how long saw logs will be produced from the stem: the larger portion of the stem is cut into saw logs the higher the value of the tree.

The volume of processed logs is required to assess the amount of wood sold/purchased. The geometry of the logs and pulp wood largely defines the value of wood through volume. When wood is sold as standing trees, the harvester head volume measurement determines usually the value of supplied timber, and thus the payment for the forest owner [93]. Sometimes the value of pulp wood cut down manually is evaluated in a pile by the forest road. In this case, the height, the width and the length of the pile determine the frame volume of the log pile. The timber volume is obtained by multiplying the frame volume with the pile density [92].

Timber is transported from the forest to a saw, ply wood or pulp mills and to a power plant. The processing of the wood depends strongly on the type of wood - ply wood, saw logs, pulp wood or fuel wood – and thus geometric properties of interest vary widely. Furthermore, each wood type can be handled in alternative ways at the mill. However, at all mills the

wood geometry and dimension information is utilized in processing. Normally in Finland the value of a log is determined according to its outer dimensions with bark. However, the bark layer is nearly without commercial value in mechanical or chemical wood processing. The volume of bark and that of wood under the bark are important geometric wood properties.

The volume of the pulp wood at pulp mills may be evaluated rather from piles of pulp wood logs than from the geometry of individual logs. The pile properties of interest are geometry, weight and density. The geometric properties of interest in single pulp wood logs are crookedness, curvature, forkedness, and scar deformations. Crooked and curved logs are difficult to process in mechanical pulping. Similarly, forked logs and logs with deforming scars have geometric defects that reduce the quality and thus processability of pulp wood [140].

The geometry of the log determines its processing at the sawmill. The dimensions of the individual logs, such as shape, length, diameter and roundness, are important. The optimal sawing of the log depends on its 3D-shape. Even slightly curved and/or crooked logs are difficult to saw effectively. Furthermore, curves and crooks in a log indicate a tendency for twisting of the sawn product produced from the log. Scars and knot enlargements reduce the log symmetry. The low tapering rate of a stem is a desired quality property. Because of natural narrowing of the tree towards the top, the top diameter is the more important parameter than the root diameter. The top diameter of the log determines how much and which kind of boards can be sawn of it with minimum loss of waste wood and with minimum board edge damages e.g. wanes. Thus the low tapering rate means less waste wood. The shape of the top end may also affect the sawing process and thus board edge damages. The eccentricity of the log end may indicate exceptional tension inside the tree that, after sawing, when relaxing twists the boards. At present, the shape and the eccentricity of the log end are not utilized at the sawmills in processing, but taking them into account in sawing appears to have economic potential. After sawing, the outer dimensions of single boards should be known, because typically the sawn wood products are delivered for customers in standard measures. The curvature and twisting are important 3D-geometric properties affecting the value of sawn products.

At plywood mills, the logs must be prepared before veneering. Logs are sawn to suitable length and soaked in water or vapor to soften them for veneering. Thus the accurate

measurement of the log length is essential. For plywood industry outer sapwood part of the log is more valuable than the inner heartwood part. Thus the correct centering of the log is important. For a perfectly round log the separation of inner and outer wood is made with centering, but in practice the result may be rather rough. Typically, the boundary between heartwood and sapwood is not exactly round even in a round log, so that their accurate separation is problematic. The eccentricity and the ellipticity of the logs make the separation even more challenging. If the log is eccentric so that the pith is not in the geometric center line of the log, the heartwood and sapwood layers of the log are similarly eccentric. An elliptic log should be shaped to a round one with a lathe before it can be veneered. Usually after shaping the similar eccentricity problems occur. Today the layers cannot be accurately separated in a veneering process.

Fuel wood is typically waste wood from sawmills and pulp mills, or pruning and bucking waste of a harvester, and may include stumps and roots of the harvested trees. Usually waste wood is chipped before combustion to increase combustion efficiency and to make the processing of fuel wood easier. The average size and the size distribution of wood chips affect the burning process efficiency and thus are the most important geometric properties related to quality of fuel wood. Of course, the dimensions - at least the volume - of fuel wood storage should be known for the process control and wood trade.

2.2 Material properties of wood

Material properties of wood dominate the quality of wood at all stages of the supply chain, although wood geometry may account for a part of the quality, as discussed in the previous section. The wood material properties can be affected by silviculture: when the growth increases due to thinning or fertilization, the annual rings become wider and the strength may decrease. The pruning of the dry branches of standing trees decreases the number of knots in wood and thus increases the sawn wood quality for commercial use.

Requirements for wood quality – and hence the relevant material properties – depend highly on the end use. Requirements for energy and fuel wood are rather loose and most, even defected, trees are accepted, whereas at sawmills and in ply wood industry the requirements are very tight. However, those industries accepting defects want to detect and evaluate the defects to control their production and product quality. Most quality properties of raw

material relevant for pulping and papermaking are related to material properties of wood, such as density, moisture content and fiber properties [140]. Here we limit the discussion to properties that can be evaluated before pulping. At sawmills, the optimal wood material is homogenous throughout the log and thus without knots or defects. Typically, the log with narrow annual rings is favored because of its higher strength.

The material/quality properties of wood and the properties affecting them can be divided in two categories: natural wood properties and wood defects. Natural wood quality is defined by the wood material properties, but the quality may be reduced due to defects. However, today in wood commerce the defects are considered in more detail than natural wood properties.

Wood defects are classified as (for examples see *Figure 4)*

- rot and decay,
- color defects,
- wetwood
- compression and tension wood,
- cracks and splits,
- resin pockets,
- insect damages
- wood with foreign objects and
- knots.

Knots are classified as defects though they originate from the natural growth of wood.

At sawmills and ply wood mills defects caused by fungi are problematic. Typically critically rotten logs are sorted out already in forest, but some mildly decayed logs may be transported to the mills. Rot and decay decrease the strength and processability of the wood. Color defects, such as blue stain, are also caused by fungi, but normally color defected wood material is hard and therefore the color defects are mainly aesthetic defects. Severely rotten logs are problematic also in pulp and paper industry, but mild rot is typically accepted [67].

The butt of softwood trees growing in old forests or in wet habitat may suffer from wetwood. Wetwood is a type of heartwood which has been internally infused with water. Wetwood may be problematic in the forest products industry, particularly in drying [67].

Softwood species produce compression wood and hardwood species tension wood when growing on a slope or when continuously under tension. Compression and tension wood is harder than the surrounding wood material and it is considered as a defect. Harder wood material supports the tree to grow straight upwards. Typically, a log with compression wood or tension wood has abnormal internal tension, and after the sawing process the relaxation of this tension may twist the sawn board [67].

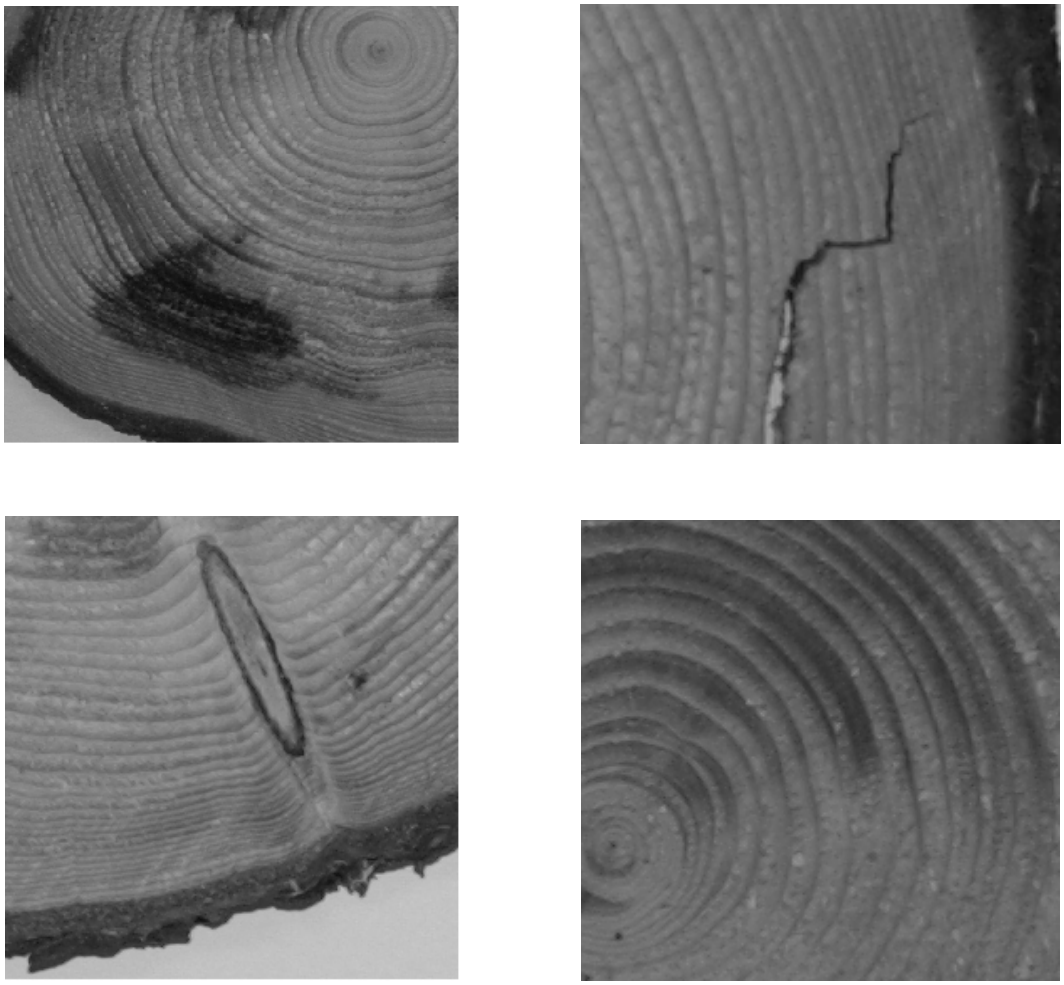

Figure 4. Some examples of typical wood defects. (a) Root decay. (b) Crack after windfall. (c) Internal knot. (d) Compression wood.

Windfall trees have often cracks or splits within the trunk. The tree falling may produce cracks as well. Typically, the cracks inside the tree cause critical damage to the strength of the sawn board and lead to problems during the veneering process in ply wood mills.

Resin pockets are cavities that are filled with resin produced by the tree. Resin pockets may weaken a board. Typically, resin dirties the board surface during the processing. The resin pockets may be problematic in the veneering process, too.

Insect damages, such as worm holes, may be extremely harmful for wood quality. Worm holes weaken wood material and complicate wood processing. Severely damaged wood material is typically accepted only in energy production.

Foreign objects, such as stones and metal particles inside logs may damage seriously the sawing equipment or peeling blade. A truck loader grab may press small stones inside the tree when lifting the logs from ground to a truck trailer. Trees supplied from the areas of past military operations often include metals due to ammunitions.

Knots are natural properties of wood, but in sawn board and ply wood they are usually considered as defects. The properties of knots of interest in logs and sawn products are their number, location, size and soundness/looseness. The number of knots within the stem can be reduced by pruning the lower branches of a standing tree during the growth, but knots in sawn timber cannot be avoided completely. Typically, knots decrease the strength of the sawn board, but the effect of an individual knot depends highly on its size, type and soundness/looseness. Dry knots are the worst, because they may drop away during processing. The resulting hole weakens the board considerably. Knots are aesthetical defects as well. For instance, when producing window frames knots are sawn out and the remaining parts are combined with finger joints to get knotless material.

The natural wood properties and the properties affecting them in trees, logs and sawn products are classified according to

- wood species,
- tree age,
- wood density,

- strength,
- annual ring width,
- latewood proportion,
- heartwood and sapwood proportion,
- grain orientation, known also as the spiral grain in standing trees,
- freshness,
- color,
- moisture,
- bark content and
- fiber properties.

Hundreds of wood species are utilized globally for commercial purposes. Typically, the commercial use of wood is highly species specific, because many material properties are species specific as well. In Finland, the most important commercial wood species are spruce, pine, birch and aspen.

The number of annual rings on the stub reveals the age of the timber. The strength and the density of wood are the higher the more narrow annual rings are excluding extremely narrow annual rings [8][33][71]. The width of annual rings depends on climate, environmental factors and nutrition. The annual rings are usually narrower in the colder climate e.g. in north and mountainous regions. Nordic softwood forests are typically ready for felling in 70-80 years, and their annual rings are typically a few millimeters wide whereas in tropical forests, in trees, such as eucalyptus, the annual rings may be several centimeters wide. Thus the life cycle of a eucalyptus forest from planting to felling is only approximately seven years.

An annual ring has two parts: lighter early wood and darker latewood. In the springtime, the trees in the coniferous forest belt grow more rapidly and produce larger early wood cells with quite narrow cell walls. In the summertime growing slows down and the latewood cells are smaller, and cell walls grow thicker towards the autumn [124]. Thus the borderline between early wood and latewood within an annual ring is not sharp. The borderline between early wood and latewood is defined as follows: “Latewood in softwoods includes tracheids in which the common wall between two cells is exactly half or over half the radial width of lumen” [8]. During the winter liquids inside the tree are frozen and trees are in an inactive

state. In the next year, after the winter, trees begin to grow rapidly and the borderline between the latewood of previous year and the early wood of following year is sharp. The sharpness of the two borderlines is illustrated in *Figure 5*. Proportion of latewood within annual ring affects the color of end products in paper industry and the strength of boards in mechanical wood processing.

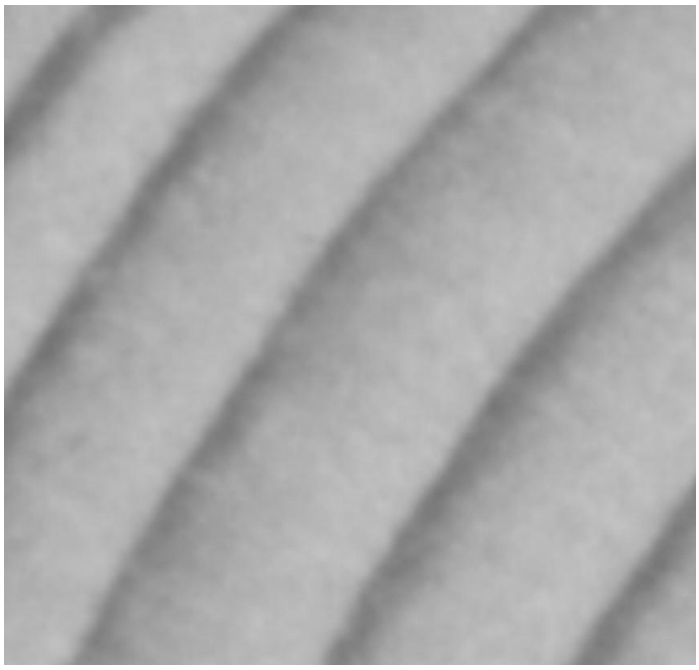

Figure 5. The boundary between early wood and latewood of the same year is blurred but the boundary between latewood and the early wood of next year is clear.

Active living cells transport inside the tree stem the nutrients and water up for leaves and needles. These cells are located on the outer parts of the cross section and have high moisture [67]. This layer is called sapwood. Inner area with inactive cells and lower moisture is called heartwood. The difference between regions is more clearly visible in Scots pine than in Norway spruce. The moisture ratio of sapwood in fresh spruce is 140% (ratio of water mass to dry mass), and in heartwood it is 33% [124]. Correspondingly, the moisture ratio in pine sapwood is 120-150% and in pine heartwood 32-37%. *Figure 6 (a)* presents a disc of Norway spruce. The image has been taken immediately after falling the tree in wintertime. Liquids within the sapwood area are frozen and thus the color difference between sapwood and heartwood is evident. The sapwood and heartwood regions can be distinguished also if a thin enough tree disc is placed in front of bright light. The visible light penetrates easier through the sapwood region than the heartwood region. *Figure 6 (b)* presents this phenomenon for a thin disc of Norway spruce. Now the heartwood appears as

the darker region. Sapwood is more valuable than heartwood for plywood mills. Thus the automatic determination of the sapwood/heartwood boundary is highly desired in order to optimize the positioning of the log in the rotation chucks of the veneering lathe.

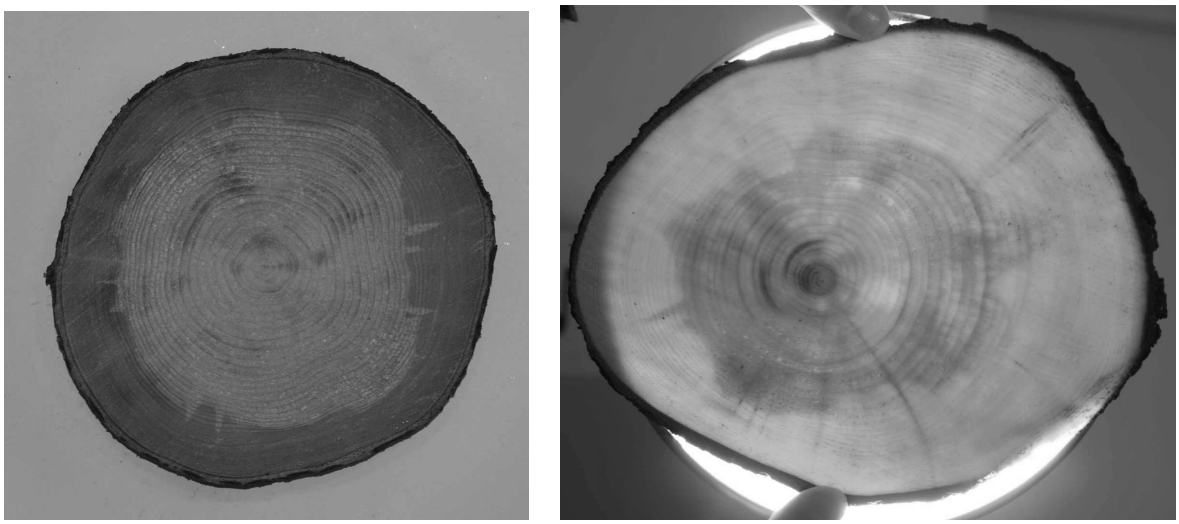

Figure 6. Sapwood and heartwood regions might be visible. The image (a) shows a frozen spruce disc just after falling the tree. The image (b) shows the different penetration of visible light through sapwood and heartwood regions of a thin spruce disc.

Nordic softwood trees twist during the growth. The helical orientation of grains, i.e. spiral grain, can be seen e.g. in dead standing trees after bark has dried out and fallen off. The spiral grain has a close connection to the orientation of wood fibers. The spiral grain of the tree is the main reason for the twisting of boards after sawing and during drying: the sawn product made tends to twist the more the larger the spiral grain angle in the log is. The spiral grain angle may also affect the strength of the wood product [67].

In particular for pulp mills it is extremely important that incoming wood is fresh. Freshness is a prerequisite for good quality of paper and sawn products. In Finland, the wood must be delivered to the pulp mill within two weeks after falling. Long-time storing in forests exposes wood material for decay and insect damages.

The color of wood material in an individual pulp wood log can be evaluated by the early and latewood content of the log. The log end having more latewood appears darker. The storing and the transportation of pulp wood reduces wood brightness, and in paper making more bleaching agents has to be used to get a paper of specified brightness [140]. Thus the mean color of cross section surface is an interesting wood quality property in pulp mills.

The average moisture content and bark content of chips are the most important quality properties for fuel wood. The quality of fuel wood affects substantially the burning process, and therefore the quality determines the amount of released energy and combustion gases during the process.

Pulp and paper properties are strongly dependent on properties of wood fibers. Longer fibers provide the paper strength, whereas shorter fibers yield paper with better optical properties. Largely decayed pulp wood logs are not acceptable, because decay has typically destroyed the fiber structure.

3 Testing and Measurement of Wood

This Chapter concentrates on the physical phenomena, which have been utilized in wood testing and measurement, such as interaction between wood material and visible light, infrared waves, X-rays, microwaves and acoustic waves. The chapter discusses scientific work behind the present commercial wood measurement devices and reviews the relevant research. The discussion in Section 3.1 concentrates on non-destructive analysis techniques for wooden samples, such as logs, boards and discs. The majority of the methods discussed are based on digital images, provided with various techniques.

The state of the art of wood measurement in the Finnish wood supply chain is reviewed in Section 3.2. For the dimension and volume measurements of both raw wood and processed wood many commercial applications are available, but only few for quality measurements. The viewpoint here is in industrial wood measurements within the Finnish wood supply chain though most methods are used around the world. The present solutions are based on various technologies: conventional measurements are made with simple rulers and calipers, but more sophisticated solutions based e.g. on visible light, lasers and X-rays have become more common. The emphasis of commercial application review is in camera based systems.

Section 3.3 presents shortly a few commercial and pre-commercial image analysis software packages developed for wood research purposes. Some of these tools are largely used by denrochronologists around the world.

The main objective of this Chapter is to identify gaps between the measurement needs of present and future wood supply chains, and the current technology. Section 3.4 discusses technology gaps which can be filled with novel camera and image analysis based methods and thus provides the motivation for the research work of the thesis.

3.1 Methods to assess wood properties

Wood measurement equipment was rather simple till 1970s. The measurement equipment in the forests consisted typically of a measuring tape and a hand held caliper. The rapid development of measurement technology in 1980's and 1990's brought novel approaches also into the field of wood measurements. Many non-destructive material evaluation techniques have been tested for wood samples, but most of the techniques have originally been developed in other areas of materials engineering or – quite often – in medical engineering. Ultrasound for wood defect detection and beta rays for wood density evaluation were tested already in the 1950's. The electrical impedance of the wood material was measured for wood moisture evaluation even earlier. The first commercial automatic non-destructive measurement techniques that use visible light sources and light sensors were applied for wood measurements in the seventies. The laser was first used for sample illumination in wood measurements in the 1980's. Laser and camera were first combined in dimension measurements, and later laser scattering was exploited e.g. in grain orientation measurements. Today the laser and camera based systems are the most common approach to measurements at sawmills. In the late 1980's, X-ray imaging and the computed tomography imaging were under research. Methods developed in medical imaging were transferred to the forest industry applications. At present effective commercial X-ray based measurement solutions are available for both log and sawn wood measurement. These devices measure properties, such as internal knots and foreign objects, which were impossible to detect and evaluate only a few years ago. However, X-ray tomography measurement systems are used only at the largest sawmills due to their high price.

Until recently, only few of the many promising techniques have been commercially applied in forestry. Acoustic methods for decay and crack detection have been tested for both standing and cut trees, and even for boards. These methods are non-destructive, but require a contact to the wood material. The wood material properties have been studied with infrared and near infrared (NIR) light, microwaves and radio frequency waves. So far no on-line applications for the forestry mills with radio frequency technologies are available. Magnetic Resonance Imaging (MRI) has been tested for wood samples, but the applications are too expensive to be commercialized for wood based industry in the near future.

3.1.1 Laser technology

At present laser illumination is one of the most common measurement techniques for machine vision applications in industrial wood dimension measurements. A laser device projects on the object a straight line of high accuracy and intensity. The laser line is photographed and the shape of the object surface is obtained by the shape of the laser line. When the object moves under the laser, a 3D-model of the object can be constructed from the individual profiles. Conners et al. [27][28] reported the development of such a system for the thickness measurement of boards in 1990.

Obviously, at least two laser-camera combinations located on both sides of the object are required to cover the object. Such multiple laser-camera solutions have been applied for both logs and boards. In 1992, Cicciotelli and Portala [19] reported a measurement system, in which laser lines were projected and imaged on both faces of the board. Thus, the 3D-shapes of the wood pieces were obtained.

Active laser based methods measure the distance to an object. The measurement is most commonly based on the time of flight of a laser pulse, but it can also be based on the phase shift between the emitted and the reflected laser pulse. If the laser distance measurement is swept along a line across the object, the laser device provides the 2D-profile of the object. The 3D-profile is generated with distance measurement by sweeping the laser above a moving object, for instance above a conveyor belt. However, active laser distance measurement technology is not commonly applied in the wood industry. The distance measurement hardware and sweeping of the laser makes the device more complicated in comparison with the laser-camera system, and thus more expensive. Furthermore, fast enough sweeping of the laser may be problematic at the high-speed production lines.

More recently the laser scattering has been tested in the measurement of wood quality properties. Shen et al. [128] showed in 2000 that the scattering intensities along and across fiber orientation are different, thus facilitating a laser based fiber orientation measurement. At rough wood surfaces and in porous wood species the intensity variation of the scattered laser light as a function of orientation was less pronounced, but with the polarization measurement of scattered light the orientation could be measured.

In 2003 Nyström [105] determined the grain orientation in a spruce sample by imaging a laser spot with a camera. The shape of the laser spot changes on the object surface according to the surface properties. Due to the tracheid effect a round laser spot on the barked wood surface transforms into an elliptical one extending more to the direction of fibers corresponding with the grain orientation. Thus the analysis of the imaged spot produces a measurement of the grain slope. Simonaho et al. [130] also studied the grain orientation with similar methods. They imaged and analyzed the spreading of laser spot on Scots pine and silver birch samples and were able to measure grain orientation similarly with image analysis. Hu et al. [57] [58] studied laser and camera based grain orientation measurement for Japanese beech and sugi trees. They applied modified Hough transform for ellipse shaped laser spot image analysis and succeed in grain orientation measurement as well. Zhou et al. [164] advanced the method towards a full-scale application in 2007. They produced the matrix of the laser spots on a board surface. When the board moves on the conveyor belt under the laser and the camera during imaging, the entire board surface is scanned. The spots were imaged with a CCD-camera and the wood grain orientation was measured using the shape of the spread laser spots.

A Swedish Company RemaControl utilizes the tracheid effect in bark recognition. Their product RemaLog Bark recognizes barked and non-barked wood according the spread of laser spot. When this information is combined with profile measurement, the bark thickness can be evaluated [118].

3.1.2 Infrared imaging

Electromagnetic radiation with wavelength ranging from 750 nm to 1 mm is called infrared radiation. The infrared band just above visible light from 750-1400 nm is called near infrared (NIR). All objects above the absolute zero temperature emit infrared radiation. Thermal imaging is measuring infrared radiation with a matrix sensor: a thermal image shows the temperature variations of the object. In wood science, thermographic methods have been studied since the nineties [12]. To enhance thermal imaging speed, the object may first be heated and then imaged after a short cooling period. However, even with heating the method is slow taking typically several minutes.

Infrared radiation has been used in some applications to detect the edges of the log for diameter and length measurement, e.g. in the production line of a sawmill, but this is not actually thermography, as the spectral content of infrared radiation is not analyzed.

According to Kollmann and Côté [71] the thermal properties of wood, in particular thermal conductivity, depend on its density. Quinn et al. [115] developed an infrared based method for locating knots in wood in 1998. They heated samples of southern yellow pine lumber. After a short cooling period, the lumber was scanned with an infrared detector and the resulting infrared images were analyzed. Knots were detected, because the temperature of the knots after cooling time was generally higher than that of the regular wood. Heating/cooling process of 240 seconds was required in order to detect a significant difference between temperature in knots and regular wood.

Also Tanaka and Divós [142] concluded in 2000 that within single wood species, knots and decayed regions can be recognized from regular wood using thermography because of the difference in density. Six wood samples of different species were heated using an external heating device, and knots, decayed regions and artificial cavities were detected as temperature variations in the samples. Knots and decayed regions could be detected even without external heating device, based only on natural temperature variation during the day.

Wyckhuyse and Maldague [160][161][162] in 2001 and 2002 had a hypothesis that rotten wood defects have moisture content different from regular wood and that thermal properties depend on the moisture content of the material. They heated the samples both with a radiator and with a microwave heater. Their conclusion was that defects having higher moisture content than surrounding material can be detected with infrared thermography when the defects are near the sample surface. They applied the results for wood pole defect detection.

In 2002 Arnerup [3] imaged log cross section surfaces with an infrared camera instead of a visible light camera and achieved a contrast between heartwood and sapwood in Scots pine that was better than in visible light imaging. In order to measure the size of the heartwood area within the log cross section Arnerup tested both global and adaptive thresholding methods and three model based algorithms (Hough transform, RCD algorithm and snakes) to detect the heartwood boundary.

Gjerdrum and Høibø [45] published results similar to those by Arnerup in 2004. They imaged log cross section surfaces with infrared cameras on a conveyor belt at a sawmill to measure the heartwood fraction within logs. However, they analyzed only a line crossing of each IR image instead of full images. The line was chosen visually to avoid knots and other defects that may disturb the heartwood fraction assessment. They proposed that heartwood fraction information can be used for evaluating the average annual ring width. They proposed also that the temperature gradient provides information about the freshness of the logs.

3.1.3 Acoustic and ultrasonic methods

The acoustic methods for detecting and evaluating wood properties are based on the mechanical vibrations of the material. The frequencies above 20kHz, higher than human ear can detect, are called the ultrasonic waves [35]. In acoustic wood measurement systems, ultrasonic waves are typically generated to the object and transmitted waves measured for identifying the transfer properties of wood.

Ultrasonic methods for wood defect detection were tested already in the 1950s. Waid and Woodman [152] applied ultrasound for regular, rotten and drilled wood samples in 1957. They coupled the transducers to small wood samples with a coupling agent to ensure good contact. Transmitted ultrasound energy was measured on the opposite sides of the sample both across and along the grain direction. The energy received in proportion to the one transmitted was substantially less in defected wood samples than in healthy wood.

The requirement of good contact between the wood sample and the emitting and receiving transducers made applying ultrasonic devices at production lines difficult. In 1978, McDonald [87] solved this problem by placing a wood board in a water basin so that water provided the required contact. At that time there existed many methods reported for detecting internal defects in wood, but McDonald's invention allowed to locate the defects in board with much improved accuracy. McDonald presented a commercially applicable system for defect detection using ultrasound.

In 1989, Sandoz [123] graded construction timber nondestructively by applying longitudinal ultrasound along the longitudinal axis of the wood beams. He measured more than 300

beams and found good correlation between the propagation speed of sound and the modulus of elasticity (MOE) and the modulus of rupture (MOR) in flexure of the beams.

Han and Birkeland [50] reported ultrasonic scanning of logs in 1992. With ultrasonic scanning for a short log sample placed in a water basin they were able to detect the location and the size of the wood defects (mainly knots) roughly. The results were confirmed by comparing them with the X-ray scanning results.

Ross et al. [121][122] studied the sorting of logs based on acoustics measurements in 1998 and 1999. Instead of ultrasound they impacted one end of the log with a hammer and then measured the propagation time of the impulse with an accelerometer attached to the other end of the log. Ross et al. measured the propagation time of acoustic waves for full length logs, short logs and veneers processed out of the logs with the aim to predict the quality of veneer from log quality. They compared the acoustic measurement results for veneers with measurement results for corresponding logs, and found a correlation.

In 2000 Tsehaye et al. [146] used an acoustic method similar to the method of Ross et al. The logs were typically graded according to length, diameter, sweep, taper and visual features (knottiness, scars etc.). However, even after grading logs within the same class had differences that were detected using acoustic measurements. Tsehaye et al. tapped one log end and measured the time of flight for sound from one end of the log to the other. Measurement of the acoustic response allowed the pre-sorting of the logs according to intrinsic wood quality.

3.1.4 Microwaves

In the electromagnetic spectrum microwave frequency is in between the frequencies of infrared radiation and radio frequency waves, i.e. roughly between 1GHz and 100 GHz, or of wavelength between 1 mm to 1 m [6]. However, the borderline between microwaves and infrared waves or radio waves has not been defined exactly.

Microwaves excite vibrations in polarized molecules, such as water molecules. The rate of microwave power absorption in most materials is proportional to the water content of the material. Thus also in wood technology the first microwave devices were applied for timber

moisture measurement. In 1979, Tiuri and Heikkilä [144] reported on a microwave-based instrument for the moisture measurement of timber. The microwave attenuation through the timber depends not only on moisture content, but also on the density and the temperature. To compensate for density and temperature variations Tiuri and Heikkilä combined the microwave measurement with a gamma-ray density measurement and infrared temperature measurement. The device measured the moisture content, density and temperature of boards on a conveyor belt at 10 cm intervals.

In 1985 James et al. [61] combined grain angle measurement with that of moisture and density of wood. All these measurements were based on the polarized microwave radiation. Both transmitted and reflected microwave radiation were detected. Moisture determined mainly the attenuation of the microwaves. The phase shift of microwaves was affected by both moisture and density, and the grain angle determined the microwave depolarization.

In 1987 Martin et al. [85] were able to measure the wood characteristics in boards, such as density and moisture, and the slope in grain with internal wood scanning by microwaves. In comparison with research described above, Martin et al. reported that they detected defects, such as knots and metallic objects with the microwave methods.

In 2000, Eskelinen and Eskelinen [37] applied the microwave measurement to logs, contrary to earlier work that had been on boards. By measuring microwave attenuation, time-of-flight and the rotation of the polarization angle Eskelinen and Eskelinen were able to obtain real time information about the moisture, material bends, number and location of knots, and sections of wood spoiled e.g. by insects.

In 2004 Fuentealba et al. [43][44] measured with microwaves the internal properties of wood products. However, the use of measurement was novel: they identified each wood piece according to its microwave characteristics. A product can be traced throughout the production cycle of the wood product with such identification.

In 2005 Kaestner and Bååth [65] were the first to report microwave tomography images about the internal properties of wood. They measured the polarization of microwaves in wood. The polarization depends on the local fiber orientation. Thus e.g. the internal knots of logs can be located.

3.1.5 Radio frequency scanning

Radio waves are electromagnetic radiation having the lowest frequency and the longest wavelength within the electromagnetic spectrum. Electromagnetic radiation below 1 GHz is considered radio frequency (RF) waves.

RF-radiation has been little applied in wood technology. However, in 2000 Steele et al. [135] differentiated knots, grain distortions and regular wood by radio frequency scanning. The wood sample was moved through a gap between the plates of capacitive sensors and 500 kHz alternating current electrical field was passed through the sample. During the scanning, differences between wood properties were obtained from the statistical analyses of the dielectric signal. Steele and Cooper [136] estimated lumber strength with radio frequency scanning in 2003. This method requires moisture compensation. A sensor for moisture and density of wood and wood based materials based on radio-frequency sensing was patented in 2004 [137].

3.1.6 X-ray, gamma ray and computed tomography imaging

X-rays are electromagnetic radiation having high energy, high frequency and short wavelength. In the electromagnetic spectrum X-rays are located between ultraviolet (UV) and gamma rays i.e. between wavelengths 10 nm and 0.01 pm. Gamma radiation is the radiation with the highest frequency and energy and the shortest wavelength, below 10 pm. X-ray imaging was first applied in medicine. An X-ray (or gamma ray) source emits the radiation through the object to the detectors. The radiation is attenuated depending on the internal characteristics of the object. Thus a transmittance image reflecting these characteristics of the object is generated.

In 1978, Polge [113] reported in his review of radiation densitometry that in wood technology first tests for X-rays were made already in early sixties. The early applications were related to microdensitometry: the wood core sample was studied with X-ray radioscopy that revealed the wood density. Cown and Clement [32] reported an automated X-ray based wood core densitometry in 1983.

Already in 1981, Hopkins et al. [56] presented that X-ray imaging is able to provide information about the internal properties of wood, such as annual rings, knots, rot, worm damage, cracks and in certain cases moisture or preservative content. They used a small Douglas fir power pole sample and measured local wood density with the X-ray imaging.

X-ray images, in particular X-ray tomography images, require heavy computation capacity. Hence the development of these techniques has been tightly connected to the development of computer processing capacity. X-ray tomography began in the 1980's and is known as computed tomography (CT). The CT images are constructed from a set of transilluminated images taken at various angles to the object. The smaller the angle difference between the emitter-detector pairs around the object, the more accurate the tomogram will be, and the more computation time is required. Backprojection is a common method to construct the tomogram from transilluminated images [66]. In medical applications the filtered backprojection with Fourier domain filtering is typically used when tens of transilluminated images are available of the sample. X-ray tomographic devices for wood technology have typically only 2-4 imaging directions, because the response time requirement is considerably tighter than in medical use. In comparison with a medical matrix type X-ray source-detector pair, a line X-ray source is enough in wood industry because the object is moving.

A study on the tomographic imaging of entire logs was published by Taylor et al. [143] in 1984. They used a gamma radiation source to generate tomographic cross section images of a log. The study demonstrated that knots can be recognized and located in tomographic images by computer assisted image analysis.

In 1989, Wagner et al. [151] reported the 'ultrafast' X-ray imaging device which makes it possible to apply such devices at conveyor belts of sawmills. The scanning speed of logs was 0.43 m/s with one scan every 1.27 cm. The X-ray slice images of the tomograph were only visually inspected, not analyzed further. All macro-scale defects were visible.

In 1991, Zhu et al. [165] [166] reported the development of image analysis methods for X-ray image data to locate and identify internal structural failures in wood. The three dimensional filtering method developed in conjunction with segmentation and labeling successfully detected potential wood defects. Filtering suppresses unwanted details, such as annual rings in the hardwood log images. In addition to the histogram segmentation

presented in an earlier publication, Zhu et al. proposed segmentation by 3D-volume growing algorithm for the extraction of defects [167] [168]. Defects were identified with a rule-based approach.

In the late 1990's many researches developed X-ray devices and CT methods for wood applications. Numerous articles about detecting and locating defects, such as knots and rotten regions, have been published. In addition to defect detection, methods for measuring the properties of regular wood were developed. Wang [153] studied the annual ring measurement from X-ray images in 1998. Observing annual rings accurately was not possible, but Wang was able to classify logs in two categories according to the annual ring width, with a classification error of 11%.

Sepúlveda [126] reported on the measurement of spiral grain of Nordic spruce with CT in 2002. He used a medical X-ray tomography device to generate images of concentric surfaces and measured the surface pattern angle. The correlation between CT-based surface pattern angle and the grain angle in destructive tests was 0.81. Sepúlveda et al. [127] measured also with an X-ray Log-Scanner the variables that can be used in estimating the spiral grain. The most important properties for estimation were the sapwood content, the variation in the ratio between the heartwood and the log cross section areas, and the standard deviation for the mean log density in 10mm thick cross slices along the log. The logs were sorted in two groups according to the estimated spiral grain with a classification error of 16%.

CT images of red oak, yellow poplar and cherry were studied by He [53] in 1997. In addition to defect detection, He was able to distinguish heartwood and sapwood in yellow poplar, but not in the other wood species. For Norway spruce, Longuetaud et al. [80] were able to determine the heartwood/sapwood boundary very accurately from CT images in 2007. The algorithm for heartwood/sapwood boundary detection required a pith location as a prerequisite. The algorithm for locating the pith from CT-images was published by Longuetaudet al. [79] already in 2004.

3.1.7 MRI imaging

Magnetic resonance imaging (MRI) is based on nuclear magnetic resonance (NMR) and is better known as the highly sensitive method in medical imaging and diagnostics. Under the

influence of a strong external magnetic field, magnetic moments in nuclei having an odd number of protons and/or neutrons are aligned with the external magnetic field, instead of the random ordering in the absence of the field. This alignment is deflected with a short RF-pulse. After the RF-pulse, the nuclei return into the alignment with the external magnetic field releasing a specific transient radio signal that is detected.

Chang et al. [15] reported NMR imaging of wood in 1989 . They used a medical device and chose only hydrogen protons (in water) for scanning white oak and black cherry logs. Thus the MRI image was the distribution of water inside the logs. They demonstrated that defects, such as knots, worm holes, cracks, decay, wetwood and tension wood can be detected with MRI technique from internal 2D-slice images. The location and size of the defects can be detected, and the heartwood and sapwood regions were distinguishable.

In 1998 Coates [21] developed an algorithm to detect defects in logs with two dimensional MRI image slices. Coates observed that simple thresholding methods were not adequate for separating defects from the undefected wood because of the variation caused by early wood and latewood regions within the annual rings. Thus Coates extracted defects with the region-growing method, beginning from a defect region seed.

In 2002, Contreras et al. [29] proposed an improvement to the MRI scanning of the wood by applying the transverse 1-D projections with a pattern that was helical and undersampling. Slice images were reconstructed by filtered backprojection. The technique increased the scan speed considerably.

In 2004, Morales et al. [97] made a 3D-reconstruction of pine with MRI technology revealing annual rings and describing the ring evolution along the log. In addition, individual characteristics such as knots and defects were included in the 3D-reconsruction although not all types of defects were distinguishable.

3.1.8 Electric measurements

Electric measurements have been applied in wood assessment for decades [62]. Typically, these are straight forward resistance or frequency dependent impedance measurements with

two electrodes. Variation in impedance is then interpreted as variation in wood material properties.

The simplest electric measurement system for a wood sample is to measure the resistance of the sample. Because the resistivity of wood is highly dependent on the water content of the sample, resistivity measurement may serve as moisture measurement. According to James' review about electric moisture meters in 1988 [62], the first resistance based moisture meters were tested already in the 1920's. Capacitive sensors generate an electric field between the sensor plates. The capacitance of the sensors changes according to the changes in the dielectric properties of wood, e.g. due to moisture variation.

Rice et al. [119] reported in 1992 a method for detecting knots, voids and wane in lumber with dielectric sensors. They placed seven adjacent capacitor plate pairs on the board surface and applied a voltage between the plate sensor pairs. The conveyor belt moved the board, and thus the board was scanned. The dielectric properties of wood varied with voids and knots, which was detected by the sensors. The variation of dielectric constant with the grain direction is the basis for the detection of knots, because the grain orientation changes significantly near knots. Voids are detected, because the dielectric constant of air is significantly different from that of wood.

In electrical impedance tomography (EIT), several electrodes are placed around the sample to be analyzed. Currents are applied in the sample through the electrodes and the resulting voltages are measured. Thus impedance between all electrode pairs are known and the impedance distribution inside the sample can be estimated.

In wood technology, the impedance tomography has been little applied. White and Waterfall reported the first attempt for detecting decay in power line wood poles in 1996 [157].

Savolainen et al. presented a simple and inexpensive EIT measurement device in 1996 [125]. They measured the internal impedance distribution in spruce logs. Screw electrodes were fixed around the log. After impedance measurements between the electrodes, the tomographic image revealed knots clearly near the electrode plane.

Steele et al. patented in 2004 an electrical impedance tomography device for detecting density variations in logs, such as those due to juvenile and compression wood and knots or rot [138]. In comparison with earlier research, the electrodes in the device were non-penetrating brush electrodes and allowed the movement of saw logs past the electrodes. Cooper et al. [30][31] demonstrated the device in 2007 and 2008 and compared their results with CT-images to determine the accuracy of juvenile and knot wood detection of electrical impedance tomography.

3.1.9 Visible light imaging

The wavelength of visible light is between 400 and 700 nm in electromagnetic radiation spectrum. The invention and commercialization of digital cameras have boosted the applications in wood measurements as in many other fields. Most visible light range cameras used are line scan cameras located above a conveyor belt. Over the last decade color cameras have been replacing the gray scale cameras. In order to turn the image into wood geometry and quality information, advanced image processing methods are required. Thus wood image processing is reviewed here as well. The field is here divided into three categories:

1) board face imaging typically for the detection of defects, such as knots,
2) board and log cross section imaging inferring about the wood properties based on e.g. the annual ring pattern, and
3) full log and bark imaging e.g. for recognition of wood species.

Watson and Latshaw [154] from Morvue Inc. patented a non-imaging veneer inspection system in 1972. Their on-line apparatus detected cracks, knotholes, voids and similar type wood defects in a moving strip of veneer. This was the first sensing system based on optical line detector in wood measurements and thus the predecessor of modern imaging methods. The system illuminated the sample with a stroboscopic light and studied transmission through the veneer sheet under inspection. Obviously, the defects affect the transmission of the light. The difference between cross-grain and with-grain dimensions of individual defects was measured, and that was the basis for distinguishing splits and cracks from knotholes and other voids.

Board face imaging

Matthews and Beech [86] from Plessey Handel und Investments A.G. patented an apparatus for detecting knots in planed timber in 1976. Their patent comprised the device emitting light on the board face and sensors detecting the reflected light. The output of the sensors was used in the knot, blue stain and rot detection. Based on this patent Plessey developed a laser based optical defect detection system in co-operation with Weyerhaeuser Co..

Conners et al. [26] developed a fully automatic system for the control of wood cutting and sawing. Their system scanned logs using computed tomography for optimal cutting and sawing. After sawing the logs into boards, the board surfaces were prepared and then scanned optically. They published research results about board face scanning, defect detection, defect location and identification in 1983. The system analyzed gray scale images of size 512×512 pixels and was able to detect, locate and identify eight most common defect types correctly in 88% percent of cases in board faces. After defect detection, the system cut the clear wood blocks with a laser, and finally classified with image analysis products free from defects. This research group published numerous articles about the system during the following decade. McMillin et al. [89] described the system more in detail. Klinkhachorn et al. [70] described an updated version of the system with improved grading capability: the system was able to take images and analyze both faces of the board and algorithms were improved to cover a wider range of wood species. Cho et al. [17] [18] reported a color camera based system that was able to detect, locate and identify defects also in rough boards and independently on wood species.

Lampinen et al. [74] presented a camera based wood defect recognition algorithm in 1994. In particular, the system was able to classify different types of knots. The first algorithm was based on the percentiles of color histograms and on the location information about the knot on the board. The comparative algorithm was based on general defect shape related features, such as dark ring around the knot, dark blobs inside the ring or width and severity of cracks in the knot. Lampinen et al. also studied the self-organized feature selection with SOM (self-organizing map) [75]. The method continues to be used in full-scale defect detection applications in sawmills. After these pioneering publications, a considerable amount of literature has been published on detecting, locating, identifying and classifying defects in

boards and plywood using the face images. (e.g. Kauppinen et al.[68], Silvén et al. [129] and Niskanen et al.[100])

In 1999, Nyström and Hagman [104] were the first to image spectral composition in wood applications. Their line camera system divided the line information into 256 wavelength bands, each 1.2 nm wide, with an imaging spectrograph instead of the three color bands of conventional color cameras. The spectral information obtained from a wood sample face was analyzed to distinguish compression wood from normal wood in Norway spruce. The results were compared to those obtained with a scanning electron microscope. The automatic classification of compression wood was correct in 11 out of 14 cases.

In 2002, Kellner et al. [69] applied a camera based machine vision system to track grains on the board face. The purpose of grain tracking was to analyze the relationship between the visual features - the regularity of the grain - and the stiffness and strength of the board. Furthermore, their real-time system was able to classify boards into appearance categories. The system consisted of a gray scale CCD line camera at a distance of 1m above a conveyor belt, which moved the board under the camera allowing the overall scanning of the board. Only a few image rows were analyzed rather than the full scanned image because of the response time requirements in the online analysis.

Cross section imaging

In 1982, McMillin [88] demonstrated the potential of image analysis, though semi-automatic mode, in wood quality assessment. This was probably the first publication discussing wood sample imaging and matrix image analysis using computers. McMillin used a 'minicomputer' with 64kB memory and a scanner. Images were obtained through a microscope or directly from specimens using an illuminated macroviewer. The macroviewer image was focused on the scanner unit similar to early video cameras. The scanner unit produced the analog video signal from the sample, which was displayed on the operator's monitor. The operator adjusted the image gray levels, after which the image was converted by a binary code and sent to the processor. The system required the operator commands to determine the region of interest and threshold values for the image. McMillin measured early wood and latewood ring widths and areas (and thus annual ring widths and areas were known as well), and the average growth rate in an area of 1.54 square inches (9.94 cm^2) of a

loblolly pine sample. He also macerated the loblolly pine sample in chemicals to obtain some tracheids and measured the fiber length with microscopic imaging. In the microscopic scale, the determination of cell scale characteristics was demonstrated: the void volume, the lumen area and the radial lumen diameter of prepared and stained shortleaf pine sample were measured. McMillin also measured the amount of defects in percent in plywood shear. Finally, McMillin demonstrated the analysis of a slice tomographic image of a log. He measured the maximum and minimum diameters, the area and the growth rate of the log, and the knot diameters and area.

Rauschkolb [116] discussed in 1994 in his master's thesis algorithms for automatic identification and measurement of annual rings. The algorithms required an idealized cross section image and samples had to be carefully prepared. He proposed that the boundaries between annual rings are best detected along several paths from pith to bark in the direction of the radius although he also studied boundary tracing algorithms in gray scale images. However, the methods required that the wood disc sample should be located or the image cropped so that the pith location is at the geometric center of the image.

In 1995 Smith [132] described an image analysis prototype for measurement of annual ring area. A system was developed to determine the area of annual rings for discs in which annual ring boundaries are clearly defined and without disturbances. Thus the method was suitable only for ideal and perfect wood discs. Three attributes for the ideal wood disc are: a distinct boundary between the annual rings, one threshold value defines the boundary between all annual rings, and no annual ring has breaks or gaps. The system was based on 8-bit gray scale images. Smith's method started by detecting first the most outer annual rings and proceeded towards the center. Then he applied a contour-tracing algorithm first to detect annual ring boundaries and then the area enclosed by all ring boundaries was calculated. After subtracting the two areas enclosed by adjoining annual rings the area of individual annual ring was obtained.

A dating system for annual rings assisted with computer vision has been developed at the University of Arizona since 1998 by Conner et al. [23] [24] [25] and Gopalan [49]. The system was developed for the dendrochronologists to provide support to the tedious manual annual ring dating work. The system consisted of a camera and a microscope. A series of overlapping images was taken and the separate images were patched semiautomatically into

one large image for the analysis. The annual ring edges were determined using Canny edge detector algorithm [13]. The system required sanded and polished samples thin enough to fit under the microscope.

Viitanen and Mattila [150] patented a new imaging method for tree cross section surfaces in 1999. Their invention was to attach a row of imaging sensors in a chain saw flange similarly to a line-camera. Thus the cross cut image of the log is obtained during the tree cutting. Imaging in the chain saw flange was developed for harvester head measurements. The prototype of the device is being made and the tests in a real environment are in the starting phase.

In 2003 Hanning et al. [52] developed analysis of board end images for the measurement of average ring width according to the German norm DIN 4074. This study is related to the method development of this thesis in that it applies 2D Fourier transform. DIN 4074 specifies that the ring width has to be evaluated along the lines from pith to the furthermost corners of the board cross section. Thus the pith location has to be known first. Hanning et al. determined an estimate for the pith location with two methods. The first method was based on the local connectivity components and quantization of color images, and the second one on the 2D Fourier transform. Both of the methods determine the gradient lines perpendicular to the annual ring orientation, and the pith was located by applying the Hough transformation [7] for a set of gradient lines. Hanning et al. concluded that the first method was not robust enough for unprepared board ends, whereas the FFT was more robust. They found that the FFT was an appropriate tool also for annual ring width determination. They concluded that more research is needed, but the group has not published further results on the topic.

Vaz et al [148] proposed a camera-based annual ring width measurement in 2004. Their local image scale definition and image segmentation levels solved the problems caused by irregular contrast variation in wood samples or very narrow annual rings that occurred in earlier systems. The local scales are automatically computed using a multi-scale detector approach based on the idea of normalized derivatives introduced by Lindberg [76], and applied for the ring center detection. After ring center has been identified, the system segments annual rings by using a local minimum distance - minimum cross-entropy principle. This is a two-step procedure. First, the image along the radial analysis direction is

reconstructed by using a low-pass filtering with cubic polynomials. Then, a maximal resemblance measure between a filtered annual ring intensity profile segment and the original curve, computed upon minimum cross-entropy is applied to divide gray levels in two classes.

Laggoune et al. [73] introduced a semiautomatic system for annual ring detection, counting and areas measurement in 2005. Wood disc samples were sanded and then imaged with a scanner. The annual ring detection was based on the optimal 3rd order recursive filter dedicated to blurred and noisy images. After filtering the edges were extracted by thinning the annual ring boundaries in one pixel wide ridges and thresholding the image with low and high thresholding levels. The method finds annual ring boundaries accurately for prepared and sound samples without knots. If knots are present, the intervention of an expert is required. Finally, after analyzing an entire set of sample discs the system builds a 3D reconstruction of annul rings within the tree.

In 2006 Norell [101] published the method for locating the pith in the images of untreated and rough cross sections of logs (see *Figure 7*). The method has similarities with that of Hanning et al. At first the method evaluates local orientation to compute the direction normal to the annual rings. Then the location at which the lines of normal direction intersect is determined. The result is refined by multiplication with a filter having circular pattern properties. In 2008, Norell and Borgefors [103] presented two ways to compute the local orientation of the annual rings: the quadrature filter method and the Laplacian pyramid method. The pith location is detected with the Hough transformation [7].

In 2007 Norell et al. [102] introduced the polar distance transform (PDT) in wood image analysis. PDT is a tool for images with circular shapes. It finds the shortest paths along the ring in the tangential direction. The metrics of PDT is such that the step in the radial direction is considered longer than the step in the tangential direction. PDT was multiplied with a cost function that uses the intensity values in the image as a cost function of the path. The result was called the grey weighted polar distance transform (GWPDT). The method was applied for tracking annual rings in the cross surface images. The result was improved with back tracking.

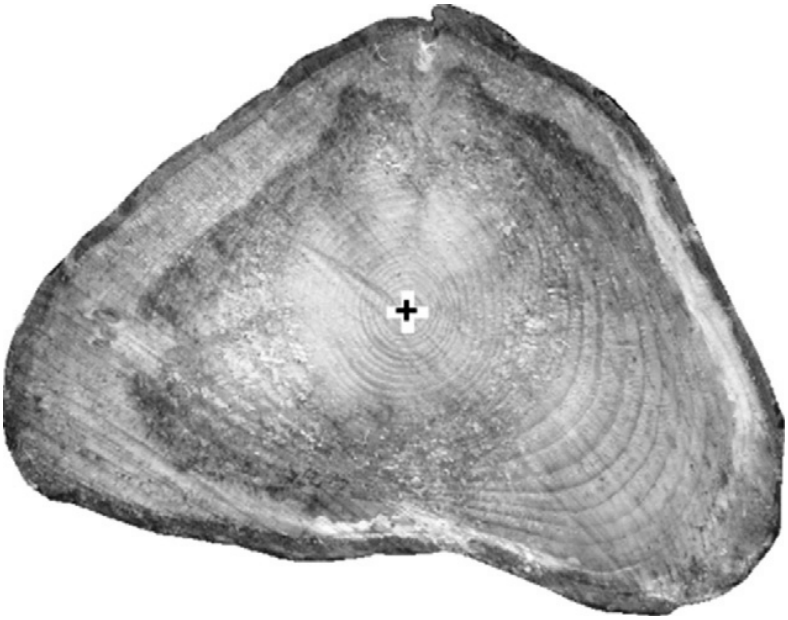

Figure 7. The result of pith locating algorithm of Norell et al.

Enarvi [36] presented algorithms for the image based detection of defective logs in his master's thesis in 2006. He developed a machine vision system for a wood handling terminal to ease the work of human wood quality graders. The system automatically detects defects from log end images in a real industrial process. Thus the log end surfaces are unprepared. With the system a human needs to grade only those logs that the system suspects to be defected, instead of all logs as has been practice until now. Detection of the log end position is based on three-dimensional tables that represent typical wood colors and the circular shape of the log end. Defects are detected according to the statistical features of the log end pixel colors.

Cerda et al. [14] proposed in 2007 an automatic tree ring detection algorithm that works well with the images of smooth and non-defected wood cross-sections. At first, the canny edge detection [13] is applied to the saturation component of the image. Then a filtering that preserves only edges from dark-to-light, not vice versa, was applied. The filtered edge detection data is combined with a growth model, which was based on a variant of generalized Hough transform [7]. The model requires that the perimeter of the wood sample disc and pith location are obtained from the filtered edge data.

Pont et al. [114] made in 2007 a 3D model of a tree stem and its internal structure by imaging with digital cameras slices of the stem. They developed the G2Ring software to delineate annual rings and to map compression wood areas. The samples were chain saw cut wood discs. Annual rings could be tracked in spite of the noise caused by the uneven chain saw cutting surface. Image distortions were corrected and the image was mapped from polar coordinates to rectangular coordinates. The re-mapped image was median-filtered to remove the majority of the noise while preserving the edges, most notably the annual rings boundaries. Thus the re-mapped image was smoothed, focusing more in the tangential direction along ring boundaries, rather than in the radial direction across ring boundaries. The oriented edge enhancement with filtering results in high contrast. The gradient operator picks up the transition from latewood to early wood and the annual ring boundaries are represented as discontinuous vertical bands, which are however, rather noisy. The annual ring boundary detection algorithm searches local maxima with an iterative multi-scale process. Line segments are moved to the locations of the local maxima in neighborhoods that reduce iteratively in size. As inner rings are quite circular, the ring detection begins at the pith wood boundary and proceeds towards the bark. Thus the pith location has to be given. The shape of each new ring is based on the shape obtained for the nearest ring already delineated. The process is rather slow and takes 5-10 minutes for discs such as the ones shown in *Figure 8*. The computation time increases with the number of annual rings. The operator may digitize manually the incorrectly delineated boundary. Compression wood was detected from the smoothed gray scale image by thresholding. The authors used the fact that compression wood may exist only on one side of the stem. Hence the other side provides a reference when selecting the compression wood threshold. The threshold value was finally given by the operator. Several wood disc samples were cut from the tree stem. The 3D structure of the tree and its internal properties were constructed by using the annual ring and compression wood data of discs, and by using the stem coordinate data obtained with profile measurement software based on the images taken before cutting (e.g. PhotoMARVL).

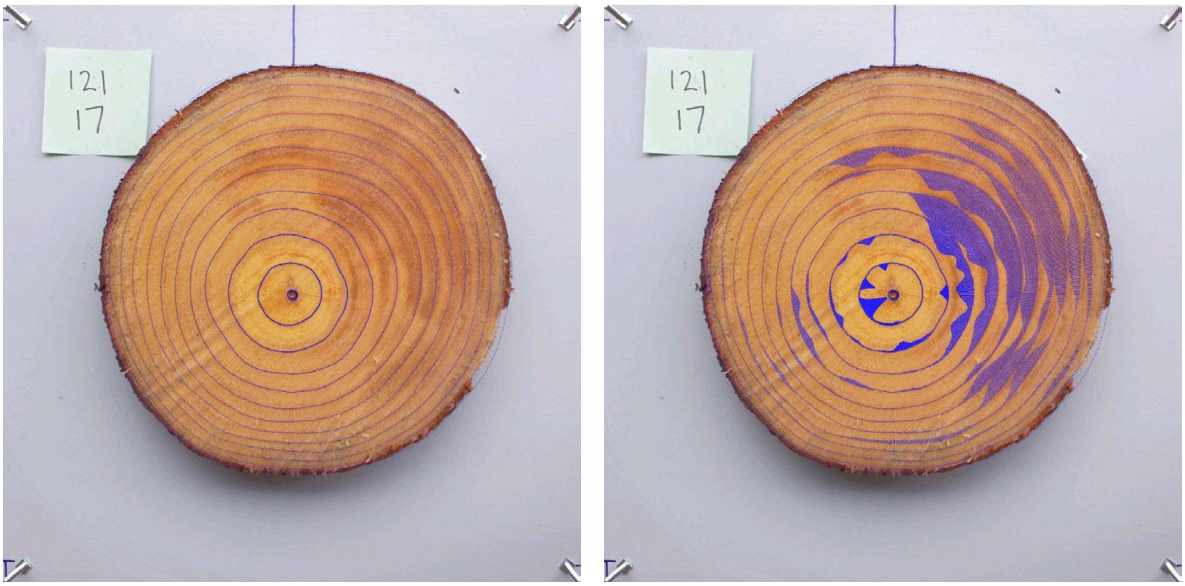

Figure 8. (a) Annual ring boundaries delineated by Pont et al. [114]. (b) The result of the compression wood detection algorithm.

In 2008, Marjanen et al. [84] studied the annual ring measurement from the wood cross sections outdoors. This work is a continuation of the work in this thesis. The long-term goal is to apply the camera-based measurements and the analysis algorithms reliably in a harsh outdoor environment, in particular, in a harvester head. The matrix camera was not located orthogonally to the log end, and thus the log end image was skewed due to perspective projection. The skewed image was transformed and interpolated to a constant resolution orthogonal image. Powerful Laser and LED based lighting solutions solved the problems due to variation in lighting during the day, in particular, those due to straight sunlight. The effects of the object movement during the imaging were reduced with a short flash time and short exposure time. The mean annual ring width and its standard deviation were evaluated using the local 2D Fourier power spectrum methods based on the studies in this thesis.

The research for full logs or bark images

In 1992 Ciccotelli and Portala [19] presented a system for optimizing the geometric positioning of logs prior peeling. The camera-based machine vision system developed for the plywood industry commands the positioning control, so that the theoretical peeling axis coincides with the log's longitudinal axis. The system has two cameras facing both log ends producing image data for the analysis system.

In 2005 Suomela [141] studied as a Master's thesis recognition of wood species from the bark images taken with a conventional SRL camera. The calibration plate was included in each image to obtain correct color and distance information. The classification of the four most important wood species for the Finnish forest industry was based on statistical color histogram parameters and texture parameters.

Kosonen [72] applied image analysis in the recognition of tree species similar to Suomela's work in his master's thesis published in 2007. He developed the method towards an application in the forest environment. The method was based on the bark images of standing trees. The images were taken with a machine vision camera from varying distance that was measured with a laser scanner attached in a vehicle. The texture and color parameters of the four most important domestic tree species in Finland were analyzed. The color parameters were the statistical values of color image histograms and the texture parameters were obtained with six algorithms. A combination of texture and color parameters specific for tree species was chosen for the recognition of species. The correct classification rate was over 80%. In addition to standing trees, the recognition system can be applied for logs before debarking.

3.2 Wood measurements in industrial wood supply chain

The measurement of wood is an essential part of the wood supply chain management in the forest based industry. Term 'wood measurement' covers the quantity and quality measurement of standing trees, the measurement of cut and bucked trees or sawn wood, such as boards, and that of wood in mechanical industrial processes. Measurement results support the economic transactions in wood handling and trade: the trade of timber, the wages of the forest workers, and the business of wood logging and transportation. Measurements are made to maintain and develop the wood supply chain efficiency. Today wood measurements are needed increasingly in the production control at mills. All the methods approved for the measurements within wood trade are regulated by law in Finland [92]. The law commands how to control the accuracy of measurement devices. The law also provides the guidelines how the conflicts between wood supplier and forest owner are moderated.

The measurement method of industrial wood is defined in the trade agreement signed by the forest owner and the buyer. The wood can be measured in the forest, at the roadside wood

storage or at the forestry mill. Forestry companies buy trees as standing trees or as ready cut and bucked logs. Typically, the trees are measured after cutting to evaluate the price of timber for the forest owner. However, after cut down the trees are thinned before measurement. For decades the measurement of trees, stems and logs has been manual work, and even today most manual methods continue to be acceptable by the Finnish law, though they are becoming increasingly rare.

The majority of Finnish timber is cut with harvesters. Harvesters are able to measure log volumes in the forest quite accurately, and in most cases this measure is used as the trade measurement. If the forest owner cuts the trees himself and transports the logs to the roadside, the volume and hence the selling price of logs is typically determined at the measurement stations of pulp mill, sawmill or plywood mill. Quality properties of the wood are measured automatically only rarely, and for defect detection rather than overall quality assessment for end use.

The logs of high diameter having the best quality are transported to plywood mills. Straight logs with a low taper are optimal for peeling. Good quality logs are required also at sawmills, so that waste wood is minimized during the processing such as board sawing and edging. The low diameter logs of lower quality are utilized in pulping industry. Even rotten logs are often accepted. The worst wood material, such as totally rotten parts, branches and rootstocks can be utilized in energy production. However, when logging waste is left in the forest, it is expected to preserve diversity of the forests. The majority of the wood nutrients remain in logging waste after logging [111].

3.2.1 Measurement technologies through wood supply chain

Most of the measurement methods discussed in this thesis are in global use, but the emphasis of the thesis is in measurement systems used in Finland. A great variety of measurement techniques are applied for wood measurement throughout the wood supply chain. In the forest, the dimensions of standing trees can be measured with a handheld caliper. The breast height diameter is an essential geometric measure of standing trees in forest management. An electronic caliper saves the data automatically. Measuring before cutting the height, and the tapering, or the higher diameters of standing trees has a high economic potential: this information allows accurate estimation of the number and the grade distribution of sawmill

logs and pulp mill logs. Laser based measurement devices are under development for this application.

Today harvester dimension measurements require physical contact with the log. The thickness of a log is measured with either delimbing knives or feed rollers, depending on the manufacturer of the harvester. The distance between the blades or the rolls determines the thickness of the log [147]. The diameter can be measured also by triangulation, which requires three contacts with the log. The measurement interval along the log in the harvester measurement of the thickness of the log is 10 centimeter or more. However, the first thickness measurement value is obtained further than 10 cm from the first cutting surface because of the geometric constraints due to the chainsaw bar and the measurement unit. The length of the log is measured using the cog wheel, which rotates on the log as the log passes through the harvester head during pruning. The accuracy of the measurements in the harvester must be verified daily with reference samples. This continues to be manual work requiring a handheld caliper and a carpenter ruler. Harvester measurement tends to be more repeatable than the manual one, but the verification measurement is needed for the detection of systematic errors.

The volume of a pulp wood pile in a roadside pile can be measured with the frame volume method. The frame volume measurement of pulp wood at the roadside storage is typically manual work with a simple ruler. The volume of the standard length saw logs in a roadside pile can be measured by the top diameter of individual logs with a handheld caliper. However, new methods based on cameras and image analysis are being commercialized for the measurement of pulp wood and saw log volume in piles.

In addition to measuring piles at roadside, wood piles can be measured at the receiving terminal of the forestry mill in the timber truck before the piles are removed or in the grab loader vehicle during/after removing. Pulp wood piles are more commonly measured at the measurement stations of pulp mills than at the roadside. The conventional way for measuring pile volume at the terminal has been the manual frame method i.e. the stacked measurement in a vehicle. The distances between timber bunks in the truck or the trailer are known, and thus the width of the pile is known. The height of the pile is measured manually and the compactness of the pile is evaluated visually by a human. The compactness depends on the log diameters and on how much branches there were in the logs. During the winter, there

tends to be snow and ice between the pulp wood logs causing error in the frame volume measurement. This is taken into account with experimental scaling factors. Both the laser scanner and the camera based automatic measurement devices have been developed for measuring the log piles in a timber truck. A truck drives through the measuring gate and the lasers or the cameras scan the wood pile. The volume of the pulp wood pile on the truck is estimated by first measuring the 3D-profile of the pile with image analysis. Such automatic measurements are verified with occasional and randomly sampled volume measurements: the sample pile is spread on the ground and the volume of each single pulp wood log is measured with a handheld caliper and ruler. At the same time the pulp wood quality is evaluated visually. It is assumed that the evaluated quality thus represents the entire pulp wood unit obtained from the forest stand. A few pulp mills in Finland have machine vision based measurement stations, which measure each pulp wood log within sample automatically instead of manual caliper and ruler measurement. According to Finnish law the evaluated compactness of the sampling pile may also be taken as representing the entire pulp wood unit. Only seldom are all the pulp wood logs measured one by one. Automatic commercial devices measure accurately the volume of the logs arriving at the mill, but commercial system for adequate quality evaluation do not exist. In addition to automating the volume measurement the machine vision solutions are able to determine the 3D shape of the sampled pulp wood logs. Logs curved or crooked, and thus problematic in the mechanical pulping, can be detected. However, non-shape related quality properties such as rot and color defects cannot be evaluated with these systems.

Another conventional way to measure the volume of the pile of logs at the pulp mills is that a grab loader vehicle places them into a water container and then the volume of escaping water is measured. The pile of logs can also be weighed and the volume of the timber is evaluated e.g. with local volume-weight tables that are specific to wood species and seasons. The volume of the pile is obtained directly using the combination of the systems above: the pile is weighted in a water container and the volume is calculated using the known density of water.

Forest industry applies machine vision solutions widely, in particular at sawmills. The 3D shape of logs is measured with laser based devices. The sawing of the log can be optimized with information about the shape and the outer dimensions, such as the length, the taper and the top diameter, and thus the amount of waste wood is reduced. The log should be placed at

the sawing station so that edge damages, in particular the wanes of saw products, are avoided. In addition to outer dimensions and shape the X-ray devices are able to detect inhomogeneities inside the log. The X-ray devices provide considerable benefit through that they can detect foreign material, such as nails, small stones or lead before sawing. Similarly knots, knot ringlets and internal cracks observed with the X-ray devices can be taken into account in sawing. The main limitation of the X-ray applications is their high investment cost. The machine vision camera based systems measuring the 3D geometry and the surface quality of sawn boards – twisting, bending, wanes, holes, knots, breaks and color defects – are widely used at sawmills. Acoustic measurements to recognize harmful internal cracks are being developed. Classification of the board is based on acoustic signal analysis. Laser has also been used to measure the strength of boards through vibrations.

At sawmills, X-ray devices are able to measure the bark content of the log directly. The new device based on laser scattering measures the bark thickness, but requires the log to have both barked and unbarked regions.

In the peeling process of the plywood industry, the roundness of the log is important. Waste wood is produced less, if the logs are round and have low taper. Laser based devices assist to position the log in the rotation chucks for peeling. Color line camera based solutions similar to the board face analysis are largely used in quality control, sorting and patching of the plies before gluing.

3.2.2 Commercial machine vision applications for wood measurement

Machine vision systems for wood measurement are a rapidly developing business. The commercial wood measurement systems combine several techniques, such as digital cameras, X-rays, ultrasound and microwaves. The most common machine vision solutions in wood industry are the devices that measure the dimension and the profile of logs and sawn timber with laser scanning often combined with cameras, and the camera based quality control devices for board surface analysis. In this section, we focus on camera based products operating in the visible range of light.

Oy Decon Ab was founded in Finland in 1974 and continues its operations under the name FinScan [40]. It developed camera based wood measurement systems called Optilog and

Optiedger, for sawmills already in seventies. In Optilog, the line cameras detected the shadow of the log in three directions, and the dimensions of log were estimated. Optiedger was for the automatic edging of boards. At present the company has products based on color cameras for automatic grading and sorting of board and veneer sheets. BoardMaster-NT scans each face and edge of the board with several cameras so that it detects several defect types, such as knot types, bark, pitch pockets, splits and stain. The system is able to detect the deformation of the board.

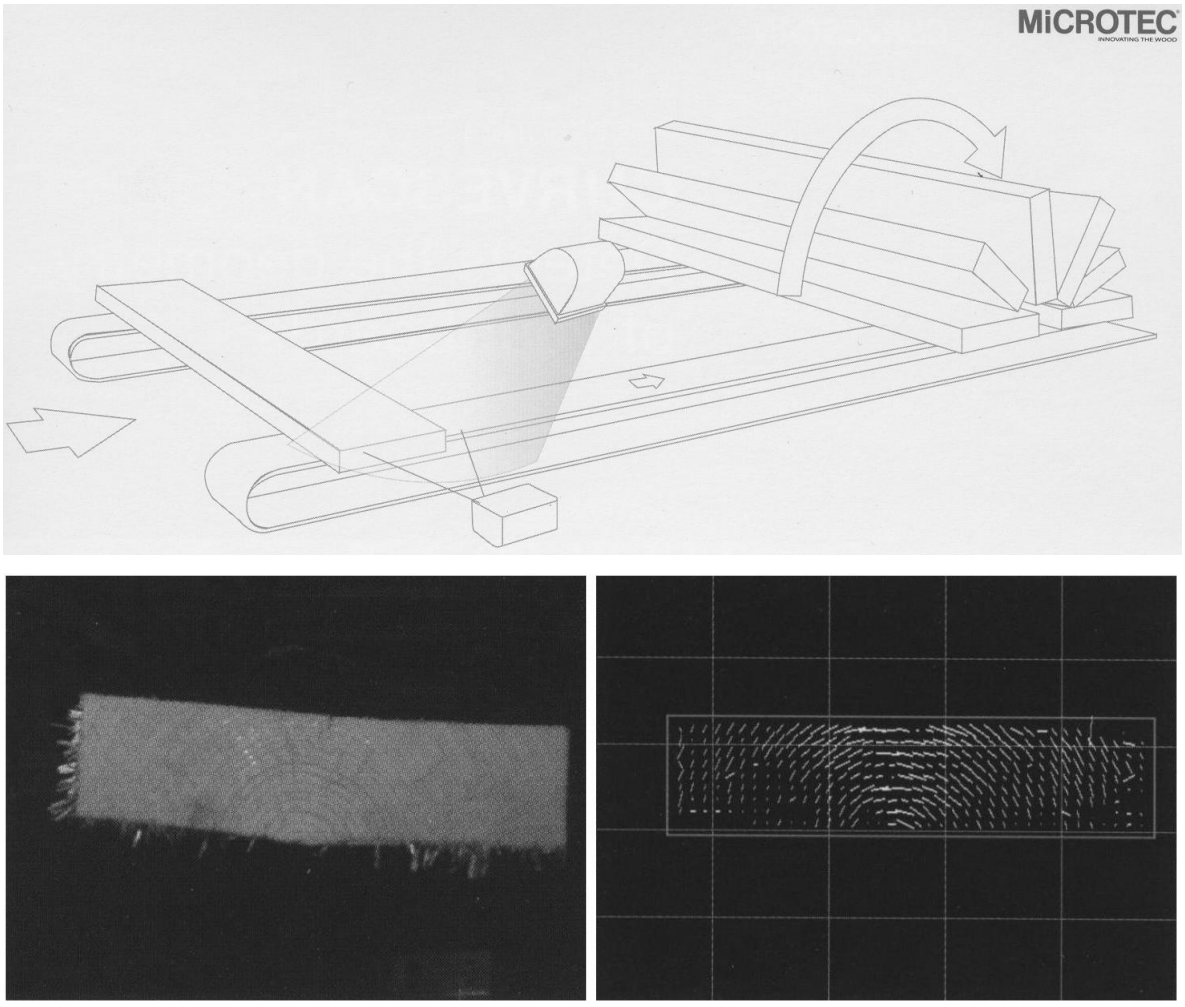

Figure 9. The Microtec's board end analysis device called Optiside. Image from [95].

Microtec [94], founded in Italy in 1980, has optoelectronics products for timber processing industry, for both logs and sawn wood. The products of Microtec combine many of the imaging techniques, such as X-rays, laser, infrared and visible light. The devices measure the dimensions and the shape of wood pieces, and detect internal defects with tomography systems and surface defects with camera based systems. The devices are claimed to assess the strength and the moisture of wood. The camera based measurement system for board

ends, Optiside, was introduced in 2007 [95]. Optiside images the ends of boards that move on a conveyor belt, and then estimates the cup of board, the pith location and the distance between annual rings. Optiside measures also the width and the thickness of boards. *Figure 9* shows an overall schematic view of the Optiside measurement system, a slightly cupped board end and the annual ring pattern detected.

LuxScan Technologies [83], founded 1998 in Luxembourg and acquired recently by Weinig Group, has developed machine vision systems for lumber processing. The LuxScan solutions are designed for boards only. In the LuxScan solutions color cameras, lasers and X-ray sources detect wane, holes, knots, cracks/splits, pith, resin, stain, decay and sound wood color. These systems measure also the shape parameters such as bow, bending and twist. An acoustic sensor is available for stress grading. LuxScan has also the Front End Scanner, which estimates grain orientation, heartwood position and the curvature of the cross section of a board end. In particular, the Front End Scanner classifies boards according to their grain orientation. *Figure 10* shows a camera for board end analyses and scanned images with detected grain orientations.

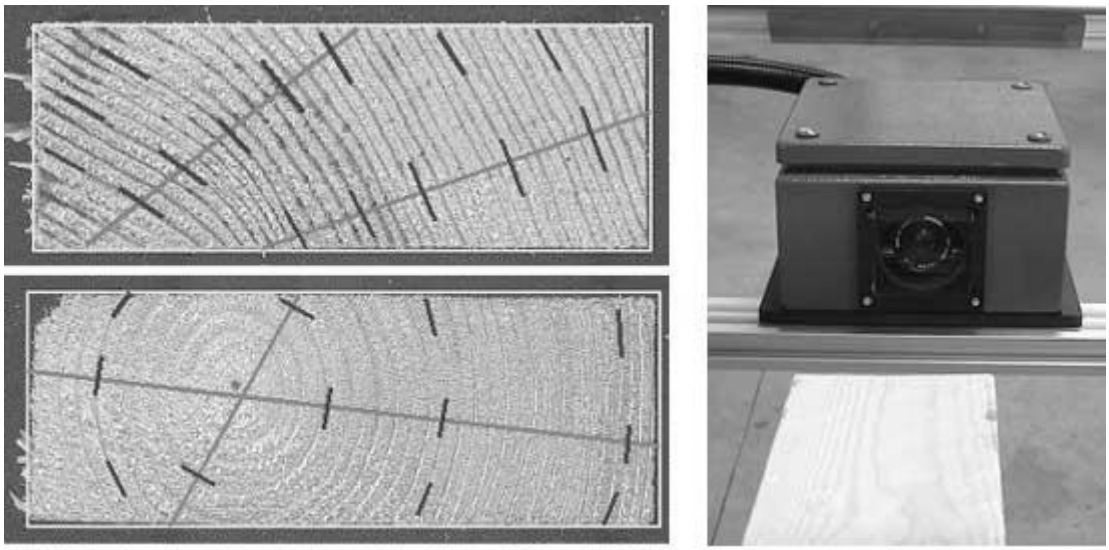

Figure 10. Luxscan's Front End Scanner measures grain orientation using the image of the board cross-section. Image from [83].

The Canadian company Comact Inc. [22] designs and manufactures sawmill technology and equipment for the lumber industry. For instance, they provide equipment for log handling, lumber trimming and sorting. Their lumber grading device, GradExpert^{TM}, is based on laser devices and line scan color cameras. The board passes the camera so that the geometric

properties, such as bow, crook, twist, warp and wane of the board, are measured. The vision system is suitable for several American wood species and detects accurately knots, pith, blue and red stains, decay, bark pockets, paint marks, splits, shakes and worm holes. Comact has also solutions for the shape measurements of logs. The Blue stain detector (BSD) takes color images of the log cross-section surface of a board and detects blue stain and cracks visible on the surface. The blue stain caused by fungi is a visual defect that does not weaken the wood. *Figure 11* shows the principle of BSD and some color images processed during the analysis.

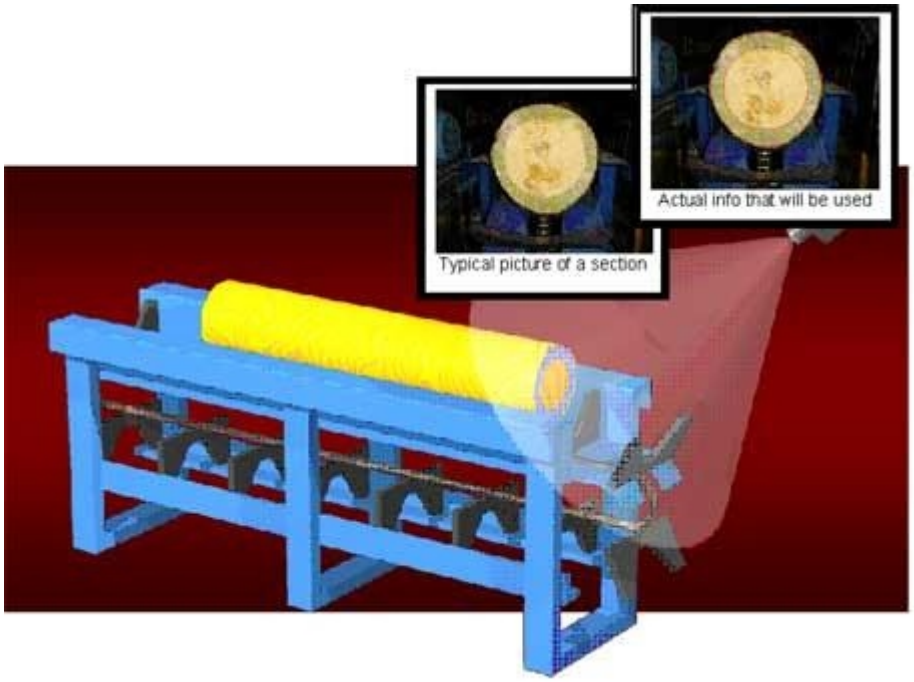

Figure 11. Comact's Blue stain detector utilizes color images taken from the log cross section surface. Image from [22].

Swedish RemaControl [118] has been more than half a century in the sawmill equipment business. RemaControl products are scanners based on laser devices and cameras for both log and sawn wood processing. The systems measure the shape of the log, including roundness, taper and sweep. Scanning devices detect knot enlargements and handling damages. The X-ray based log scanner of RemaControl detects knot ringlets and heartwood, and gathers information about annual rings. The most recent product, RemaLog Bark, distinguishes the bark region from the missing bark region with a laser by utilizing the tracheid effect. The log dimensions on and under bark are evaluated and information about bark thickness produced. For board quality control RemaControl has camera based devices that detect and classify wood defects, such as knot types. The defect classifying algorithm of OptiGrader is based on the self-organizing map (SOM). The technology for OptiGrader is provided by a Finnish company InX-Systems [59].

Sprecher Automation [134] from Austria has two solutions based on board cross cut image analysis: one detects the alignment of the annual rings in order to estimate the position of pith, and the other is a camera based crack detection device developed particularly for the parquet flooring industry. *Figure 12 (a)* shows the pith detection and the distance measurement between the pith and the center of a board cross cut surface. *Figure 12 (b)* shows a result of the crack detection algorithm.

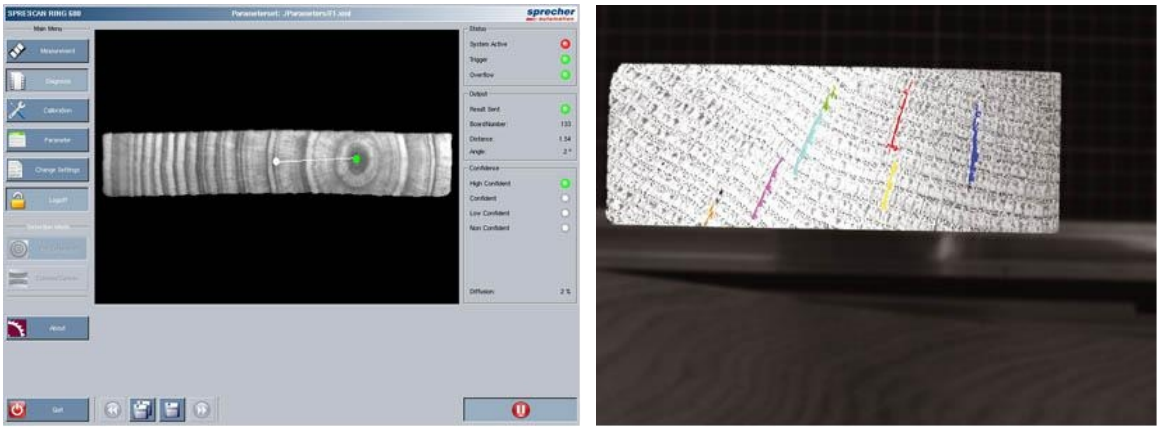

Figure 12. (a) A screen grab of SPRESCAN RING, the pith detection device. (b) An image of SPRESCAN CRACK that detects cracks of in the board. Images from [134].

North-American Newnes-McGehee [99], acquired recently by USNR, offers measurement solutions for logs and sawn wood based on cameras, lasers and X-rays. The Linear High Grader (LHG) with DataFusion™ and AddVantage™ scanner combines four sided multi-channel color vision, infrared laser measurement of the geometric profile, and an optional X-ray measurement of density. The vision scanning detects cracks, insect holes, stain, decay, tight/loose knots and grain angle. The laser profile scanning detects 3D defects, such as wane, holes and crooks. The X-ray scanning detects internal knots and rot. Furthermore, LHG is claimed to detect planed bark and pith location, and even to provide information about fiber structure and its quality.

Swedish Innovativ Vision AB [159] has developed the WoodEye scanner that inspects and optimizes sawn and planed timber. The camera based defect detecting and locating system measures the position, the shape and the extent of the most common defects, such as resin pockets, knots, checks, blue stains, holes and wane. Light and dark knots are classified by

type, size and position. WoodEye measures the fiber direction with a laser, and the width, thickness and length of the timber with a laser profiler.

Canadian Autolog [5], founded in 1987, manufactures laser based devices for measuring the profile and dimension of logs and sawn wood. Visual Defect Detector detects knots and grades the boards by the knot properties based on images taken with a CCD camera under high-power LED lighting.

LMI technologies [78], founded in 1976, produces machine vision sensors, components and software for several branches of industry. For wood industry LMI offers DynaVision chroma+scan sensors that combine 3D laser profiling and light curtain with color vision for accurate dimension measurement and defect detection. DynaVision sensors are applied in measuring, grading and sorting of sawn wood, logs and plywood.

Finnish Mecano Group Oy [90], a member of the Raute group, founded in 1992, develops and delivers machine vision systems that detect defects and measure the roughness of peeled wood sheets. Clipping and patching in veneer and plywood manufacturing is optimized with the data produced. Most of the solutions are based on color camera technology.

Color camera based machine vision systems of American Ventek [149], founded in 1991, detect defects and grade the plywood using surface images. They offer solutions also for plywood patching and moisture measurement.

In Finland, Lisker Oy [77] offers the shape measurement systems of logs and boards at sawmills. For grading sawn timber, Lisker has a system, ProfiGrade, which can detect wane, knots, resin pockets and faults in shape and structure. The equipment is based on laser devices and digital matrix cameras.

Finnish Mikropuu Oy [96] manufactures measurement devices for single log dimension measurements based on line laser and cameras. Mikropuu also has a one-dimensional X-ray scanner combined with a 3D-laser scanner. The company offers dimension measurement devices also for sawn wood.

For pulp wood measurement, a member of the SKS Group, Finnish SKS Vision Systems Oy [131] offers solutions for measuring log dimensions at the pulp and paper mill woodyards. The profiling method of the Automatic Quality Sorting (AQS) system is based on camera and laser technology. However, the operator evaluates the quality of wood from the color images of cross section surfaces.

Danish company Dralle A/S [34] has a camera based solution to measure dimensions of piles of wood at the roadsides or at wood storage. The system has two cameras mounted on the roof rack of a vehicle. When the vehicle drives by the pile, it takes stereo images of the face of the wood pile (i.e. the cross sections of the individual logs are towards the cameras). The wood pile compactness, the mean diameter and the diameter distribution of the logs, and the net and the gross volume of individual piles are estimated. Furthermore, a 3D presentation of the stack can be constructed.

3.3 Applications for wood research

Wood researchers and dendrochronologists have analyzed cross sections of wood for decades. Typically, the measurements have been made manually with simple rulers or under a microscope. During the last decades, only few commercial analysis systems have been developed for wood research. In this application area the careful preparation of samples is often required and user interaction during the analyses is commonly needed.

WINDENDRO™ by Regent Instruments Inc. [117] requires a prepared wood sample that may be a wood disc or a core sample. Alternatively, a high quality X-ray image on a film is analyzed. The sample or the film is scanned, and then the user defines a straight line along which the widths of the annual rings are measured. The most recent version is able to change the line direction to follow the normal of the annual rings. Unrecognizable annual rings can be corrected manually. *Figure 13* shows an image captured from WINDENDRO™ user interface. After the user has located the pith manually, the software determines the annual rings of the prepared wood disc in vertical and horizontal directions.

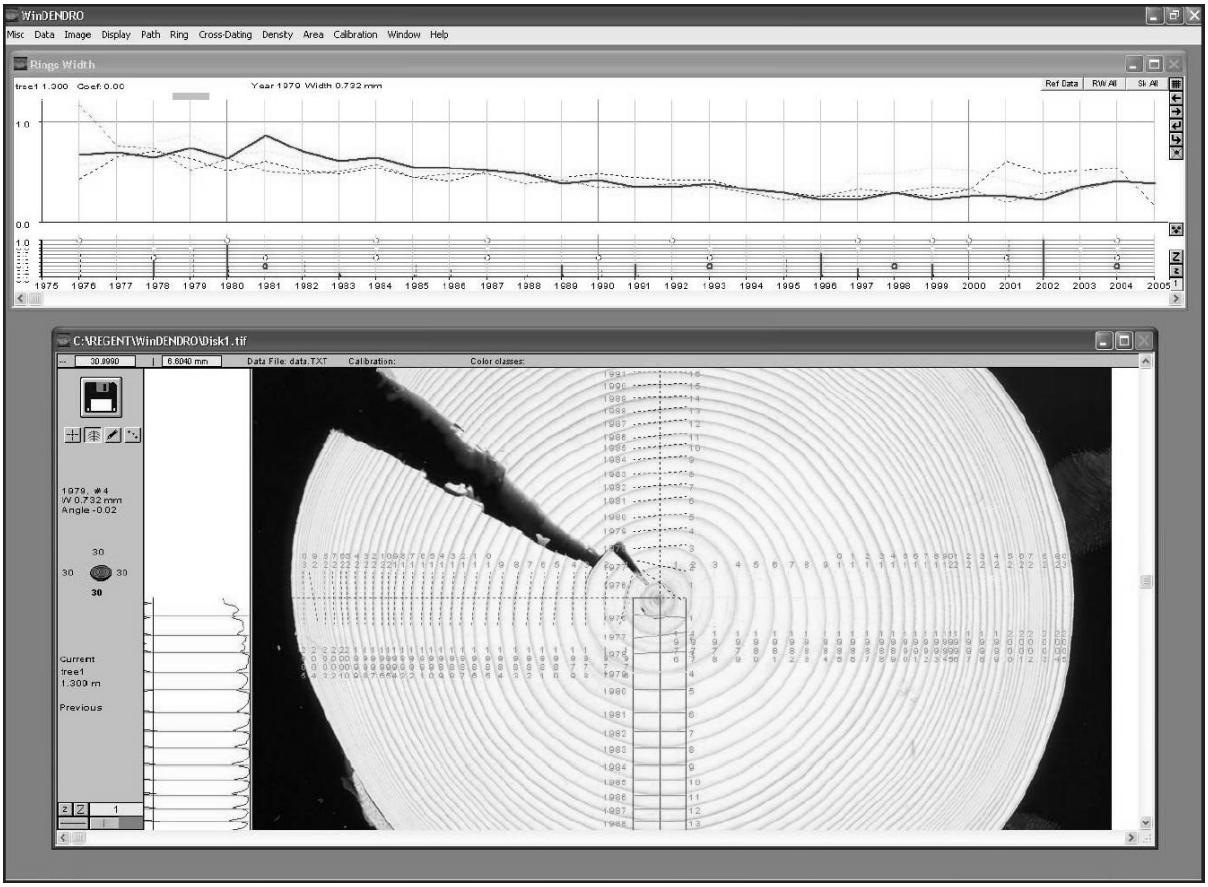

Figure 13. The image capture of the WINDENDRO™ software. Image from [117].

LIGNOVISION™ by Rinntech [120] analyzes the width, the early wood and the latewood of the annual rings along a path perpendicular to each annual ring. The system is suited for softwood and some foliage trees and analyzes either scanned images or photographs. The scanned images must have a high resolution and the photographs must be free of distortion. The results can be edited manually.

A non-commercial software measuring compression wood was developed in the Swedish University of Agricultural Sciences in an EU project [1]. Cross section surfaces of the wood disc samples with compression wood were imaged. During the teaching process the user defines small typical areas of normal wood, and those of mild and severe compression wood in the cross section surface image. After the teaching process, the software is able to divide the entire cross section surface into these three pre-defined wood types. The software also defines the geometric parameters of the wood disc, such as out-of-roundness and pith eccentricity. *Figure 14 (a)* shows the example on the teaching process for the prepared wood disc and *Figure 14 (b)* the result of compression wood detection and classification.

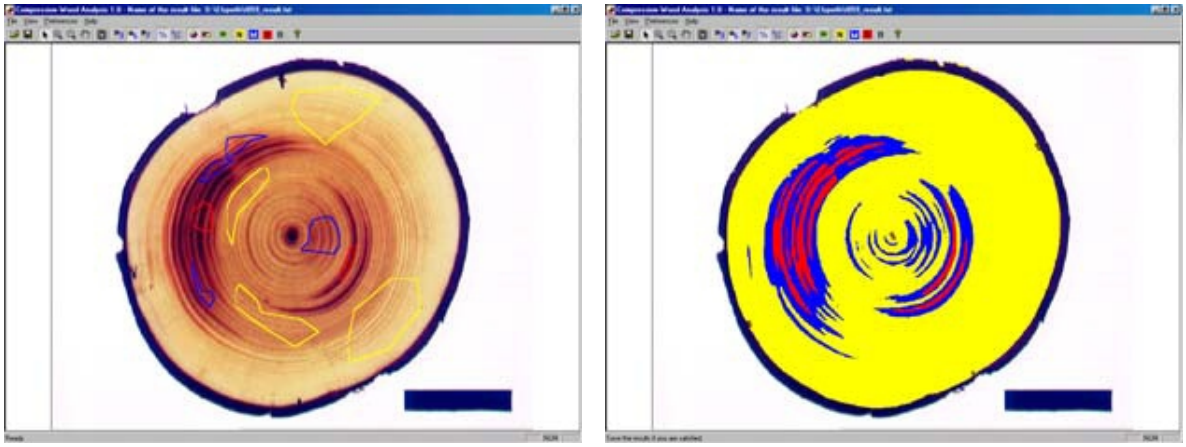

Figure 14. The Compression Wood Analysis 1.0 software. Image (a) presents the user defined typical areas for normal wood (yellow), mild compression wood (blue) and severe compression wood (red). Image (b) shows the detected areas in the disc. Images from [1].

SilviScan® is a wood material measurement system developed in CSIRO Forestry and Forestry Products in Australia by Robert Evans [38]. It has been developed further in cooperation with STFI-Packforsk in Sweden [82]. SilviScan® measures wood properties such as fiber diameter and fiber wall thickness, ring width and wood density. SilviScan® is developed primarily for fiber and microscopic-level analyses. SilviScan® combines X-ray densitometry, X-ray diffractometry and image analysis. Image analysis is made from cross-sectional surface of the core sample with an auto-focusing microscope. Image analysis provides ring orientation, ring width and fiber width. The X-ray absorption provides wood density measures and the X-ray diffraction fiber orientation and microfibril angle. STFI-Packforsk has developed the SilviScan® into an automatic measurement device, which takes samples from wood pile on a wood truck and analyses them.

Von Arx and Diez [4] developed ROXAS© a tool for the analysis of annual rings in root cross sections, based on image processing. Images of well-prepared samples are taken with standard digital cameras through a microscope. Uneven illumination is corrected during the analysis. ROXAS© estimates mean ring width, ring area, number and size of vessels in each ring, vessel density, and the percentage of area occupied by vessels. The core of the analysis consists of common color analysis methods: the image is first enhanced and then segmented in order to determine morphometric parameters. The algorithm requires detailed manual calibration. The microscope image in *Figure 15 (a)* shows the cross-section image of a root taken with a camera. The vessel walls are stained with red color to make the image analysis easier. The right side image shows the growth ring borders as yellow lines and vessels of consecutive rings with as red and white spots.

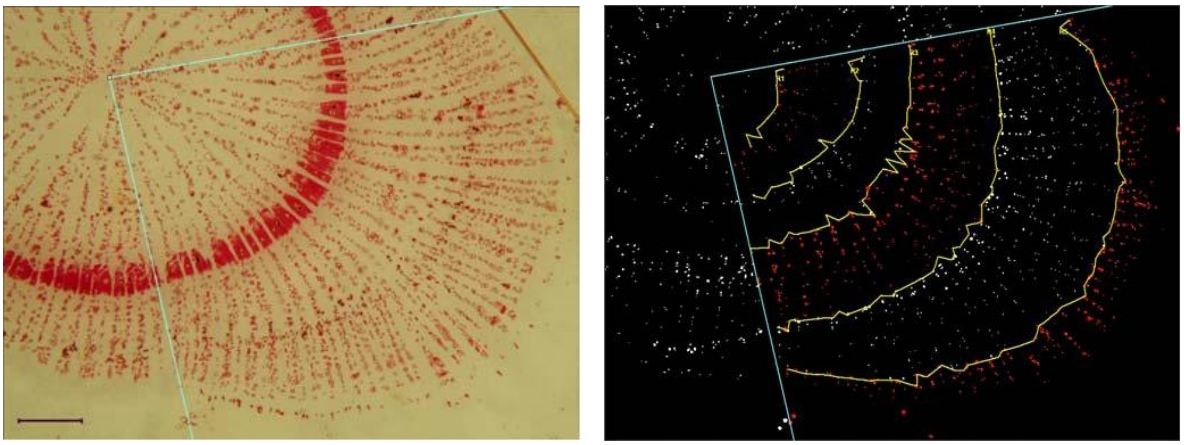

Figure 15. (a) The vessel walls are stained during the sample preparation for better contrast. (b) The yellow lines indicate the annual ring borders. Images from [4].

3.4 Technology gaps as opportunities for image-based measurements

Novel wood measurement methods support existing wood measurement devices to operate more efficiently and provide added value for wood material throughout the wood supply chain. Providing of novel wood property information may enable new solutions within wood supply chain and thus the novel measurement methods may change the entire wood trading. However, it is easier and faster to apply the novel measurements methods so that they support the existing solutions in wood supply chain rather than to re-engineer the wood supply chain. Supporting the existing methods is restricted to providing increased accuracy to the volume and geometry measurements, and to improve the quality grading at sawmills. More detailed quality assessment may change the wood supply chain considerably: the earlier the quality of the wood is evaluated in the wood supply chain, the more versatile are the exploitation possibilities of the quality information. Today, the wood measurement technology, in particular the quality assessment, is rather crude at the beginning of the wood supply chain, but becomes more advanced towards the end of the chain. Thus the largest gaps for novel wood measurement methods are at the beginning of wood supply chain, in forest.

The long term goal is to collect the geographical and the climate information about the forest stands and to measure the quality and geometry properties of the trees and logs in the forest.

When this measurement data is attached to the individual logs through the wood supply chain, the log will be used exactly where it has the highest value.

The quality of wood is currently not measured in the forest at all. Measurement of the bark thickness, the presence and the severity of rot, and the shape and roundness of logs are opportunities for image based measurements. These measurements must be made from rough cross section surfaces. Fortunately, the log end surface is always fresh and quite clean after cutting, which makes image analysis easier. The more detailed quality measurements based on annual rings is the second important opportunity. The number and the widths of annual rings, the annual ring distribution, latewood ratio, heartwood-sapwood boundary, and log eccentricity are pieces of information that help to optimize sawing and peeling, and that are correlating with the strength of the log. Recognition of wood species would allow the detection of rare wood materials and species, and would prevent the faulty sorting of single logs. At present no machine vision or other non-contact measurement methods are utilized in wood cutting and bucking. Current harvester head measurement requires physical contact with the trunk surface, which is why measurement results vary with the season. Methods that provide season-independent results are needed. The accuracy of the diameter measurement in a harvester may be improved with image based methods as the sampling frequency along the trunk can be increased.

Bucking determines a large portion of the commercial value of a tree. Optimizing bucking with measurement information about rot and other defects, and stem geometry has a huge economic potential, but requires new measurements.

The novel camera based measurement system for wood piles measures the outer dimensions of pile, the mean diameter and the diameter distribution of logs and the pile compactness. Additional information, useful in wood logistics, may be obtained from the roadside piles. In particular, the roundness of logs, the presence and the frequency of occurrence of rot could be determined from wood pile images. However, the poorer resolution of pile imaging compared to that of single log end imaging either limits detailed measurements, such as annual ring width, or requires multi-image techniques.

Pulp mill wood would benefit from automatic defect detection: both geometric defects and material defects cause problems in wood processing. At present, defect detection is at best

only semi-automatic: The most geometric defects can be detected, but still the operator must browse through the images that are proposed as defective logs. The annual ring width, the late wood proportion and the bark content measurements could provide wood quality parameters that are important when controlling the paper quality.

The importance of detailed quality control is already well understood. This is manifested by the many machine vision solutions for veneer and ply sheet quality control and patching, and when centralizing the logs for peeling. However, the economic performance and quality in peeling of the veneer sheets may be improved with log cross section information. Information about the annual ring width, the early wood/latewood content, the pith location, the eccentricity, the roundness and the sapwood/heartwood content of the logs may provide essential economic impact, if obtained before peeling.

In the forest based industry, the sawmills are the most advanced users of the machine vision solutions and quality management based on them. The log is positioned for sawing with its 3D-profile obtained with camera and laser based devices. The X-ray devices evaluate the internal properties of the logs to be sawed. The 3D-profile and the defects of the boards are evaluated with solutions based on laser and line camera, the moisture content of boards is evaluated e.g. with microwaves, and the strength of boards e.g. with acoustic measurements. The most recent solutions measure the cup of the boards by using the images of board cross section surfaces. Propagating all these measurement methods to the earlier stages of the supply chain is with high potential. However, making the techniques reliable and affordable at the conditions of the timber trucks, the road side piles and the harvesters is challenging.

Although sawmills are in the forefront of image-based measurement technology, the shape of the log end, the heartwood/sapwood content, the number of annual rings and the width and their distribution are properties currently not measured but with potential in sawing optimization. The high cost of the X-ray based methods is a considerable constraint for smaller sawing operations. The X-ray based technique allows the accurate annual ring measurement, but it requires many measurement directions and thus many expensive X-ray source-detector pairs, or a moving x-ray source detector pair. Recent commercial devices have typically 1-4 measurement directions and thus the ring width measurement and the early wood/latewood measurement based on cross section images produces more accurate results. Less accurate but also less expensive solutions that evaluate wood properties using

the cross section surface images of both log ends may find commercial market. Similarly, the volume of bark or the heartwood/sapwood ratio can be estimated on the basis of the bark thickness, respectively the heartwood/sapwood area, at both log ends. The presence of knots in a log can be evaluated by counting the annual rings in both logs ends. Difference between the annual ring numbers reveals the number of knot ringlets within the log and thus evaluates knottiness. The area and the color of the rot reveal the severity of rot and the propagation of the rot inside the log can be predicted. Eccentricity and pith location can be used in predicting if compression wood or tension wood is present in a saw log. It may be possible to interpolate single annual rings through the log volume by detecting and identifying individual annual rings at both ends with methods commonly used in dendrochronology.

Today, sawn boards are analyzed in detail with machine vision systems, but further development is still possible. The systems based on line-cameras can locate and classify accurately knots on the board. If this data is combined with the annual ring number, the information about the ring width and the latewood content, the strength of boards can be evaluated with improved accuracy. This may lead to finer grading and hence better price-performance correspondence of boards. Evaluating the pith location within the board cross section surface or even outside the cross section surface allows detecting automatically the inner and outer face of the board. The measurement of the annual ring curvature can be used in predicting the bending properties of the board during drying.

Table 1 presents a conclusion of wood properties and measurement techniques discussed. First, costs, applicability and safety of each measurement technique are evaluated in the range of - - - to + + +. The suitability and the performance of a measurement technique for the measurement of any wood property are assessed. The applicability and the performance of any method vary with wood species and along the wood supply chain. This evaluation is subjective based on information collected by the author and his personal priorities of these factors. Applicability and performance are typically the highest for sawn boards at the sawmill and the lowest for trunks in the harvester. E.g. microwaves penetrate through boards rather well, but penetration through logs is poor. Similarly camera based systems can detect every knot in boards but not in logs. Gray color behind the sign in the table denotes that a commercial industrial on-line measurement application is available at least for boards.

	Laser	**IR**	**Acoustic**	**µ-waves**	**RF**	**X-ray**	**MRI**	**Electric**	**Visible light**
Cost	+ +	+ +	+ +	+	+	- -	- - -	+ +	+ + +
Applicability	+ + +	-	+	+ +	-	+	- - -	-	+ + +
Safety	-	+ + +	+ + +	+	+ +	- - -	+	+ +	+ + +
Performance:									
3D-shape	+ + +	+ + +[2)]	- - -	-	- - -	+ + +	+ + +	- -	+ + +
Eccentricity	+ +	+ +[2)]	- - -	-	- - -	+ +	+ + +	- - -	+ + +
Rot and decay	- - -	+	+ +	- -	- -	+ + +	+ + +	+	-
Color defects	- - -	- - -	- - -	- - -	- - -	- - -	- - -	- - -	+ +
Wetwood	- - -	+ +	+	+		+ + +	+ + +	+	- -
Compression and tension wood	- - -	-	+	+	+	+ + +	+ + +	+	+
Cracks and splits	- - -	+	+ +	+	-	+ +	+ +	-	+
Resin pockets	- - -	-	- -	+	-	+ +	+ + +	- -	- -
Foreign objects	- - -	-	- -	+ +	+	+ + +	+ + +	+	- -
Knots	- - -	+	-	+ +	+	+ + +	+ + +	+	+
Wood Species	- - -	- -	- - -	- - -	- - -	- -	- -	- - -	+ +
Tree age	- - -	- -	- - -	- - -	- - -	+	+	- - -	+ + +
Wood density	- - -	-	- -	+ +	+	+ + +	+ +	+	+ +
Strength	+ +	+	+ +	+	+	+ + +	+ +	+	+ +
Annual ring width	- - -	-	- - -	- - -	- - -	+	+	- - -	+ + +
Early/latewood	- - -	- -	- - -	- - -	- - -	-	-	- - -	+ +
Heart/sapwood	- - -	+ +	- -	+ +	+	+ + +	+ + +	+	+
Grain orientation	+ + + [1)]	- - -	- - -	+ +	+	+	+	+	+
Freshness	- - -	-	- - -	-	-	+	+ +	-	- - -

The table continues on the next page

	Laser	**IR**	**Acoustic**	**µ-waves**	**RF**	**X-ray**	**MRI**	**Electric**	**Visible light**
Regular wood color	- - -	- - -	- - -	- - -	- - -	- - -	- - -	- - -	+ + +
Moisture content	- - -	+ +	- -	+ +	+	+ +	+ + +	+ +	- - -
Bark content	+ + [1)]	- -	- - -	- - -	- - -	+ + +	+ + +	- - -	+ + +
Fiber properties	- - -	- - -	- - -	- - -	- - -	-	-	- - -	-

1) when combined with image analysis
2) is not thermography, i.e. no spectral content is utilized

Table 1. The conclusion presenting the suitability of discussed measurement techniques for measurement of various wood properties. The evaluation range is between three minus signs and three plus signs. Gray background color reveals if commercial solutions are available.

On the basis of this analysis, this thesis work has been focused on the image-based measurement methods that – at least in principle – can be applied throughout the value chain, and that predominantly classify wood quality according to the annual ring information. Of course, laboratory background in image based measurements and existing equipment affected the choice of measurement method. Also other measurement techniques on wood cross section reviewed in this thesis may provide methods both for supporting the present value chain structures and for opening up new ones. As the conclusion, however, the best measurement solutions have been achieved and will be achieved when combining information obtained with several imaging and measurement technologies.

4 Research Equipment, Image Acquisition and Calibration

This Chapter discusses the research equipment, the image acquisition and the calibration in this research. The imaging setup is presented in Section 4.1. Imaging devices, image types, lighting solutions, wood samples and their preparation are discussed. Section 4.1 describes also briefly the image analysis software. Section 4.2 presents the calibration of the imaging system: the correction of distortions due to camera optics, the scale calibration for converting pixel distances to real world measures and the color calibration to remove the effect of the variation of lighting between and within images. However, most methods developed, in particular all texture analysis based methods, are quite insensitive to lighting variations, and thus color calibration is not essential for most of the analysis methods described in this thesis.

4.1 Measurement devices and imaging setup

Digital color system cameras were the main imaging devices in this work. Digital scanning of some wood disc samples was tested as a means to make log cross section images. The lighting solutions have been provided rather simply, either with a camera flashlight or with tungsten bulbs and umbrellas. The applicable image formats are considered, and how they can be used in the analyses. In particular, common image types such as JPG that are highly compressed appear often problematic. Thus more suitable image types for texture analyses are discussed. In this section the analysis software, MATLAB®, is presented shortly and the motivation why we decided to use this software is given. At the end of Section 4.1 the wood samples and their preparation for this study are discussed. As spruce and pine are the most important wood species for the Finnish forest industry, a majority of the samples in this study have been spruce and pine discs, or blocks. Section ends with a short description of the general imaging setting.

4.1.1 Imaging devices

The first high resolution images for this study were obtained by scanning carefully prepared wood samples. Images were made at the Finnish Forest Research Institute with a scanner suitable for wood discs. Obviously, the scanner image is generally the best for image analyses because of the uniform lighting. However, in the on-line application phase at the forestry mills and at the harvesters scanners are very cumbersome. Typically, in processes and at harvesters the images must be taken from a distance. Thus after succeeding in imaging with a scanner a decision was made to start using system cameras as imaging devices. This is closer to the intended real-life applications. However, providing sufficient and uniform lighting for the cameras in the intended applications is a further problem. The digital cameras were found adequate for the purposes of this study and they provide a feasible basis for real-time applications in the processes of the industry and at harvesters.

Most images analyzed in this research were taken with conventional system cameras (SLR-cameras). We tested four system cameras each with a different imaging sensor: Canon EOS D30, a camera with a 3.11 Megapixel CMOS-sensor, Nikon D70 with a 6.24 megapixel CCD-sensor, SIGMA SD10 with a 3.4 megapixel Foveon X3® three-layer CMOS-sensor, that corresponds to a 10.2 megapixel conventional Bayer-matrix type imaging sensors, and Canon EOS 5D with a 12.7 megapixel CMOS sensor. Several cameras were used because of the rapid development of digital cameras during the thesis work.

Figure 16 (a) shows the structure and operating principle of the Foveon sensor: the light with wavelengths of blue color are absorbed and thus measured in the first layer, wavelengths of green color in the second layer, and the rest of the incoming light is detected in the third layer as red color. *Figure 16 (b)* presents the structure of the conventional Bayer-type sensor, in which the imaging sensors of the three colors, sensitive at their specific wavelength bands, are tiled on a rectangular grid. The Bayer sensor has in every 2×2 sensor block two green sensors, one blue and one red sensor. The Bayer matrix raw image has missing values in each color channel. The missing values are interpolated on the basis of values of the surrounding pixels so that all the three color channels have an intensity value at every pixel location of the resulting TIF-image. Thus the true resolution of the cameras with the Bayer-type imaging sensor is lower for all color channels than the resolution corresponding to the number of the pixels in the sensor.

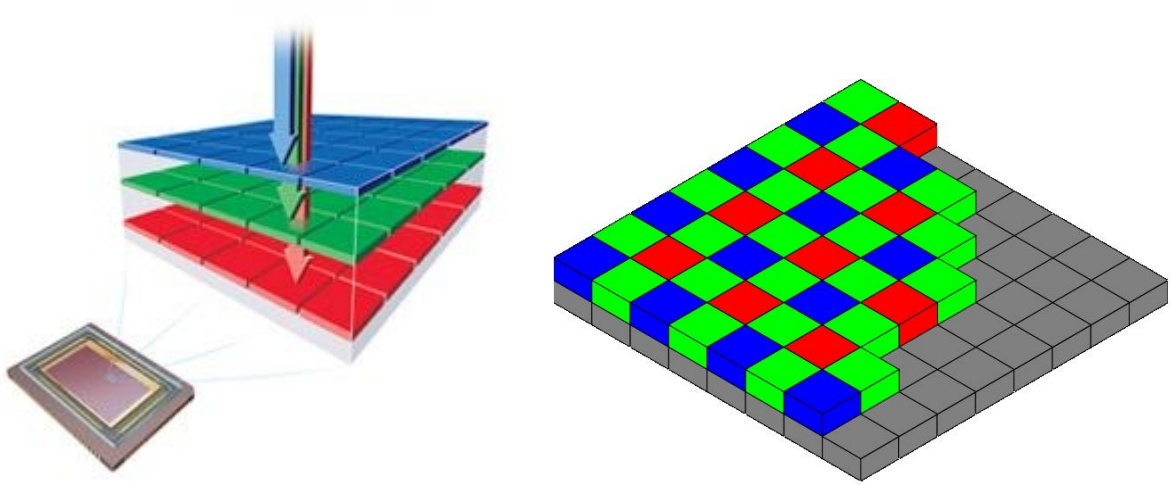

Figure 16. (a) The Foveon X3® three-layer imaging sensor. Image from [42]. (b) A conventional Bayer-type imaging sensor.

Cameras were equipped with normal objectives, such as Canon 50mm, or with macro objectives, such as SIGMA 50mm 1:2.8 DG macro D. In the applications following up the research discussed in this thesis, system cameras are being changed over to commercial machine vision cameras. The applications have more stringent response time requirements and the image transportation challenges are being faced. This is discussed more in the future outlook of Chapter 8.

Most of the images obtained with the cameras specified above can be analyzed successfully with the algorithms discussed in the thesis. However, in some cases the resolution of cameras, such as 3.14 megapixels in Canon EOS D30, was not sufficient to distinguish the thinnest annual rings in an image that covered the wood cross section surface. The higher resolution cameras, such as Sigma SD10 and Canon EOS 5D, allowed even intra-annual ring measurements such as the latewood content in boards cross section surfaces.

4.1.2 Image formats

The choice of the image format is a highly relevant issue. In particular, the texture analyses require high quality images. All cameras produce first a raw image. The raw image typically consists of 8-bit to 16-bit values of the red, green and blue channels. Most point-and-shoot consumer cameras do not provide access to the raw image, but the raw image data is processed with the camera software into some other image type, such as JPG (also noted JPEG) or TIF (also TIFF). The digital system cameras typically provide the raw image, but

the header information in the raw image with e.g. current camera settings, is manufacturer and device specific. This is reflected also by that the extension name of the raw images is camera specific. The raw image types of the cameras in this research are as follows: Canon EOS D30 is of CRW-type, Sigma SD10 is of X3F-type, Nikon D70 is of NEF-type and Canon EOS 5D is of CR2-type raw image. The use of raw images is not straight forward, because most image processing and viewing software, including MATLAB®, are not able to read the raw images without conversion. Therefore a system camera package includes a software, which converts the raw image to a more usual image type, such as JPG or TIF. An imaging sensor converts linearly the photon radiation to an electric charge. Thus the raw image appears very dark, and typically conversion makes nonlinear gamma correction that results in color intensities better for visual inspection. It is the image conversion that makes also the interpolation for red, green and blue color channel to fill missing pixels in a Bayer-type imaging sensor. Because of the interpolation of all the three channels, the TIF image is about three times larger than raw image. The high-resolution TIF images preserve details, but because of their large size, TIF images may not be practical. The raw or the TIF images are typically compressed to reduce the size of the image files. The most common compressing technique is JPG. This technique compresses the image files to a fraction of the original size and yet the images appear acceptable in visual inspection.

Compressing the images leads easily to blurred edges and other details in the image processing phase. Thus the JPG-images should not be used in texture analyses. However, JPG compressed images are more suited for color measurement. TIF images are suitable for image processing with texture analysis. This is particularly so with MATLAB®, because TIF images can be readily loaded into MATLAB®. However, the TIF images are quite large to transfer and to store in the computer memory. The author of this thesis had available MATLAB® functions for reading the raw images directly from our cameras. Although the functions are not contributions of this thesis, they have been extensively utilized when developing the analysis methods. The benefit for using the raw images instead of the TIF images is that image file size is smaller. Furthermore, the computation time is reduced remarkably, because the time consuming conversion from raw images to TIF images can be avoided. Hence, the raw images have been chosen as the basis for the method development in this thesis. However, the raw images are very dark and not good enough for visual inspection due to that gamma correction is not made. Thus whenever images needed to be

inspected visually during the research, TIF images were made. The example images in this thesis are high quality JPG-images.

4.1.3 Analysis software

The main analysis tool software in this research was MATLAB®, versions 6 and 7. The analysis software is a high-level language for technical computing with functions to visualize data and results as graphs. MATLAB® has a large amount of advanced built-in functions for data analysis, and there are sets of extensions available for various research areas. The Image Processing Toolbox was extensively used when carrying out this research and method development.

MATLAB® allows the user to implement his own functions and routines and it has a quite user friendly interface. MATLAB® is particularly effective tool for routines demanding heavy matrix computation. For MATLAB® there are available also some freeware components useful for this research, such as camera calibration toolbox to be described in Subsection 4.2.1. In this research MATLAB® was found an efficient tool for method development. However, when developing high speed real-time applications e.g. C++ routines may be needed for computational efficiency. User interfaces sufficient even in commercial applications can be written with MATLAB®. Because of these reasons and because of the long experience with MATLAB® in the research group, MATLAB® was chosen as the method development tool in the thesis work.

4.1.4 Lighting

An artificial light was used as the lighting in all the studies of this work. First prepared wood discs imaged with the digital scanner were analyzed. In scanned images the lighting was generated by the scanner itself, and thus the lighting was even, and reasonably constant in all images. For images taken with the digital system cameras the lighting was provided in a typical setting with two 500W tungsten bulbs and white umbrellas diffusing the light. Thus the contrast between the illuminated background and the adjacent shadow near the object edge is rather weak. As an alternative, lighting with several office lights aimed at the wood sample was used. Some cameras had built-in flashlights and also they were tested for lighting. However, built-in flashes or other straight bright lights cause heavy shadows, in

particular at the border between the wood disc and background. This tends to pose difficulties for the analysis. The mounting of adequate shades for built-in flashes is a rather demanding task. Thus it was concluded that the external continuous tungsten lights with umbrellas are the best alternative for this research. Differing lighting conditions were tested to see how the analysis algorithms perform for images with different light sources. The texture based analyses produced quite the same results independently on the lighting conditions studied, but automatic extraction of wood cross-section was more complicated with straight light illumination than with diffused lighting due to the heavy shadows around the sample. Obviously, the spectrum of lighting devices affected the results of the color measurements. In real-life applications, such as those at sawmills, pulp mills and harvesters a short lighting pulse should be used because of the short imaging time available. Several external flashes with diffusing shades, based on high-power LEDs for instance, may be a good alternative.

4.1.5 Wood samples and their preparation

The research was focused on two industrially important wood species: Norway spruce (*Picea abies*) and Scots pine (*Pinus sylvestris)*. These are particularly suited for method development as the high color contrast between the early wood and the latewood in the Finnish softwoods makes the discerning of the annual rings in the image analyses easier than with the hardwood species.

At first the algorithms were developed for highly prepared wood samples free from defects. Cut wood discs were planed and sandpapered to get high quality cross section surface for imaging. At a later stage non-prepared healthy wood discs were imaged, and finally the somewhat defected samples cut with a sharp chainsaw were analyzed. Typical defects in the samples were rot and decay, color defects, knots and cracks. With a sharp chainsaw, the fibers are rather cut than ripped. Ripping leads to poor wood sample surface, that not all the analyses can be carried out successfully.

Moistening of the cross-section surface is an inexpensive, harmless and easy way to prepare the sample both in the laboratory and in most of the real-life applications. Moistening increases particularly the contrast between the early wood and the latewood. Moistening works particularly well for chain saw cut surfaces, because the water soaks more easily in

the rough wood cross section surface than in the planed or sandpapered surface. Extensive soaking must be avoided so that the surface does not shine. It is noteworthy that in the forests the fresh cross section surface has typically good contrast just after cutting because of natural wood moisture content.

Both log end and board end samples were studied. Typically samples were wood discs and blocks, but end surfaces of full logs and boards were tested as well. In total 530 rotten spruce wood surface disc images, 2316 healthy spruce disc images, 2224 healthy pine disc images, all unprepared were available for the analysis. For the first tests of methods there were also 20 prepared pine disc images and 8 prepared spruce disc images. Additionally, there were 200 prepared pine and spruce board cross section images each. Not all the images were used, but a variety of the images was chosen for development and testing of each algorithm.

4.1.6 Imaging setting

Producing the image of the object is the key stage of any machine vision and image processing system. Lighting should be even so that the areas with similar properties appear similar to the camera. The lighting source, its spectrum and geometry, and its location with respect to the object affect considerably the imaging and thus the analysis. The lighting intensity and the geometry should be made constant. Therefore, the artificial lighting is used both in the research phase and in the industrial applications. The cross section surface of the log may be rough. In this case, the light source should be located so, that the light comes from the imaging direction and the shadows due to the surface roughness are minimized.

The distance between the camera and the object is a compromise between the largest wood sample size and the camera resolution. An imaging sensor with more pixels allows longer imaging distance at a given imaging resolution. Zoom objectives provide a degree of freedom for selecting the distance, but zoom objectives typically cause more image distortion than ones with fixed focal length. Therefore, fixed objectives are recommended in the measurement systems.

A typical laboratory imaging setting is shown in *Figure 17*. The camera is fixed to the camera stand and the stand is attached to the table. The wood sample lies on the floor, having an even background board, white, gray or black. The camera is aimed at the sample

and the optical axis of the camera is perpendicular to the floor level. Distance between the camera and the wood sample is varied between 0.4-1.5 meters. Board cross section surfaces of constant size are imaged from the shortest distances. Respectively, the longest distance is chosen according to the largest cross-section area in the wood disc sample set. At the borders of the background board, there are calibration targets for scale calibration, and also for color calibration when required. The camera is calibrated as described in Section 4.2. Light stands are on both sides of the samples. The lights with umbrellas are located near the camera so that the lights, stands or umbrellas are not visible in the image, but the light does not come to the sample from a steep angle. Lights are set away from the wood sample towards the umbrellas and the umbrellas reflect and diffuse the light. Typically, the camera is operated remotely to avoid shaking. In most cases focusing was automatic.

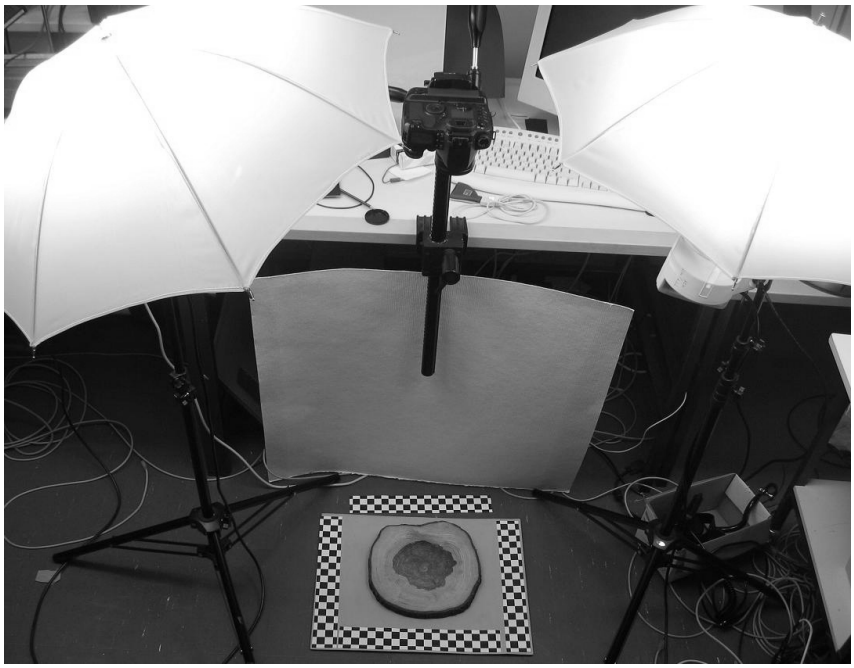

Figure 17. The typical image setting for the imaging of a wood disc cross section surface.

Preliminary tests for imaging the cross section surfaces of full logs and boards were made. The log or the board was placed on the stands and the camera was attached to the tripod. Lights were on both sides of the camera. Light was diffused and reflected towards the log cross section by using umbrellas. In such a setup, the even background board for 3-4 meter long logs is difficult to arrange. The background light should be minimal in comparison to the lighting of the cross section surface. The depth of field was kept shallow, and the camera was focused precisely on the cross section surface. Furthermore, placing the calibration targets at the same distance with the cross section surface is cumbersome. Therefore, in this

case scale was calibrated based on a distance measurement between the camera and the imaged cross section surface. The distance was measured with a laser distance measurement device.

4.2 Calibration

An imaging system becomes a measurement system only through appropriate calibration. This section reviews three calibration tasks: the camera calibration, the scale calibration and the color calibration. The optics of the camera causes radial and tangential distortions to the image which must be taken into account via camera calibration. In image based measurements, the pixel dimensions of the image have to be converted to the real-world distances, e.g. millimeters, via scale calibration. Varying and uneven lighting are error sources causing significant color variation between and within images. Such color differences and variations may be disturbing in the image analysis. Hence color calibration is commonly required in machine vision applications, in particular in tasks using absolute color values. However, color calibration is less important in the measurements based on texture analysis.

4.2.1 Camera calibration

The lens system of the camera causes distortion in the image. Pixels may move up to tens of pixels from their correct position. The most well-known types of distortion are the radial and the tangential distortion. The radial distortion moves the location of a pixel in the direction of the radius from its correct position, either towards or away from the image center. The tangential distortion moves the location of a pixel in the direction perpendicular to the radius. Typically, wide angle lenses have a greater radial distortion than normal lenses, which can easily be noticed in the border areas of the images. As a result, straight lines are heavily curved. Although the distortion of normal lenses is not as easy to recognize visually as that of wide angle lenses, in normal lens images pixel locations may deviate several pixels from their correct position. Distortions known as the affinity and the shear describe the deviations of the image coordinate system with respect to the orthogonality and the uniform scale of the coordinate axes. Eventually, the exact deviation of pixels is determined by how the lens distortions map on the imaging array. Thus the exact deviation depends also on the size and the resolution of the imaging array. Distortions may originate from many reasons.

The lens plane of the camera objective is not exactly parallel with the imaging array of the camera, there may be inaccuracy in the lens grinding or some of the objective lenses deviate from the optical axis due to manufacturing error or inaccuracy. Positioning may have been changed, for instance, when the camera or the objective is clacked or exposed to vibration. In order to take into account all these distortions the camera system must be calibrated.

The camera system is calibrated in a field test by placing a calibration target with known dimensions in the field of view. Typically, the target is a planar grid, a checker board pattern or a pattern of round targets with known distances and sizes. In calibration the target is imaged in various positions, either moving the calibration pattern or the camera system. The distance between the camera and the calibration target is chosen approximately the same as the imaging distance in the measurement application. As the correct measures of the calibration target are known, the distortion errors can be computed. The camera system must be calibrated only once for static imaging setup. Of course, the constancy of the imaging setup should be verified frequently.

The purpose of the camera calibration is to determine the geometric camera model described by the parameters of interior orientation. The most important parameters are the image coordinates of the principal point, the principal distance and the function parameters of deviations such as those of radial distortion, tangential distortion, and the affinity and shear of the image coordinate system [81]. In the ideal case the principal point equals to the image centre. The principal distance is the distance between the principal point and the perspective centre that in the ideal case equals with the focal length.

If we know coordinates of n corresponding points in the world coordinates, which in the case of this thesis are the coordinates of corner points of the squares in the calibration target, we obtain n linear equations describing the model point coordinates M_i and its image coordinates m_i:

$$sm_i = A[R \quad t]M_i \qquad ,i = 1,2,...n \tag{1}$$

A is the intrinsic camera matrix including the coordinates of the principal point, the scaling factors of the coordinate axes and the parameter describing the skewness of the two axes.

The rotation parameters in the vector R and the translation parameter t are called the extrinsic parameters which relate the world coordinate system to the camera coordinate system. s is an arbitrary scale factor for image point m_i in the camera coordinates.

Camera calibration is an optimization problem in which the camera and the distortion parameters are determined. The set of the linear equations can be solved e.g. by using the method of least squares.

One of the first studies of the modeling of the tangential and the radial distortions in close range camera applications was presented by Brown [11] in 1971. He imaged seven plumb lines hanging vertically in the field of view and rotated the camera 90˚ to obtain straight lines for calibration of both the vertical and the horizontal direction. Tsai [145] introduced a camera calibration technique to 3D machine vision using TV cameras in 1987. In 1999 Zhang [163] presented a flexible technique for camera calibration, in which planar calibration pattern was imaged in various positions. Clarke [20] reviewed in 1998 the comprehensive historical study of camera calibration.

Calibration procedure described above is implemented in the Camera Calibration toolbox for MATLAB® developed by Jean-Yves Bouguet, and it is available in public domain [10]. The camera calibration software is based on and inspired by Zhang's [163] article. However, the intrinsic camera model differs from Zhang's solution and is based on an article by Heikkilä and Silvén [55]. The calibration target is imaged in various positions. Then images are read in the calibration software. Software is semi-automatic in that the user has to provide some data, including the four extreme corner locations of the calibration pattern and the size of the checkerboard pattern chosen for each image. With the four extreme corner locations given the calibration software locates the corners of all squares of the checkerboard more precisely. Calibration software produces the error parameters of the camera system with which the images can be corrected. The procedure of camera calibration is computationally heavy.

We calibrated our camera system with test field calibration and we used a checkerboard calibration target presented in *Figure 18*. The size of each square is 20.0mm × 20.0mm. The reason for the choosing the checker board calibration target was that the free and adequate Bouguet's MATLAB® calibration implementation available in the internet is based on that target.

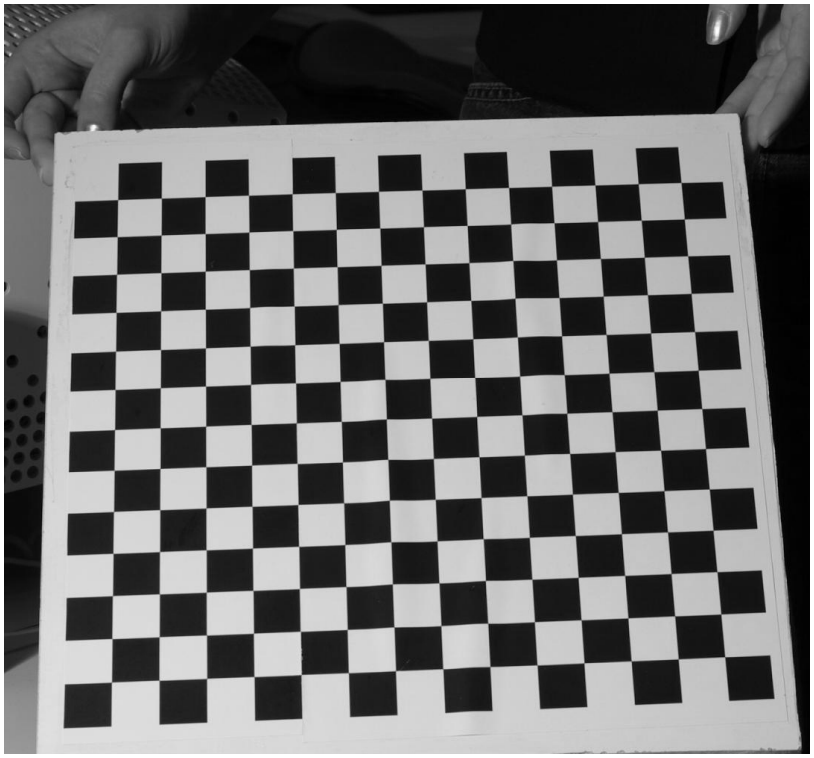

Figure 18. The planar checkerboard calibration target that is used in the camera calibration of the research. The size of each square is 20.0mm x 20.0 mm.

4.2.2 Scale calibration

Digital images consist of pixels. Thus image based measurement systems produce pixel distances and values as their primary measures. However, the measurement systems are often required to produce measurement data in real world distances, e.g. in millimeters. Thus pixel distances have to be converted to the real world distances. This procedure is called the scale calibration.

If the object is planar and perpendicular to the optical axis of the camera, at least one real-world distance is needed in the measurement setup to make the scale calibration. It may be the distance between the camera lens and the object to be measured or a known distance in the image. In the method development of this thesis work, the cross section surface of the log or board was assumed to be planar and perpendicular to the optical axis and thus parallel with the imaging sensor of the camera.

If calibration is based on the distance between the lens and the object, the distance can be measured for instance with a laser based distance measurement device installed in the same

setting with the camera, or with stereo imaging. Laser distance measurement in three or more points allows detecting if the planar object is perpendicular to the camera or not. This can be detected also with a calibration target, if the target is in the same plane with the object.

In this study the scale calibration was made with calibration targets attached to a background board. Targets of known dimensions were approximately at the same distance from the camera as the log or board end surface. The targets should be placed on both vertical and horizontal edges in the image of the log or the board end surface, so that deviations from perpendicular set up can be detected.

The calibration procedure is simple: software seeks automatically, e.g. with image correlation, two known points, the corners of two extreme squares or the centers of circles for instance and then counts the pixels between the points. It does not matter if the line between the two points is not exactly vertical or horizontal. The correct calibration for pixel size to real distance is obtained with the Pythagoras' theorem. In laboratory environment, the calibration targets are the same from image to image, and only the object is changed. Thus seeking for the two known points can be restricted to very small areas. *Figure 19* shows two arrangements of calibration targets for the scale calibration. In *Figure 19 (a)* there is the checker board calibration grid on three sides of the image. Each square is 20.0 mm × 20.0 mm and thus the 18 squares in the vertical direction makes 360.0 mm. In this case calibration procedure seeks the furthermost corners of the squares The corners of the squares can be located quite precisely in the image when the print quality of the target is high. The number of pixels between two furthermost corners in the same row is counted, and after dividing it with the known real distance in millimeters, the dimension of a pixel is obtained in millimeters. Several estimates for pixel dimensions can be obtained from the various locations of the image. If the pixel dimension estimates differ from each other, the camera orientation is not correct or the camera calibration has not been completed properly.

Figure 19 (b) shows the calibration targets with black circles. The diameters of the black circles and the distance between two adjacent circles are both 10.0 mm. The center of the circular calibration targets is quite simple to locate, even if the object and the calibration targets were in a steep angle to the camera, by fitting an ellipse to the circle distorted by perspective. After the scale calibration, the calibration targets are left out from the further image processing.

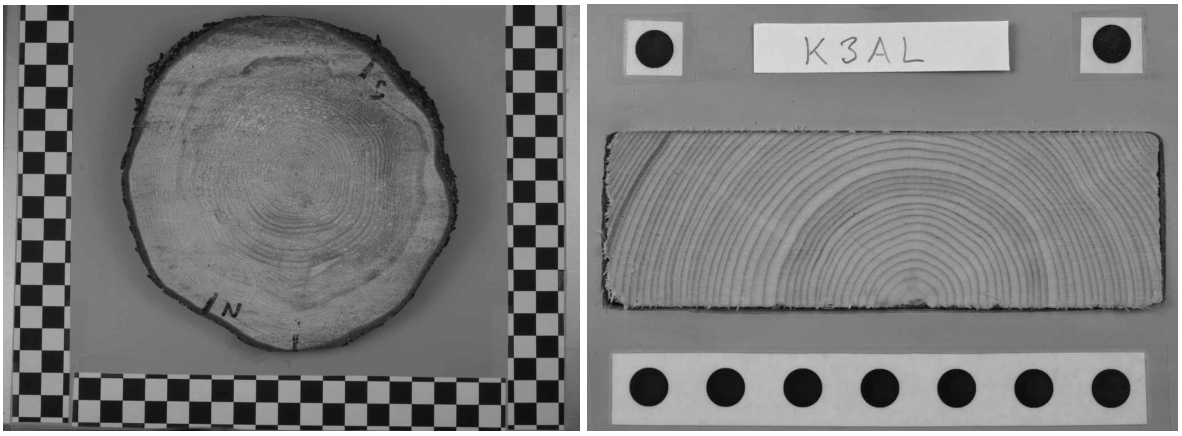

Figure 19. The examples of calibration targets. (a) shows the checkerboard calibration targets around the sample and (b) the circular calibration targets. The dimensions of the targets must be known.

In full log and board imaging it may be complicated to keep the distance between the camera and the imaged surface with the calibration targets constant. If the object is not in the same plane with the calibration targets, the scale calibration is possible only with an active distance measurement. However, the pixel size in millimeters as the function of distance must be known in advance. This function can be obtained experimentally or from camera specifications for the cameras with fixed focus. We tested such a system for full logs with a single point based laser distance measurement device.

4.2.3 Color calibration

Color calibration is required whenever absolute or relative color is used in the measurement. Color calibration corrects errors caused by an uneven or variable lighting within an image or between images. If we have a constantly colored object but the lighting intensity or the spectral content is varied in location or in time, the color appears variable to the camera sensor, too. This causes obvious problems in the image analysis based on colors. Varying intensity or spectral content can be compensated with the color calibration. However, in the case of lighting with a narrow band of wavelengths e.g. red, the change to lighting with another narrow band of wavelength light, e.g. blue, cannot be corrected with the color calibration discussed in this section.

Most system cameras at consumer markets, such as the ones in this work, are highly automated. If the object is dark, the camera adjusts image colors automatically. Such automated actions must be bypassed in the color measurement. The industrial machine vision cameras are not automated and thus they are easier from the point of view of color calibration.

Color is calibrated with a color map of a reference target. The color map may have some pure colors and gray levels from white to black. A reference target with a color map shown in *Figure 20* was used in the research. Ideally, the white surface reflects all wavelengths to the camera sensor and, respectively, black surface does not reflect any wavelength. The number of photons the sensor receives determines the detected color brightness level. Brightness is adjusted with the exposure time of the camera. However, saturating the sensor element at white regions, the overexposure, must be avoided.

Figure 20. The image shows color calibration reference targets on both sides of the wood sample disc. The targets can be used both scale and color calibration. Note the heavy shadows around the disc, because straight lighting is used instead of diffusing umbrellas.

In this work, rot analysis described in Subsection 6.3.4 is the most critical one to proper color calibration. Rot analysis compares colors of wood samples from image to image. The

color calibration was made for raw images with color calibration reference target setting shown in *Figure 20*. Only shades of gray were used. The outermost columns of squares in the color calibration reference target have squares with black, white and different gray shade colors. The white square represents 100% of color and black square 0%. The gray shades were determined to be 25%, 50%, 75% and 87.5% of full white. It was assumed that the gray shades reflect red, green and blue light in proportions corresponding to the percentage of the full white. In each image the mean colors of the squares were evaluated automatically by determining the region inside the square, and then averaging out the values of pixel intensities. The reflected red, green and blue light were measured from all the squares of gray shades.

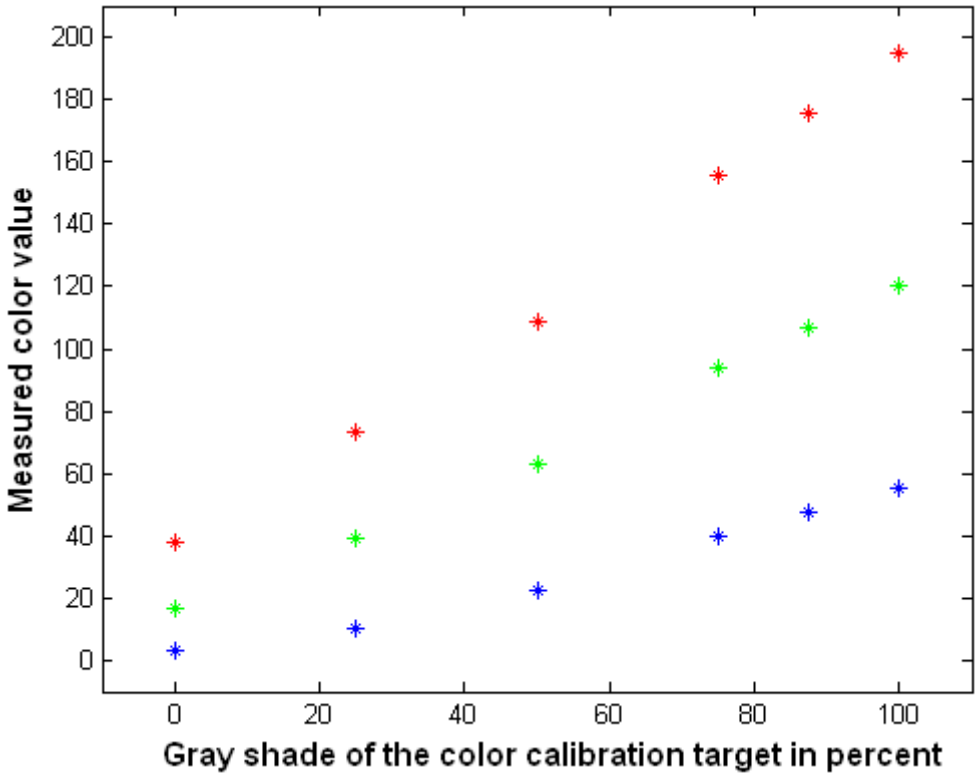

Figure 21. The diagram shows 8 bit values measured by the camera for the gray shades of the color calibration target on red green and blue image channel.

An example of a color calibration data is shown in *Figure 21*. The response to gray shades is approximately linear at all color channels as the imaging sensors are linear to the number of photons. When a photon of visible light wavelength interacts with the silicon material of the imaging sensor, the photon generates one free electron by the photoelectric effect [63]. Image enhancement algorithms such as the gamma correction, are not applied in the raw

image, and thus linearity holds quite well. After the response was found to be close to linear in all cases studied in detail, the two point calibration practice based on full white and 50% gray was adopted. This was adequate in this work, but of course the accuracy of calibration can be improved with a larger data set and by estimating the parameters of the linear relationship with the least mean squares algorithm.

However, most image analysis methods developed in this study are based on texture analysis methods. Thus they are only weakly dependent on color variations and typically do not need the color calibration.

5 Selected Image Analysis Methods

This Chapter discusses the pre-existing and widely applied digital image analysis procedures applied during this study. The Section 5.1 describes shortly local image analysis. Conventionally the image analysis procedures have been applied to the entire image, i.e. globally. During the past decade, the increased computational power has facilitated efficient local analyses of images. An image is analyzed in small regions and the information at each region is combined to form information about the entire image. In this study local analysis of digital images is based on the moving window method.

The majority of the machine vision applications in this study are based on the analysis of image intensities. The object of the gray scale image analysis system was a single channel image. The channel values were 8-bit intensity data thus ranging from 0-255. Later the color image analysis with three color channels (red, green, blue, RGB) has become the mainstream approach. Thus, the Section 5.2 describes shortly the color analysis methods used during this study. A short discussion on the global thresholding methods is included, because threshold methods have been the most common procedures in image analysis throughout all the application fields. The Chapter also discusses RGB image conversions, such as hue, saturation, intensity conversion (HSI). Principal component analysis (PCA) divides the variation into uncorrelated components so that the analysis may concentrate on the ones with highest variance. Thus the PCA of the RGB color channels can be considered as a color space conversion: the maximal covariance of R, G and B color channel components is the score image of the first PCA component.

Texture analysis methods have been applied extensively in the recent years. This is because computational power has increased radically and the methods are robust. Texture analysis methods are quite insensitive particularly to variations in lighting. The core methods of this study are based on textures. Section 5.3 discusses texture analysis. Fast Fourier Transform (FFT) with the Hanning window was applied extensively during this study as the basis for all the other texture-based methods. FFT was found very efficient in producing most of the

information required during this study, including the cases in which images were of poor quality due to unprepared samples or uneven lighting.

When the moving window is combined with the analysis routines, it produces effective analysis tools for wood cross-sectional image analyses. The most important combination during the research was with the Fourier transformation, but we used the moving window also together with PCA on color channels. The moving window was chosen for the analysis of the entire cross section surfaces due to the fact that local analyses are typically more robust than the global ones against variations of lighting within and between images. As the annual ring pattern has locally a periodic texture, FFT is a rather natural approach to analyzing the pattern. Image conversions HSI, PCA and global thresholding are rather supporting methods in algorithm implementation.

5.1 Moving window method

Global texture analyses are typically useless if the textural properties are not homogeneous throughout the object. The log end images analyzed in this study are examples of images with an inhomogeneous texture. Thus the images had to be analyzed locally in small regions. The simplest approach is to divide the image into smaller regions and to analyze them one by one. The moving window method allows the local regions of image overlap and produces smoother results. However, as a larger number of regions are analyzed, the moving window method is slower than that of simple division of the image into non-overlapping regions. Smoothness can be traded off to computation speed by selecting the overlapping of the regions analyzed, or equivalently the moving window step.

In this thesis the moving window analysis was carried out with rectangular windows. The result of the analysis of a window was associated to the location of the centre of the window in the result matrix and thus result image was formed.

The size of the moving window and the move step between consecutive windows are the parameters of the moving window approach. The content of the original image sets the restrictions to the parameters. The size of the window is a compromise between the accuracy and the spatial resolution of the results. The resolution of the image has the highest effect on the window size: the more pixels in the original image, the more pixels can be chosen to the

moving window when studying texture variation at a given real spatial resolution. In this work, the cameras had 3.1 - 12.7 mega pixels. The log cross sections were imaged approximately from distances of 130 -150 cm, and the board cross section surfaces from about 40 cm. The window sizes ranging from 200×200 pixels to 20×20 pixels were studied. For example, the window size of 51×51 pixels was chosen for the analysis methods based on the Fourier transformation and the power spectrum for images taken with 3.1 mega pixel camera from log cross section surface. Due to shorter imaging distance and better camera resolution images on cross section surfaces of boards required a larger window, such as 101×101 pixels, to cover a similar texture pattern. The number of the vertical and the horizontal pixels of the moving window was chosen odd, so that the center of the window to which the window result is associated with, is a pixel position of the original image. The moving window size for PCA based color analysis was chosen rather small, only 40×40, because PCA was applied to increase the contrast. Here the window size may be either even or odd, because we inserted the entire window (or the center part of it in improved version of the algorithm) after contrast improvement and thresholding to the result matrix.

Figure 22 shows a window of 101×101 pixels. The moving window should be larger than the largest variation scale we are attempting to capture. For the annual ring analyses the window size should thus be larger than the thickest annual ring within the cross-section of the board or the log to be analyzed. When studying periodic local image properties, the area of the window should cover at least two periods of texture, i.e. two annual rings in the case of wood images. The window may cover various periods of texture without problems in the further frequency analyses. *Figure 22* shows a moving window passing the widest annual rings in the image of cross section surface of a board.

The move step size between consecutive windows affects strongly the computation time and the resolution of the result matrix. If the move step is large, the local parameters are evaluated only in few areas within the original image. A locally sparse low-resolution result matrix is obtained, but in a short computation time. Anyhow, the results obtained from single window can be precise, but they are only obtained from fewer locations. With short move step the resolution of the result matrix is high but the computation time is much longer. We have experimented with the window move step ranging from one pixel to two hundred pixels when the image size ranged from 3.1 megapixels to 12.7 megapixels.

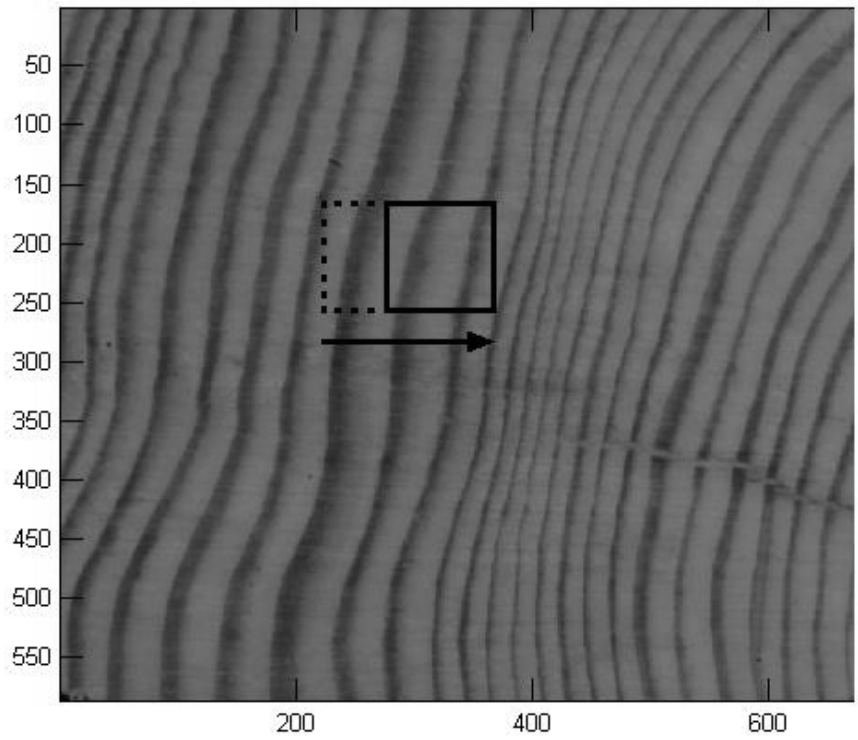

Figure 22. 101×101 pixel sized moving window sliding across the image of a prepared board cross section. The size of window is chosen larger than the widest annual rings.

5.2 Color analyses

Color analyses are based on the pixel intensities of the red, green and blue color channels that the imaging sensor of the camera detects. Because the exact values of pixel intensities are significant in the color analyses methods, the variation of lighting has to be taken into account. The detected channel intensity in the same region of the object changes, if the spectrum, location or power of the lighting changes. Thus the color calibration plays an extremely important role in color analyses.

This section discusses color image processing methods applied in this study. Global thresholding is a common algorithm for segmenting and binarizing the image. Conventionally, thresholding has been made for the RGB-images. However, new options of thresholding may open if the RGB color space is first converted to another color space. The HSI conversion of the RGB images was applied in the research. The HSI conversion is discussed more detailed in Subsection 5.2.2. PCA was applied also to RGB image and it is reviewed in Subsection 5.2.3.

5.2.1 Global thresholding

Thresholding is a simple image processing method with its roots in one dimensional signal analysis. Image thresholding has been applied widely from the very beginning of image analysis. For instance, Weszka [156] presented the histogram based thresholding already in 1974, Gonzales and Winz [46] in their book in 1977 and Otsu [110] presented an automatic thresholding method based on histogram in 1979. Thresholding is a segmentation tool based on the pixel intensities of the image and it binarizes the image. Conventionally, thresholding has been made for the 8-bit gray scale images. As the spatial resolution of the camera sensors has increased sufficiently for the color camera applications, thresholding the color channels has become a regular function in image analysis. The thresholding level is chosen either manually or automatically on the basis of the histogram of color channel data. Global thresholding means finding a single threshold for the entire image whereas local thresholding finds the threshold for small regions of the image and thus the level varies through the image. Global thresholding is problematic if the lighting is uneven. Even if the image is taken in uniform lighting, a given real color may appear darker in the corners than at the center area. This defect is called vignetting. When imaging a uniformly white paper, the changes of the 2D intensity profile can be evaluated. This imaging information eases thresholding in constant imaging settings.

Figure 23 (a) shows the red channel information of an example image and *Figure 23 (b)* its histogram, where the x-axis presents the 8-bit intensity value ranging from 0 to 255 and the y-axis shows the number of pixels having the intensity value. Thus the sum of the histogram values equals the number of pixels in the original image. The thresholding level is rather easy to choose. The result of the segmentation is typically better, if the histogram has two or more clear peaks, such as the peak for black at low intensities and the peak for white at high intensities in the histogram in *Figure 23 (b)*. However, there is also a smaller peak in the histogram between the main peaks of black and white. This corresponds to the gray regions in the background of the checker board in the original image. The effect of uneven lighting can be noticed clearly in the intensities of the white squares in the histogram: they are spread between intensity values of 140 and 200. This demonstrates that correcting the unevenness in lighting is important in global thresholding. The horizontal line in the histogram shows a possible global threshold.

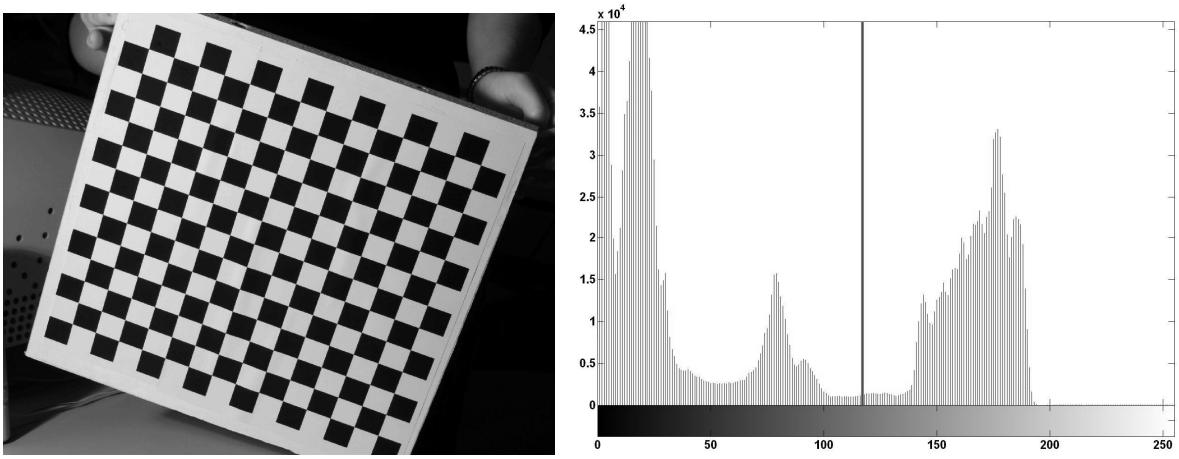

Figure 23. (a) The red channel of a checker board image and (b) its histogram. The horizontal line denotes possible threshold.

The RGB-image must not be thresholded directly, but each channel may be thresholded individually with channel-specific thresholds. The channel having the highest contrast for the property of interest is the most informative and is chosen for the thresholding in the RGB color space. Alternatively, the R-, G- and B- channel information can be combined into one channel image with color space mapping such as the gray scale intensity image of the original RGB-image and then thresholded. The combination can be made after the thresholding of all the channels as well, in which case the binary information originated from the three color channels is combined with e.g. logic operations. The automation of the thresholding can be based on Gaussian Mixture Models (GMM), with expectation-maximization (EM) algorithm [9]. If the clear peaks are not present in the histogram, proper threshold level is very complicated to determine automatically.

5.2.2 HSI color space

HSI color space is an alternative to RGB. In some applications, particularly when segmenting colorful objects from gray background, HSI is the preferred choice. The RGB color space is converted to the HSI color space with simple computation. The HSI model has also three components, the hue, the saturation and the intensity. The hue component, H, is an attribute that describes the pure color component in the pixel, the saturation component, S, describes how much white color is diluted into a pure color. Full saturation S = 1 means no dilution with white color. The intensity component, I, describes the gray scale information of a color image.

For an image in RGB format, the hue component of each RGB pixel is obtained using the equation

$$H = \begin{cases} \theta & if \quad B \le G \\ 360 - \theta & if \quad B > G \end{cases} \tag{2}$$

where

$$\theta = \cos^{-1}\left\{ \frac{\frac{1}{2}\left[(R-G)+(R-B)\right]}{\left[(R-G)^2+(R-B)(G-B)\right]^{\frac{1}{2}}} \right\} \tag{3}$$

The saturation component is given by

$$S = 1 - \frac{3}{(R+G+B)}\left[\min(R,G,B)\right] \tag{4}$$

The intensity component is the mean of all RGB components

$$I = \frac{1}{3}(R+G+B) \tag{5}$$

Here it is assumed that the RGB values have been normalized to the range [0, 1], and that angle θ is measured with respect to the red axis of the HSI space. [47][48]

For the pure main colors and their combinations, for example bright red, blue, green, yellow, cyan and magenta, the hue is easy to evaluate visually, because these colors are not diluted with white color. The hue component is sensitive to the smallest of tint of a color, e.g. in the near black, gray or white region, though such color cannot be perceived by the naked eye. Thus the hue value is independent of the intensity and dilution with white color. The saturation component for white, gray and black regions is zero, because they are fully 'white' colors, but with different intensities. This property can be utilized by choosing black, white or gray as the background color. Then the bright colored object is easy to segment according to saturation. If some part of the image receives considerably more light than others, the colors in the lighted area appear to be brighter, and the saturation component can again be used in segmentation.

5.2.3 PCA for RGB-Image

Principal component analysis (PCA) is a well-known and widely-used data analysis method [60][64]. PCA arranges the data of several variables into their linear combinations, the principal components, so that the components are not correlated. Principal components are determined by diagonalizing the covariance matrix $\boldsymbol{\Sigma}$ and they are ordered according to their contribution to variance: the first principal component has the highest amount of variance presented by the first *score*, the second principal component has more variance than the third component and so on. The number of principal components is the same as the number of original variables. In many cases, the few first components describe the majority of all the variation and the rest of components can be neglected. Thus PCA is commonly used to reduce the number of variables with the minimum loss of information. The *loadings* of a principal component are the coefficients of variables within the linear combination forming the principal component. The *loadings* describe the contribution of each original variable.

It can be shown that the eigenvector that corresponds to the largest eigenvalue of the covariance matrix, maximizes the variance and the maximized variance is the eigenvalue:

$$\max_{\boldsymbol{\beta}} D^2(\boldsymbol{\beta}'\mathbf{x}) = \boldsymbol{\beta}_1'\boldsymbol{\Sigma}\boldsymbol{\beta}_1 = \lambda_1 \qquad (6)$$

where D^2 is the variance, x is data, λ_1 is the largest eigenvalue of the covariance matrix $\boldsymbol{\Sigma}$ and $\boldsymbol{\beta_1}$ is the corresponding eigenvector. The expression $\boldsymbol{\beta_1'x}$ is the linear combination which has maximal variance, and hence $\boldsymbol{\beta_1}$ is the loadings vector of the first principal component

The score vector of the first principal component of data $\boldsymbol{x}$, is

$$y_1 = \boldsymbol{\beta}_1'\mathbf{x} \qquad (7)$$

In order to obtain the second principal component, the part described by the first principal component is projected out. It is made by setting the covariance between the first principal component and the linear combination to be zero:

$$Cov(y_1, \boldsymbol{\beta}'\mathbf{x}) = \boldsymbol{\beta}_1'\boldsymbol{\Sigma}\boldsymbol{\beta} = 0 \qquad (8)$$

The linear combination of the data, that has the maximum variance, but is uncorrelated with the first principal component, is sought.

$$\max_{\boldsymbol{\beta}} D^2(\boldsymbol{\beta}'\mathbf{x}) = \boldsymbol{\beta}_2'\boldsymbol{\Sigma}\boldsymbol{\beta}_2 = \lambda_2 \qquad (9)$$

where λ_2 is the second largest eigenvalue of the covariance matrix $\boldsymbol{\Sigma}$ and $\boldsymbol{\beta_2}$ is the corresponding eigenvector.

The score vector of the second principal component of data $\boldsymbol{x}$ is

$$y_2 = \boldsymbol{\beta}_2'\mathbf{x} \qquad (10)$$

The remaining principal components are obtained in a similarly by projecting away the contributions of the identified principal components and then maximizing the remaining variance. The result is that the loading vectors are the eigenvectors of the covariance matrix arranged in the order of ascending eigenvalues.

PCA was applied in this study to enhance the contrast of images, in particular for segmenting the annual rings and the early/latewood regions. As a pixel in a digital color image has three variables, PCA results in three principal components. All pixel values of principal components, i.e. *scores,* can be presented as an image so that the first score image provides the strongest contrast and hence typically the best information for the further analyses. The score images of the other components may offer useful information as well, e.g. about noise. If the loadings of the first principal component are equal, the first PCA component is reduced to the average value of the color channels. For RGB images, this may occur if the spectrum of lighting is uniform so that RGB components are fully correlated.

5.3 Texture analyses based on Fourier transforms

The major advantage of the texture analyses is that the methods are less sensitive to color and lighting variations than color based methods, and thus robust. In particular, the results of

texture analysis do not depend on the absolute color pixel values, but only on the distribution of the intensity over the image, most notably on differences between the neighboring pixels. Because the main wood quality measurements developed in this thesis are based on texture analysis, and hence do not require color calibration, they are easier to implement in practice. All the texture analysis methods in this study are based on the two-dimensional Fourier transformation.

5.3.1 Two-Dimensional Fourier transform and power spectrum

Any function satisfying quite loose regularity conditions can be expressed as a weighted frequency integral of the sine functions. The Fourier transformation provides the complex-valued weighting function consisting of the amplitude and the phase. The d-dimensional Fourier transformation of function *f* is a continuous integral transformation defined as

$$F(u) = \int_{-\infty}^{\infty} \dots \int_{-\infty}^{\infty} f(x) e^{-j2\pi ux} dx_1 \dots dx_d \qquad (11)$$

A two-dimensional signal on a finite size grid is continued periodically to the 2D real number plane. The integral is then replaced by sum over a discrete set of frequencies. This results in a Fourier series, the discrete Fourier transform (DFT). The DFT of a 2D function *f(x,y)* sampled on a rectangular grid of size M×N (an image) is given by

$$F(u,v) = \frac{1}{MN} \sum_{x=0}^{M-1} \sum_{y=0}^{N-1} f(x,y) e^{-j2\pi \left(\frac{ux}{M} + \frac{vy}{N}\right)} \qquad (12)$$

The DFT is computed efficiently by using the fast Fourier transform (FFT) method. The FFT is much faster than the transform calculated directly from the definition. The FFT is at its fastest when the dimensions of the sampling grid are integer powers of 2. [47]

The Fourier transformation has real and imaginary parts. The Fourier spectrum is determined to be the absolute value of the Fourier Transform *F(u,v)*.

$$|F(u,v)| = \sqrt{R^2(u,v) + I^2(u,v)}\,, \qquad (13)$$

and the power spectrum is the Fourier spectrum squared

$$P(u,v) = |F(u,v)|^2 = R^2(u,v) + I^2(u,v) \qquad (14)$$

Here *R(u,v)* is the real and *I(u,v)* the imaginary part of *F(u,v)*, respectively [133][47]. Both spectra provide information about periodic variations as peaks.

FFT assumes that the signal extend to infinity. Because the image signal is finite, any points of discontinuity at the image edges produce in periodic continuation unwanted frequencies to the spectrum. This effect can be reduced by windowing. Windowing means multiplication of the image with a weighting function that is typically zero at the edges and one at the image center. However, windowing spreads the spectrum peaks. Windowing reduces the information obtained from the sample edges. The two-dimensional Welch spectrum estimate [155][16] is an efficient tool for identifying textural structures in images in which there is an irregular component in addition to the textural component. The Welch estimate increases the reliability of the 2D spectrum estimate by calculating the sample spectrum estimates from a larger 2D signal and then calculating the mean of the estimates. Averaging the samples reduces the noise in comparison with the original spectrum and the low frequency trends are removed, but the frequency resolution is also reduced. Thus the image area to be transformed is first divided into subareas each multiplied with an appropriate windowing function, the Hanning-window in this study. The size of the subareas, the choice of windowing function and the overlap of subareas are design parameters of the methods. The size of subarea determines the frequency resolution. Overlapping produces more samples for averaging, but increases the computation time. Overlapping can be used also to fit windows of fixed size in the original image so that the last window does not cross the image edge.

For Welch spectrum estimate, the image analyzed is assumed to be large enough, so that it is meaningful to divide it further into smaller sample images, whose dimensions are in the powers of 2. Typically the original image should be larger than 256×256 pixels depending, of course, on the frequency in the texture pattern. The sample images overlap by a fixed amount, e.g. 50%, both in x- and y-direction, except close to the edges, where the selection

of sample images is more constrained. If the original image is smaller than 256×256, the straight FFT is calculated without Welch estimation and the spectrum estimate is noisier. The power spectrum is scaled so that its sum is the variance of the original image.

MATLAB® has built-in functions for the 2D-spectrum estimation with fast Fourier Transform, but Welch estimate of power spectrum is computed with the general-purpose MATLAB® toolbox, implemented in our research group but not in this work.

5.3.2 Local texture analysis based on 2D spectra

The 2D-spectrum of the entire digital image does not offer information about the possible local variations within the image. The local variations can be analyzed by dividing the entire image into several, possibly overlapping windows so small that the variation within each of them can be considered stationary. The chosen size of the window depends on the resolution of the original image. The window should be large enough so that at least two periods of the lowest local frequency are captured in it both in x- and y-direction. The more similar the periodic variations within the local image the clearer is the dominating spectral peak. The window should be chosen small enough so that it represents still local – rather than global – variations. However, it is favorable if more than two periods of the slowest local variation are within the window, so that Welch spectrum estimate can be fully utilized.

The resolution of original images taken in the early phase of this study was poor in comparison to present-day cameras. Thus dividing the window image first to local areas and further to subareas for Welch estimation was not feasible. However, the Welch estimate is discussed, because the resolution of the images increases continuously, and thus subarea size for the Welch method respectively. The direct FFT calculation offers still sufficient frequency estimates for all the FFT based methods presented in the thesis, but with higher resolution images their reliability can be increased with the Welch method.

Figure 24 illustrates the local texture analysis scheme by using the Welch spectrum estimate of 2D FFT in the moving window. The original image is first divided into local images in which the variation is assumed to be stationary and characterized by a single frequency and its harmonics. The local frequency and orientation are analyzed by calculating the Welch spectrum estimate for the local window. In order to get this estimate, the local image has to

be further divided into overlapping subareas. These subareas have to be large enough to hold at least two periods of the dominant periodic variation.

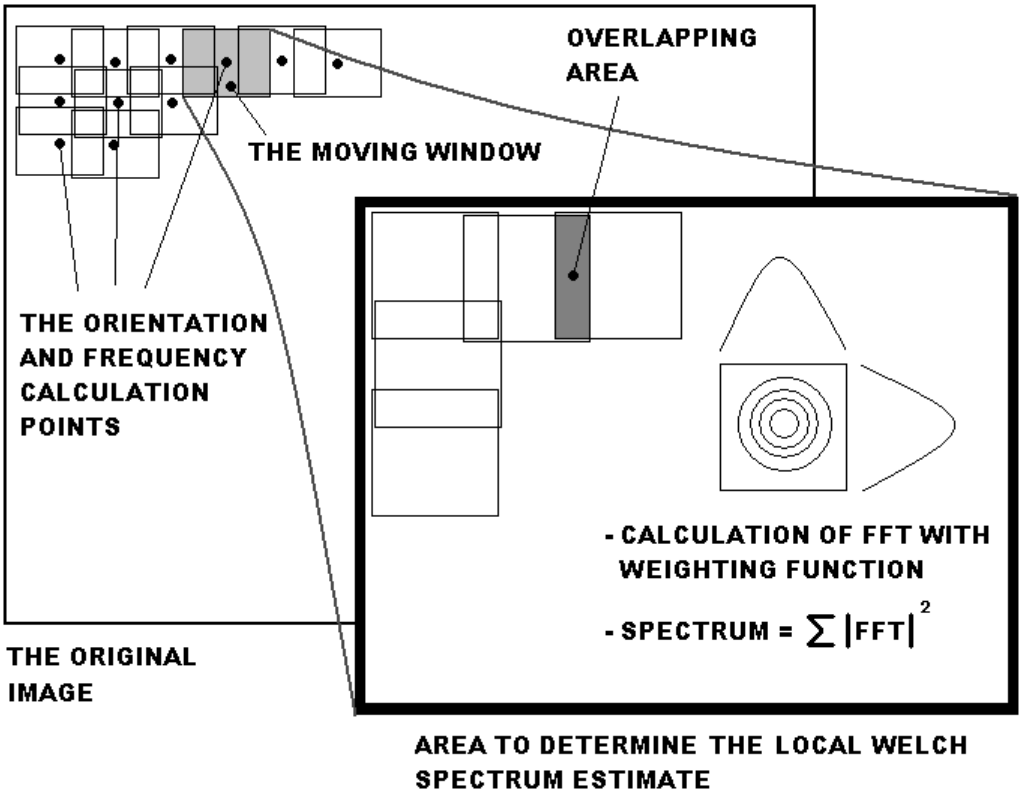

Figure 24. The scheme visualizes the calculation of the 2D Welch spectrum estimates in the moving window.

In this study, we are interested in images that can be described locally with a single frequency with possible harmonics. The dominating peak of the power spectrum is characterized by its amplitude and location. In the 2D- power spectrum, the location of the largest amplitude gives the location of the dominating frequency. Furthermore, we are not interested so much in the exact amplitude but more its location vector $k = (u,v)$ in the spectrum. The magnitude of k at each point (x,y) in the original image gives the frequency field, to be denoted as $\omega(x,y)$. The direction of k gives the orientation direction field $\varphi(x,y)$. However, the amplitude and the sharpness of the dominating spectrum peak may be used for evaluating the reliability of the measured single frequencies or orientations.

To implement a practical method for estimating the local power spectra across the original image, we have to specify the parameters of dividing the original image. At first the size of moving window was chosen based on the resolution of the image and texture in the image.

The power spectrum is calculated as described above and the local texture parameters determined from the location of the dominating peak in the spectrum are associated to the centre of the current window. The moving window moves across the original image generating local textural information, in particular frequency and orientation of the dominant local periodic variation. These are collected into the result matrices. If a resolution of the result matrix is required to be that of the original image, the step size when moving the window is one pixel. In the pixels that are closer to the edges than half of the dimension of the moving window, a part of the window crosses the original image edge. There are two possibilities to deal with this situation: the texture parameter values in the border areas are not computed, and the resulting matrix is smaller than the original image, or the area surrounding the image is filled with synthetic data, e.g. with zeros, mean values, held values or reflections of the image. We chose the first option and simply ignored border areas, because in our study there were no distinct frequencies of the log or board end area, nor information needed. In most cases border area includes background data only, so that the texture needs not to be analyzed there.

Depending on how slow the variations in the spectral properties are, it is not always necessary to evaluate the spectrum around every pixel. In images, such as 1800×2000 pixels, evaluation in e.g. every tenth pixel both in x- and y-direction is sufficient, with obvious hundred-fold speed up in computation. Respectively, the resolution of the frequency and the orientation result matrices is reduced to one tenth. However either as such or as interpolated it satisfies the requirements in most of the wood quality evaluation in this thesis.

6 Measurement Methods Developed

This Chapter presents measurement algorithms developed for quality and geometry evaluation of wood. The methods are applied to the cross section images of round wood and boards, with examples of both application cases. The images for the analysis methods discussed in this Chapter have been taken in a laboratory environment. However, the goal during the research work has been in developing a methodological basis for industrial applications. The methods developed are mainly based on texture analysis because of their robustness and because they can be applied to images of rather rough cross section surfaces of wood, in which the annual ring pattern is barely visible. The methods based on texture analysis perform well without further preparation for the surfaces sawn with a sharp chain saw. The chapter also discusses some methods based on geometry and color analysis. However, such methods require a better quality cross section for imaging. Thus they require a sharp cutting equipment and possibly further preparation in industrial applications. Wetting is a simple way to enhance the cross-section surface for image analyses and washing also removes dirt and small particles. The color and geometry based methods often require color calibration before analyses.

The texture based algorithms described in the Chapter are:

- **Thickness field of annual rings**, which gives annual ring width information across the cross section surface. Logs can be sorted in piles with the ring width information when cutting forests. The annual ring width information can be used in optimization of sawing and veneering. After sawing and veneering the resulting sawn timber and plies can be sorted according to the annual ring width. The annual ring width correlates with wood density, that is e.g. a desirable pulp property [8] [140]
- **Orientation field of annual rings**, which gives annual ring orientations in cross section surface. In industry this property has rather low significance as such, but the algorithm creates a basis for further methods.

- **Defect detection** is based on the previous algorithms and it reveals areas without clear periodic content in cross section surface. After defect detection incorrect information can be omitted in other methods.
- **Locating the pith,** that provides the growth center of the tree. Pith deviation from geometric center reveals the eccentricity of wood. Pith location can be used in veneering and in sawing optimization. Eccentric wood cross section surface is often a sign of compression wood in trunk [67]. Pith location is also a prerequisite for some later algorithms.
- **Board side and curvature detection** reveals the inner and the outer side of a board and the curvature of annual rings in a board. The curvature of annual rings correlates with board deformations during drying. Board side detection allows the packing of boards same side up.
- **Counting the annual rings** provides the number of annual rings visible in cross section surface. This reveals wood age that is a log quality property. Annual ring number is connected with wood density through the diameter of the cross section surface or across a fixed path from pith.
- **Annual ring tracking** reveals single annual rings within cross section surface Annual ring locations could be utilized in peeling.

The algorithms based on geometry are:

- **Log end shape measurement** provides an estimate for cross section shape. The shape information can be used in peeling and sawing optimization.
- **Bark thickness measurement** reveals the bark content in the log, and hence the barkless volume.

The color based algorithms are

- **Early wood and latewood segmentation** reveals single annual rings and separates early wood and latewood
- **Global latewood proportion** provides an estimate of latewood content in wood. Latewood content correlates with wood density and strength. This information can be utilized in sawing and peeling. Products can be sorted according latewood content. Content of early and latewood affect also pulp properties [140].

- **Local latewood proportion** provides local estimates about latewood content in wood.

The Chapter also discusses the global thresholding and the measurement of the color of rot that are rather supporting methods. Typically, the implementation of the global thresholding method is highly connected to the application environment. The measurement of rot color supports the modeling of rot propagation that is researched outside the scope of this study.

The wood properties, for which measurement were developed, were chosen so that they can be measured from images, they are relevant for the forest industry, and they are today either missing or obtained only with high investments, as the gap analysis in Section 3.4 shows.

Section 6.1 presents the texture based algorithms, Section 6.2 the geometry based algorithms and Section 6.3 the color based algorithms,

6.1 2D-spectrum based methods

The basis of the methods discussed in this subchapter is the two dimensional Fourier power spectrum [47] discussed in detail in Chapter 5. In the case of log and board end images, we are interested in local variations within the cross-section surface. Obviously, the local variation originates from annual rings which carry quality information about wood. To analyze locally the whole log or board cross section, the 2D Fourier power spectrum was applied with a moving window method. This provides the annual ring orientation and thickness field at any location within the cross section. However, some of the methods e.g. the pith locating algorithm, require the frequency information only in few locations. Thus the moving window is not always the way to provide the local information, but the sampling for the analysis is to be chosen specifically to the application.

Figure 25 (a) shows an example with a moving window of 51×51 pixels crossing the entire image. *Figure 25 (b)* presents a magnified local window covering several annual rings. Window size is selected such that throughout the image at least two annual rings are in the window, but annual rings within the image still appear quite straight. This kind of image provides typically a single clear peak with harmonics in the 2D Fourier power spectrum.

Obviously, in the pith area the annual rings are not straight, and therefore the results are more difficult to interpret.

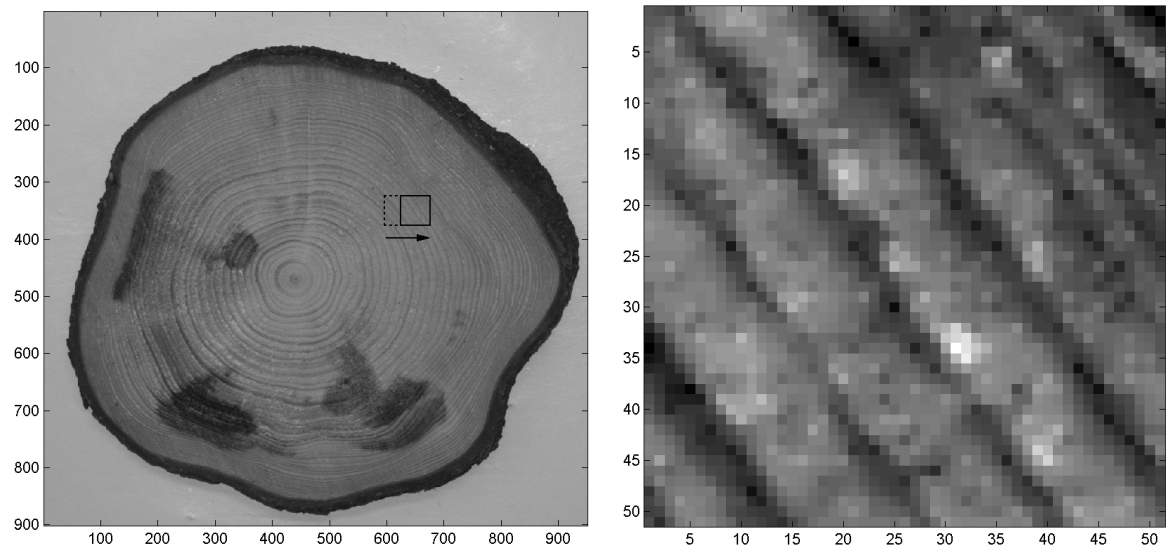

Figure 25. (a) The moving window is crossing the entire image. (b) shows a single window for 2D-spectrum calculation. The annual rings seem to be quite straight in the window. Images are in the pixel scale.

Figure 26 shows a window of size 101×101 pixels within a cross section image of wood. The annual rings within the window are slightly curved and the widths of rings are quite constant. The image is a rather clear single frequency field with harmonics. The 2D power spectrum estimate is presented in *Figure 27*. There are several methods to determine the local orientation and the frequency from the 2D power spectrum. In this study the peak location was at first determined simply as the point of maximum amplitude in the spectrum. This is an adequate method, when the spectrum is clear and there is only one sharp peak, as in *Figure 27*. If annual rings have considerably varying widths within the window, two or more frequency peaks are observed in the 2D power spectrum, but the highest peak is chosen to represent the dominating frequency. In the next moving window location that overlaps with the previous window, the situation may be changed and the highest spectrum peak and therefore the dominating frequency change as well. The amplitude and the spreading of the spectrum peak are measures of reliability for the estimate of dominating frequency within the window. If the spectrum has not a peak at all due to destroyed or hidden annual ring pattern, e.g. due to defects, dirt or other unwanted properties within the local image window, the orientation and the frequency cannot be determined. The cross section surface of wood can be segmented from the background based on that the background does not have periodic

structure and thus peaks in the local spectrum. However, this is much slower in comparison with segmentation based on global thresholding to be discussed below.

Smoother frequency and orientation fields are obtained if the peak location is determined with sub-pixel accuracy. Therefore a 2D-polynomial was fitted to the spectrum over the 8-pixel neighborhood of the original peak location. The point of the maximum of the fitted 2D-polynomial was chosen as the location of the peak in spectrum, and thus subpixel accuracy was obtained. If the amplitude of the spectral peak decreases and spreads rapidly as the moving window slides over the original image, it is likely that the area corresponds to defected or hidden texture. However, this observation was not pursued to a measurement method in this thesis.

In order to obtain the dominating frequency and orientation in the neighborhood of any point, the 2D power spectrum in the moving window centered at the point was computed first, as discussed above. For visualizing purposes one half of the 2D power spectrum was converted to the polar coordinates in Cartesian coordinate system, so that x-axis equals to the radius coordinate and y-axis to the wave vector angle in the frequency space. *Figure 26* shows a moving window of size 101×101 pixels, of which the power spectrum has been calculated. *Figure 27* presents the corresponding 2D power spectrum estimate for the window. The scale calibration provided that one pixel corresponds to 0.27 millimeters. The axes of the 2D power spectrum were scaled correspondingly to units of 1/mm. As can be observed in *Figure 27* the orientation of the 2D power spectrum peak is perpendicular to the orientation of streaks in *Figure 26* and, respectively, parallel to the maximum gradient of *Figure 26*. The half of the 2D power spectrum converted to the polar coordinates in Cartesian coordinate system is presented in *Figure 28*. The conversion of one half is enough, because the spectrum of any real valued image is symmetrical. After conversion it is easy to determine the orientation angle of the dominating frequency peak visually on the y-axis and its frequency on the x-axis. In *Figure 28*, the dominating frequency is about 0.37 1/mm. The inverse of that is about 2.7 millimeters which is the dominating annual ring width within the moving window in *Figure 26*. The orientation angle for the dominating frequency is approximately 1 radian, i.e. 57 degrees, when the angle is defined to increases clockwise from the horizontal axis in the image. The dominating orientation of annual rings is perpendicular to that, i.e. -33 degrees. From *Figure 28* one can read that the uncertainty of the frequency is roughly ±0.02 1/mm and that of orientation angle roughly ±0.2 radians. The

uncertainties seem to be uncorrelated due to elliptical shape of the spectrum peak in both spectrum images. However, the representation of the spectrum as in *Figure 28* is for visualization only, because the conversion of the spectrum takes computation time and uses interpolation.

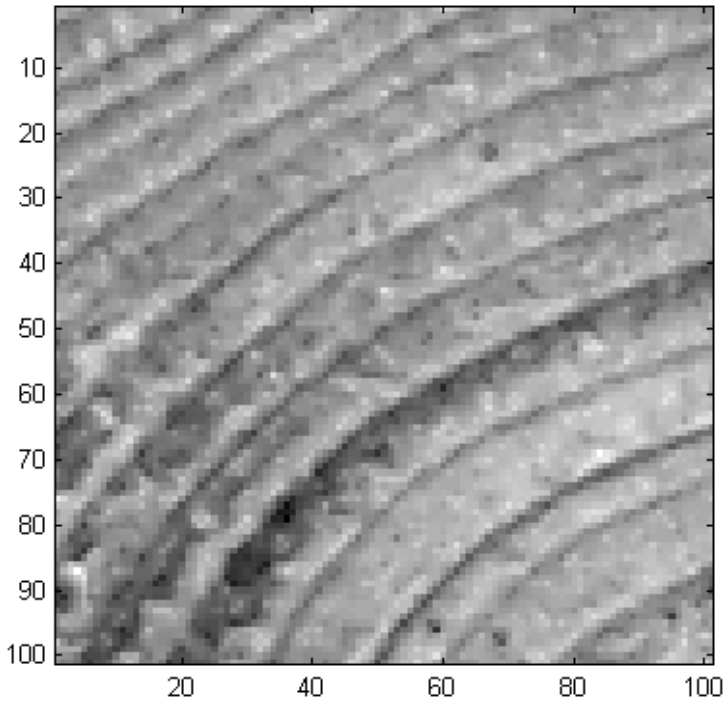

Figure 26. The green channel of a window within the original image. Size of the image is 101×101 pixels.

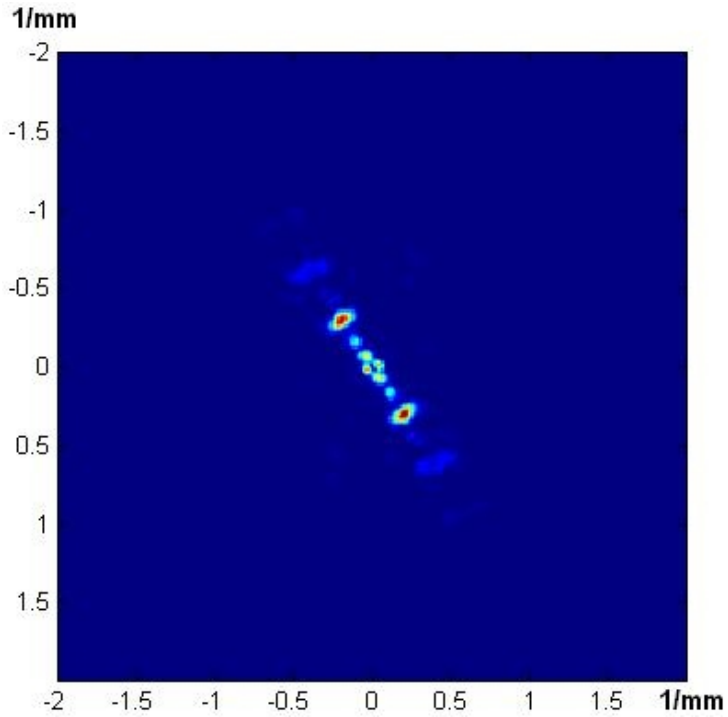

Figure 27. The two-dimensional power spectrum estimate calculated from Figure 26.

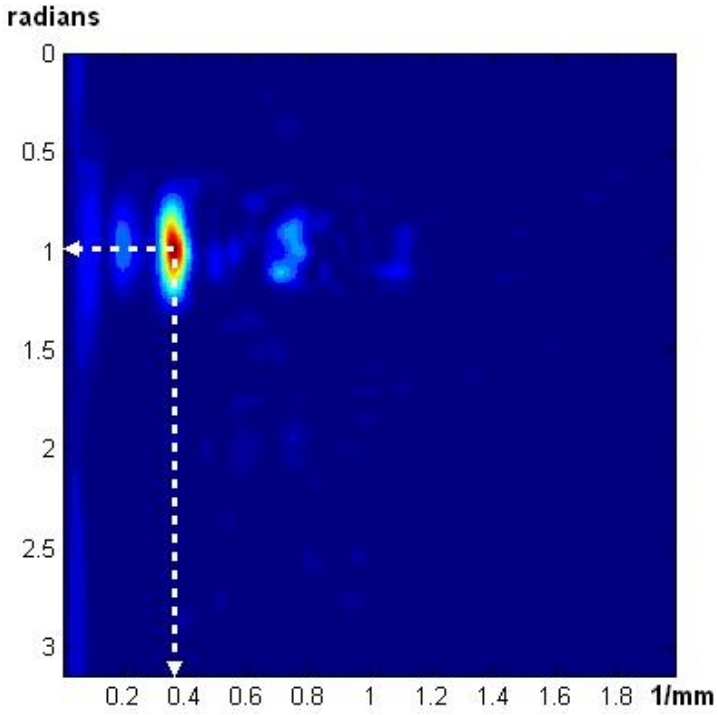

Figure 28. One half of the 2D-spectrum of Figure 27 presented in the polar coordinates for visualizing purposes. The y-axis equals orientation angle (radians), the x-axis equals the radius in the frequency scale (1/mm). The white arrows visualize the location of the dominating frequency peak.

6.1.1 Thickness field of annual rings

By sliding the moving window across the entire image the thickness field of annual rings, $\lambda(x,y)$, is constructed by repeating the local analysis of dominating frequency at each position of the window. The algorithm is following:

Algorithm 1. Thickness field of annual rings

1. A color or grayscale image $I(x,y)$ of wood cross section surface is taken.
2. An image channel or their conversion is thresholded to make a binary template $T(x,y)$ assuming the value zero to correspond to the background and the value one to the region of interest. This is not compulsory, but speeds up the computation. The saturation component of the HSI conversion is an appropriate selection in many cases, but the lighting arrangements affect the thresholding result. This is discussed in detail in Subchapter 6.3.1.
3. The moving window W of size $M \times N$ is chosen.

4. The step size of the moving window *d* both vertical and horizontal direction is chosen.
5. The moving window *W* is centered in every *d*:th location of *I(x,y)*, where the template *T(x,y)* equals with one.
6. The power spectrum *P(u,v)* is computed in each moving window.
7. The coordinates of the highest power spectrum peak *max(P(u,v))* is detected and a 2D-polynomial is fitted in the 8-neighborhood of the spectrum peak location. The peak location in subpixel accuracy is obtained as the point of maximum in the 2D-polynome.
8. The length of the location vector of the spectrum peak reveals the dominating frequency in 1/pixels and produces the frequency field $\omega(x',y')$.
9. Frequency field is inverted in dominating wavelength field and scaled in thickness field of annual rings $\lambda(x',y')$.
10. The pixel measures are converted to millimeters with scale calibration.

Figure 29 (a) shows the original image and *(b)* the corresponding thickness field for a prepared pine log cross section. Here the original 3.6 megapixel image was obtained with a scanner. The method does not give the exact local widths of the annual rings, but provides the dominating widths of annual rings in the surroundings of any chosen pixel. The resolution of the thickness field is dictated by the move step of the window. In *Figure 29*, the move step is 10 pixels and thus the resulting thickness field has 1/10 of the resolution of the original image both in x- and y-directions. As the windows were size of size 51×51 pixels, they overlap. Due to the small size of the moving window, no proper Welch estimates were calculated but the local spectrum was determined with one sample spectrum. The color of the thickness field codes the local dominating thickness of annual rings in millimeters, as given by the color bar on the right. Towards the edges near the bark annual rings are thin: the dominating thickness of annual rings in the area is less than 1 mm. In the center area the annual rings are wider, up to 7 mm. The method interprets the bark area as a single thick annual ring. Thus the thickness field of the annual rings can be used for rough bark thickness evaluation as well. However, this measurement result is not very accurate because the bark region does not have periodicity.

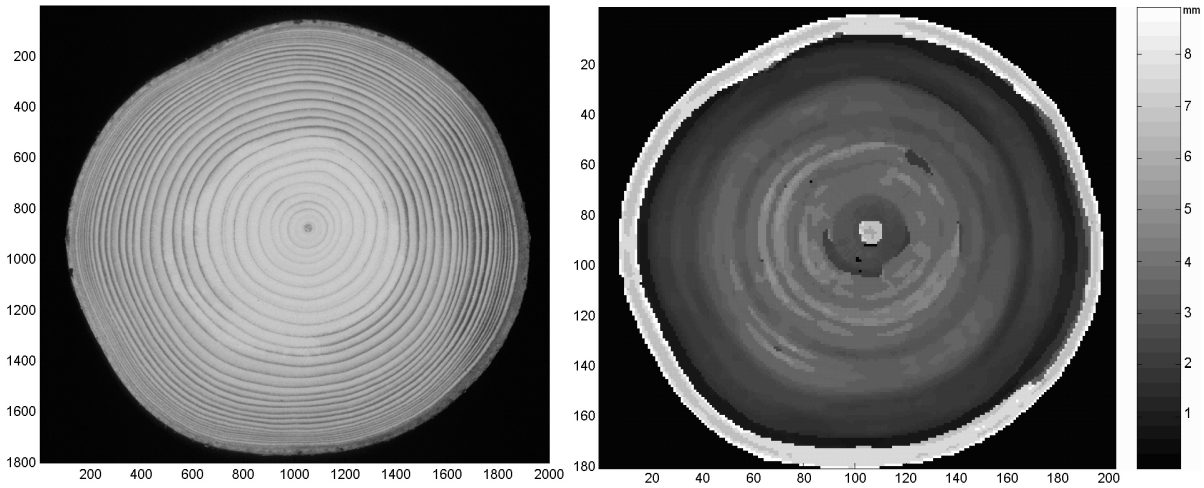

Figure 29. (a) A prepared pine disc image. (b) The thickness field of annual rings in millimeters evaluated from (a).

Figure 30 (a) shows an unprepared spruce cross section surface image with some root decay as an image of 0.9 megapixels. The thickness field of the annual rings with 1/10 resolution both in x- and y- direction is evaluated and shown in *Figure 30 (b)*. The annual ring width is evaluated correctly in sound wood regions, ranging from about 1 to 4 mm, but the analysis provides the abnormal results of over 10 mm at the decayed regions and bark area. Thus the thickness field of the annual rings can be used also in defect detection. The measurement results having rapid transitions along the annual ring direction (or perpendicular to the radius, if annual rings are not recognizable) can be interpreted originating from defective regions.

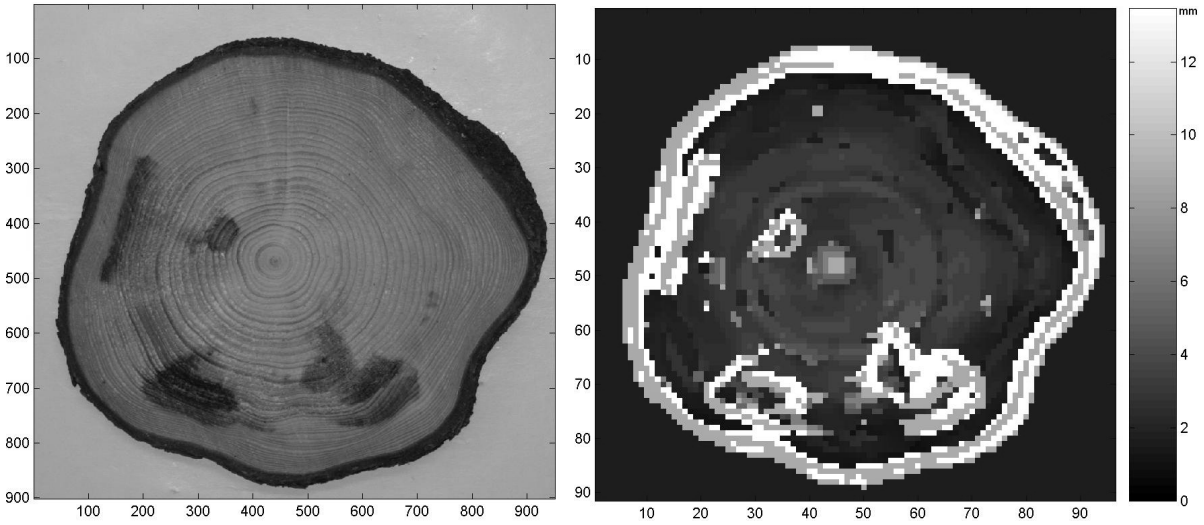

Figure 30. (a) An unprepared decayed cross section surface of spruce. (b) The thickness field of annual rings with 1/10 resolution both x- and y-direction in comparison with original.

For Scots pine and Norway spruce the annual ring width correlates with wood density, excluding extremely narrow annual rings. Furthermore, wood density correlates with the strength and the stiffness of wood [71][8][33]. The distribution of annual ring widths is expected to correlate with the strength of the sawn product. The annual ring width distribution analysis allows assessing the homogeneity of wood and sawn products. The thickness field of annual rings offers a new way to measure and characterize the quality of wood. The method allows the analysis of annual rings from region to region, e.g. in sectors or in circular bands so that positioning, sawing and peeling of a log may be optimized according to the thicknesses of the annual rings. The thickness field of annual rings provides parameters such as the variance of annual ring widths within the whole log or in areas determined locally, in particular the variance of annual rings in the inner or the outer regions. These parameters also can be utilized in log quality classification and in sawing and peeling optimization. The thickness field of annual rings can be obtained from rough and slightly decayed or color defected areas, if the annual ring structure is visible. Thus the application possibilities at least in the sawmill industry without log cross surface preparation are evident.

6.1.2 Orientation field of annual rings

The orientation field of annual rings, $\varphi(x,y)$, is evaluated together with the thickness field using the 2D Fourier power spectrum and the moving window. The location of the peak in the 2D power spectrum provides not only the dominating frequency in the moving window, but also the orientation of the wave front corresponding to that frequency. The orientation of the dominating frequency in the moving window gives the normal for the local orientation of annual rings. The step by step algorithm is the following:

Algorithm 2. Orientation field of annual rings

1-7. Steps are as the steps 1-7 of the algorithm 1.

8. The angle of the location vector of the spectrum peak reveals the orientation of dominating frequency.

9. The orientation of the normal to the location vector equals the orientation of local annual ring pattern and reveals the orientation field of annual rings $\varphi(x',y')$.

The determination of the local orientation of annual rings is an essential stage for further methods, such as the defect detection and locating the pith. The orientation of a texture within a log end image reveals irregularities in the wood structure. Thus defective areas can be detected with the orientation field. *Figure 31 (a)* presents a low resolution full image of the orientation field of an unprepared log end image with root decay. Here the resolution is lowered due to visualizing purposes: with the lower resolution the orientation marks in the window are far enough from one another to be seen clearly. The cross section sample has been cut with a sharp chainsaw and the sample was not prepared before imaging. In *Figure 31 (b)*, a close up of the original orientation field image is shown. It is noteworthy that in the decayed area the annual ring texture is distorted as the orientation follows the borders of the decay but not annual rings. This property will be used in defect detection as presented in the next subsection.

Alternatively local orientation information can be determined without 2D-frequency spectrum by evaluating the direction of the highest gradient in the moving window. Such a procedure is faster, but it is not equally robust and reliable with unprepared wood samples. This was proven in an unpublished application development outside this thesis but as its follow up.

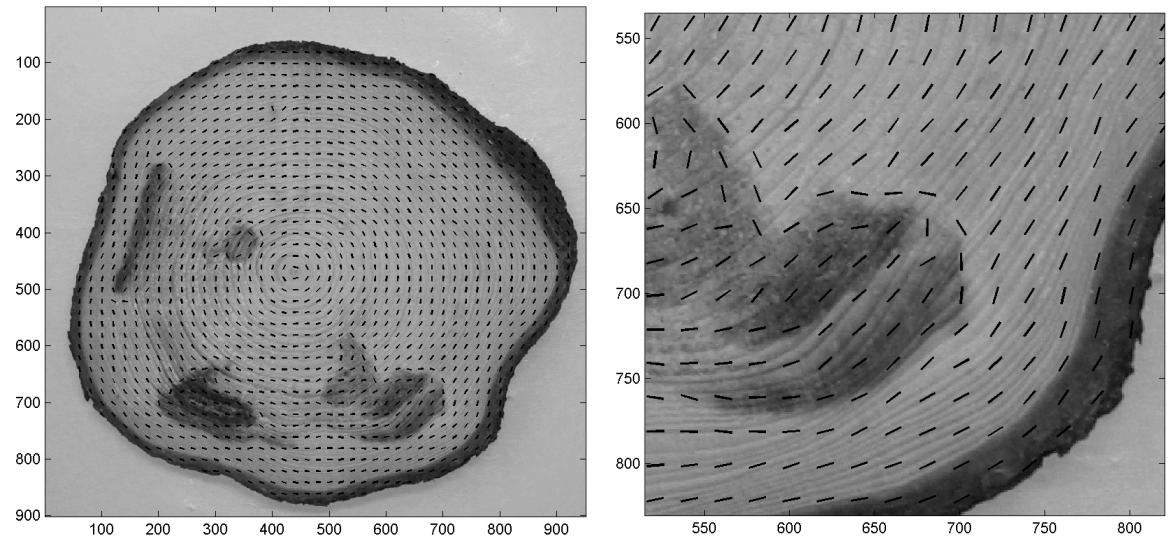

Figure 31. (a) The orientation field of annual rings in an unprepared and decayed log cross section. (b) A zoomed decayed area of image (a) and local orientations within the area.

6.1.3 Defect detection

Both the thickness field and the orientation field discussed above may serve individually as a basis for defect detectors. The previous section manifested that the estimated orientation field changes rapidly when the regular texture of annual rings breaks in a defected area, e.g. in decay, knot or crack. Similarly, the evaluated thickness of the annual rings deviates often significantly from its regular behavior in a heavily rotten and knotty area, close to the pith, and in the bark area. If the methods are combined, the reliability of the defect detection is improved further. The rapid orientation change can be interpreted originating from the defected region. However, if the border line of the defect equals with the local annual ring orientation, the rapid orientation change is not observed, but a rapid change in annual ring width may be present. Defect detection works regardless of the variations in lighting. However, incipient rot is difficult to detect because it typically changes only the color but does not destroy the annual ring structure. The step by step procedure for annual ring orientation field based algorithm is the following:

Algorithm 3a. Defect detection

1-9. Steps are identical to those of 1-9 in algorithm 2.

10. a) The circular standard deviation of the orientation e.g. in the 8-neigborhood of each pixel of $\varphi(x',y')$ is evaluated according to [41] and inserted in the corresponding locations of the standard deviation matrix $S(x',y')$.
    b) alternatively: the gradient of the orientation field both in the vertical and in the horizontal direction at each pixel of $\varphi(x',y')$ are evaluated. The vertical and the horizontal gradient vectors in the matrices are combined for matrix $G(x',y')$ having the length of the gradient vector at each location.
11. The matrix of the circular standard deviation $S(x',y')$ or the gradient $G(x',y')$ is thresholded with fixed threshold and the mask reveals the defected areas.

The step by step procedure for the algorithm based on the annual ring thickness field is the following:

Algoritm 3b. Defect detection

1-9. Steps are as in the algorithm 1.

10. a) The standard deviation of annual ring thicknesses e.g. in the 8-neigborhood of each pixel of $\lambda(x',y')$ is evaluated and inserted in the corresponding locations of the standard deviation matrix $S(x',y')$.

    b) alternatively: the gradient of the annual ring thickness field both in the vertical and in the horizontal direction at each pixel of $\lambda(x',y')$ are evaluated. The vertical and the horizontal gradient vectors in the matrices are combined for the matrix $G(x',y')$ having the length of the gradient vector at each location.

11. The matrix of the standard deviation $S(x',y')$ or the gradient $G(x',y')$ is thresholded with fixed threshold and the mask reveals the defected areas.

The results of the two algorithms can be used individually or combined with the 'and'-operation to a tighter requirement for defect detection. The gradient based algorithm is more rapid but less robust than evaluating the local standard deviations in the thickness and orientation fields of annual rings.

Figure 32 presents an example of the defect detection process. *Figure 32 (a)* shows the original gray scale image of a prepared board cross section with knot defects. In *Figure 32 (b)*, the orientation of the annual rings is evaluated using the 2D Fourier power spectrum with the moving window. In this image, the orientation information is presented in gray scale, the black color denoting the orientation angle of -90 degrees to the horizontal and the white color denoting +90 degrees. In the knotty board end case the information about orientation is evaluated in the neighborhood of every 70^{th} pixel in the x- and y- directions. Thus the resolution of the resulting orientation matrix is rather low, but the computation is fast. However, the resulting matrix has high enough number of samples of the orientation field for the defect detection. *Figure 32 (c)* shows the standard deviation of the orientation in the 8-neighborhood of each location. The resulting matrix is binarized with a fixed threshold, and as a result a mask indicating defect locations is obtained, see *Figure 32 (d)*.

When evaluating the annual ring thicknesses within the image, irrelevant values originating from knotty areas can be omitted with the defect mask. The defect mask generates also a safety margin of sound wood around the defected regions to ensure that measures originating

from the defected or nearby regions will not be included in the further calculation, e.g. when evaluating the mean width of the annual rings. The same procedure works also with heavy decay and cracks. However, the procedure is not able to distinguish which type of defect is detected.

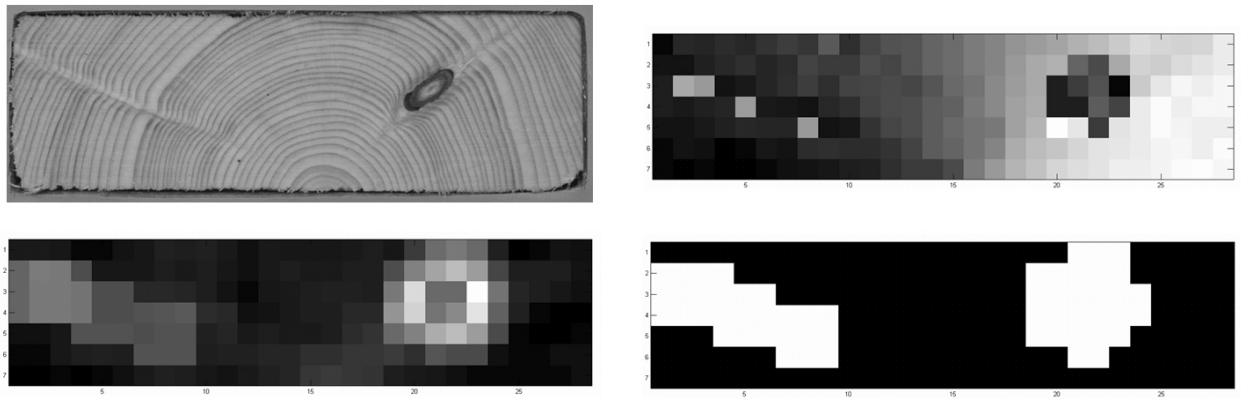

Figure 32. Detecting and ignoring the defective areas within a board cross section. (a) The original image. (b) The orientation of texture in gray scale colors with low resolution. (c) The gradient of the orientation matrix. (d) The areas suitable for measurement as the black color and the defective areas with tolerances as the white color.

6.1.4 Locating the pith

Locating the pith in the log cross-section image is also based on the local 2D Fourier power spectrum, but no moving window through the image is needed. The iterative search of the pith location starts with an initial guess. An appropriate initial guess easy to construct is the geometric centre of the log end surface, which requires that the log cross section is segmented from the background for instance with an appropriate lighting arrangement and the global thresholding. In the first iteration two further points are chosen so that these three points form an angle of 90 degrees. The distance between the two points and the initial guess was chosen to be half of the distance between the initial guess and the edge of the log cross section surface in the directions of the two points. The local orientation of the annual rings is determined in a window centered at the chosen points and the lines of normal to the annual rings are determined. The intersection of the lines of normal provides the next estimate for the pith. The second iteration begins by choosing two new points for orientation determination. The distance between the present estimate and the chosen points is reduced by a factor $0 < d < 1$. The reduction factor selected, d, is a tradeoff between robustness – d close to 1 – and computational speed – d close to 0. The scheme of an iteration round is

presented in *Figure 33 (a)*. The termination condition of the procedure is that two most recent estimates are closer to one another than a prespecified value. Minimum distance between the most recent estimate and the points at which the orientations are to be evaluated can be constrained, to prevent that all the points were near the pith and annual ring orientations would not be straight within the window. In practice a good choice for the minimum distance is 1/10 of the distance between the centre and the edge of the cross section surface. For practical purposes, termination after a fixed number of steps is also sufficient. The step by step algorithm for the pith locating is the following:

Algorithm 4. Locating the pith

1. A color or grayscale image *I(x,y)* of wood cross section surface is taken.
2. An image channel or their conversion is thresholded to make a binary template *T(x,y)* assuming the value zero to correspond to the background and the value one to the region of interest. The saturation component of the HSI conversion is an appropriate selection in many cases, but the lighting arrangements affect the thresholding result.
3. An iteration counter is set n=1.The geometric center of the cross section surface c_n, that is the initial guess for pith location, is evaluated (*centroid* in Matlab).
4. Two random points p_n and q_n are chosen so that these form a 90 degrees angle with c_n as the corner point. The location of p_n and q_n is half the distance between the c_n and the edge of a cross section surface.
5. The local window W of size $M \times N$ is chosen.
6. The window W is centered in p_n and q_n.

7-10. The local orientation at the neighborhood of points p_n and q_n is evaluated with the 2D power spectrum similarly to the steps 6-9 in algorithm 2.

11. The normal to the both local annual ring orientations is evaluated. The intersection of the normals produces the next pith estimate i.e. new pixel coordinates for c_{n+1}.
12. The location of the new pith estimate c_{n+1} is compared with the template *T(x,y)*. If the location in the template equals with zero, the estimate is outside the cross section surface and the points p_n and q_n are rotated an fixed angle around the previous estimate and procedure is continued from step 6.

13. New coordinates for p_{n+1} and q_{n+1} are given so that the distance between current pith estimate c_{n+1} and p_{n+1} and q_{n+1} is reduced by a factor *d*. Iteration counter is incremented by one.
14. The loop is continued from the step 6 until the two most recent estimates c_n and c_{n-1} are closer to one another than a prespecified value, or the iteration counter exceeds a prespecified value. The final estimate is the result for pith locating procedure.

Figure 33 (b) shows the result of estimation in the zoomed center area of an unprepared log cross section image presented after six iterations. The plus sign shows the geometric centre, which deviates significantly from the correct pith location. The cross sign in *Figure 33 (b)* shows that the pith location process produces a good result. Among others, the Finnish conifer trees have normally round first annual rings around the pith, which helps the procedure to estimate the pith location with good accuracy.

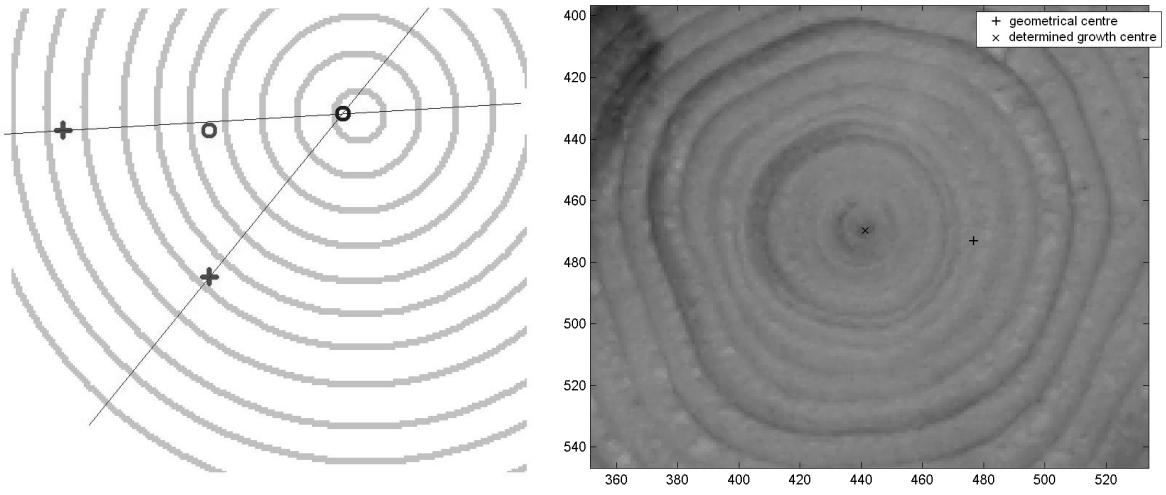

Figure 33. (a) The scheme of one iteration round of the pith location process. The plus signs mark the points where the local orientation is evaluated. The circles are the previous and the present estimate for the pith. (b) The geometrical centre with the plus sign, and the final pith estimate with the cross sign in the zoomed center area of a log cross section.

The algorithm is able to estimate the pith location despite the defects. *Figure 34* shows the pith location for a partly decayed wood disc. In the first iteration, the points at which the local orientation of the annual rings was evaluated are in the decayed region. However, the local orientation can be evaluated and the intersection of orientation lines i.e. the new estimate for pith location is rather good one and is located a slightly in the upper left direction from the final pith estimate marked with the green asterisk. The points in the

decayed region, at which the local orientation was calculated, are marked for visualization with white circles instead of the blue circles of the other points. In the second iteration one of the two points chosen is still in the decayed region, but the algorithm succeeds determining the local orientation and improves the pith estimate. The rest of the pith estimates are all quite close the correct pith location. The geometric centre, which is the first estimate for the pith location is marked in *Figure 34* with the red asterisk.

Figure 34. The pith location process for a decayed log cross section. Even the first pith estimate is rather good, though the both chosen points are in the severely decayed region.

If the decay is so severe that the local orientation of the annual rings cannot be recognized visually at all, the algorithm still provides the orientation, but the peak in the 2D power spectrum is typically low and wide so that it is recognized as an error. Fixed threshold values for the maximum value, the maximum variance and the kurtosis of the 2D power spectrum can be set. However, the orientation analysis based on spectrum may give a false orientation,

e.g. due to a crack. If the measured annual ring orientation is entirely false, the intersection of the orientation lines will be far away from the correct pith location and from the previous estimates as well. A good constraint is that not any of the pith estimates may locate outside the cross section surface. When this occurs, the algorithm discards the estimate and chooses two new points in 90 degrees angle at the same distance from the recent pith estimation, but in different location. This is an attempt to avoid the defected regions, at which the orientation of the annual rings cannot be determined correctly. The algorithm continues the iteration process from the new location until the pith is located or no acceptable estimates are generated in a prespecified number of attempts. In this case the most recent estimate, or e.g. the mean of the most recent three, is taken as the final estimate. If no pith estimate can be generated, the geometric center of the log cross section is taken as the estimate. In practice the approximation with geometric center is needed if the cross section surface is fully rotten or covered with mud.

6.1.5 Detecting the inner and the outer side of board and the curvature of annual rings in board

The algorithm to estimate pith location has been applied also for board end images. The process is similar to that in Section 6.1.4. However, it is noteworthy that the algorithm produces an estimate for the pith location even if the pith does not lie within the board end. The first estimate is the geometric centre of the board cross section surface and the first locations for orientation evaluation are at the half point between the line from the center to one or the other of the two vertical and horizontal edges. The iteration continues until the points, at which the local orientation of the annual rings is evaluated, lie outside the imaged target. The intersection of the final orientation lines or the mean of some of the most recent estimates close enough to one another gives the final estimate for the pith location. The distance for close enough estimates can be set according to the board dimensions.

The inner and outer side of the board can be determined with the pith location data: if the pith estimate is above the middle line of the board, the inner side of the board faces up and vice versa. The distance from the pith location estimate to the middle line corresponds to the curvature of the annual rings within the board. The curvature of the annual rings may correlate with board distortions during drying at the sawmill. The step by step algorithm for the side of the board and the curvature detection is the following:

Algorithm 5. Board side and curvature detection

1-11. Steps are as the steps 1-11 in the algorithm 4.

12. New coordinates for p_{n+1} and q_{n+1} are given so that the distance between the current pith estimate c_{n+1} and p_{n+1} and q_{n+1} is reduced by a factor d.

13. The loop is continued from the step 6, until the two most recent estimates are closer to one another than a prespecified value. If either or both p_{n+1} or q_{n+1} are outside the cross section surface before the termination condition is fulfilled, the current estimate for pith location c_{n+1} is the final estimate. Iteration counter is incremented by one.

14. The final pith location estimate c_n is compared to the vertical middle line revealing the inner and outer side of the board.

15. The distance between the vertical middle line and the final pith location estimate c_n provides the estimate for the curvature of the annual rings in the board.

Figure 35 presents the algorithm for estimating the pith location in a board cross section when the pith is at the edge of the board cross section. Five pairs of circles denote the points, at which the orientation of the annual rings is evaluated during each iteration. Some of the estimates are outside of the image and some inside, but obviously that does not cause any problems here. The intermediate estimates of the pith location are marked with black stars. The final estimate for pith location is marked with the white star. The median line of the board is drawn in the image. In *Figure 35* the estimate of the pith location is under the median line and thus the board lays the outer side up. The distance between the median line and the pith location estimate is a short one. Thus the curvature of the annual rings is quite heavy within the board.

Extremely large trunks can be sawed so that the orientation of the annual rings in the board is almost straight. In this case, the pith location cannot be estimated reliably. However, in Finland the trunks with such huge diameters are extremely rare, and because constraints in harvesters, they do not arrive at the sawmill through the normal transportation chain.

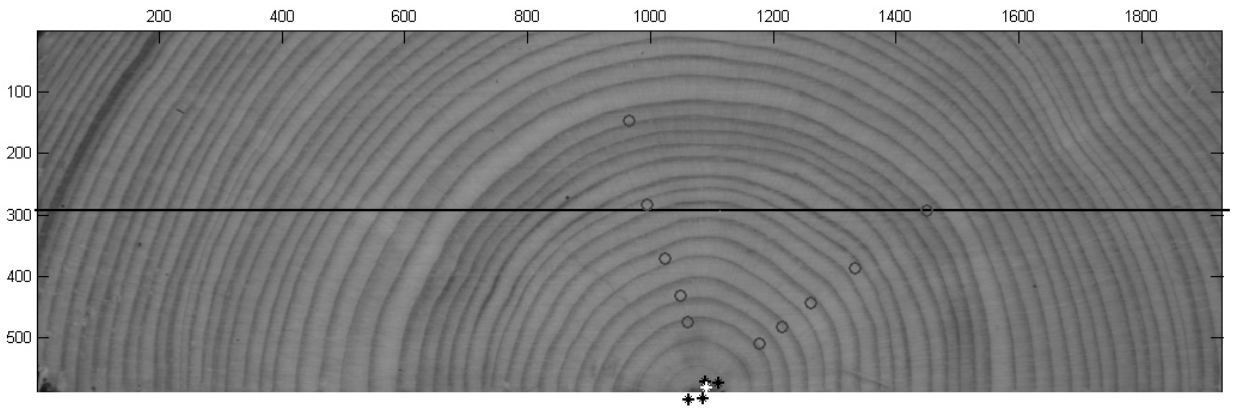

Figure 35. The estimation of the pith location in the board cross section image. The intermediate pith estimates are marked as the black stars and final estimate as white. The circle pairs denote the points where the local orientations of annual rings are evaluated.

6.1.6 Counting the annual rings

The method for counting the annual rings along a path is also based on the local 2D power spectrum. The path can be chosen as any straight line segment between two points when the line crosses the pith. The path can be also determined according to the normal of the present annual ring by evaluating the annual ring orientation with the local 2D power spectrum. However, with path determined by the normal of the annual ring the algorithm cannot be started exactly at pith because the annual ring orientation there is ambiguous. Thus the first annual rings have to be counted within the line segment, e.g. until 2 cm distance from the pith and then the algorithm may proceed the path normal to annual rings. The error is minimal, because the inner annual rings are mainly round, and thus the normal equals to the line segment.

Knowing the pith location, the edge and the thickness of the bark in the cross section are prerequisites for counting all the annual rings automatically within the cross section surface. Scale calibration is not required unless the number of the annual rings within a known distance from the pith is to be counted automatically, but then the edge of the cross section and the thickness of the bark need not be known. The algorithm evaluates the local frequency of the annual rings in the moving window covering the surroundings of every pixel along the chosen path. Thus the window moves along the path only, rather than throughout the cross section. The dominating frequency is evaluated with the 2D Fourier power spectrum and the result is given in 1/pixels. The frequency at each window location is associated for the corresponding pixel along the path. The inverse of the frequency tells the wavelength, i.e. how many pixels one annual ring covers on the average in the neighborhood

of the pixel that is under inspection. After integrating the dominating frequency at each pixel along the path we get the number of annual rings. As the integration is numerical and the pixels lie on a square grid, the slope of the path must be taken into account. With the scale calibration, the algorithm is able to count the number of the annual rings over a fixed distance, such as the distance range of 2-8 cm from the pith, which is a log quality parameter in Sweden. The step by step algorithm for the counting of the annual rings is the following:

Algorithm 6. Counting the annual rings

1-14. Steps are as the steps 1-14 of the algorithm 4. The estimate for the pith location *c* is a prerequisite for automatic annual ring counting algorithm.

15. If all the annual rings are to be counted, the edge between the bark and the regular wood is located with the bark thickness algorithm, see below in 6.2.2. Else for counting over given distance the, scale calibration is required.

16. A line segment from pith *c* to an edge point or point with known distance *d* from pith forms the counting path

17. The moving window *W* of size $M \times N$ is chosen.

18. The moving window *W* is centered at each pixel location of path from *c* – over distance *d*.

19. The dominating frequency in the neighborhood of all the pixels belonging to the path is evaluated with the 2D power spectrum described in the steps 6-8 of the algorithm 1.

20. Dominating frequencies along the path are integrated. Integrated annual ring number has to be scaled according to the slope of the path and rounded to integer. The scaling factor is the length of the path vector divided by the number of elements in the path vector.

Figure 36 shows three results obtained with the algorithm. The log cross section surface in the image has not been prepared after chainsaw cutting. In the case of the short path near the pith, the algorithm provides five annual rings, in accordance with the human visual inspection. Near the bark area, the length of the chosen path is approximately the same as near the pith. The algorithm finds 10 annual rings, again in accordance with the human visual inspection. Third path spans from pith to bark and the algorithm finds 35 annual rings. However, the annual rings near the bark area are so narrow that they cannot be distinguished

from the original image, not even with the human eye. We can deduce that there are at least five annual rings more, but the algorithm finds the blurred area as a single thick annual ring. In this case, the method gives an incorrect result, but correct result cannot be found either visually from this image. However, the number of the annual rings is correct until the algorithm arrives at the blurred area. The problem can be solved with higher resolution imaging sensors. The cross section can also be imaged from a shorter distance as only a small portion of the cross section is analyzed. Imaging a half of the cross section surface is sufficient, but the image has to include the pith.

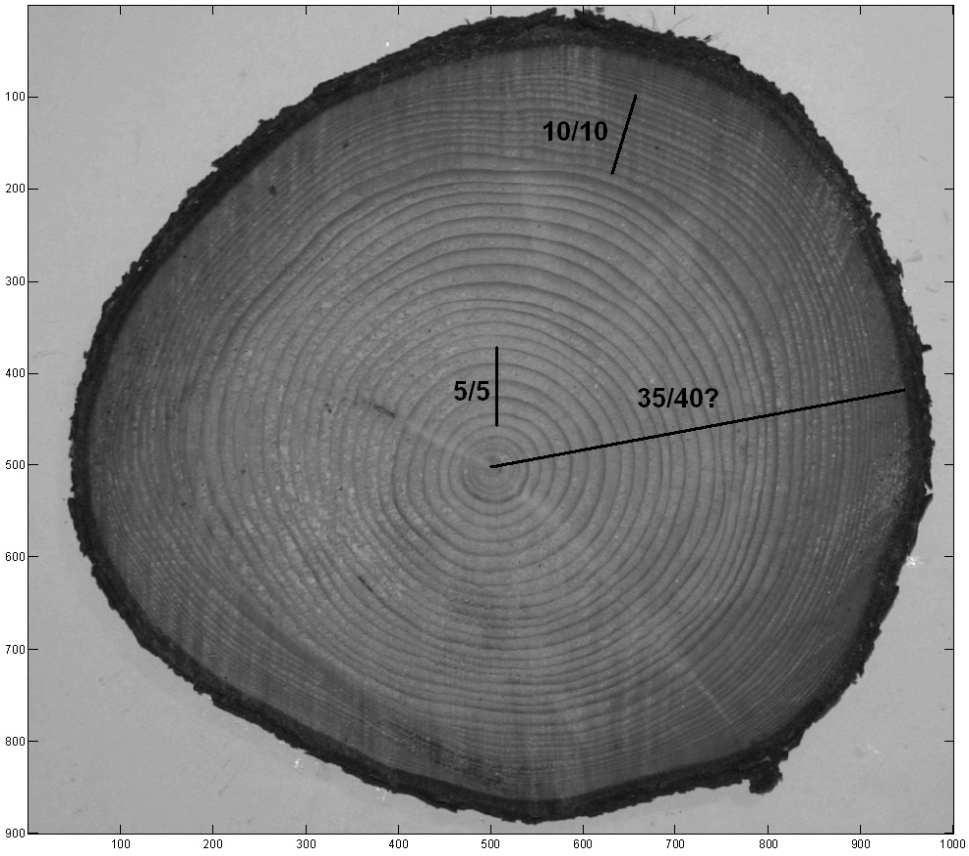

Figure 36. Counting the number of annual rings along three line segments. The first number is the value the algorithm produces automatically. The second number is the number evaluated from the image using human vision.

6.1.7 Tracking the annual rings

The method of tracking individual annual rings was developed based on the 2D Fourier power spectrum. The algorithm starts with the full resolution thickness field of the annual rings giving dominating annual ring width at any pixel within the original image. Each annual ring should have a width of several pixels, so that the thickness field is based on clear

peaks in the local spectrum. The pith location is computed next. When inspecting a line from pith to bark and the local frequencies the line covers, the total number of annual rings can be counted as discussed in the previous section. Instead of counting the annual rings from pith to bark, the ring tracking algorithm considers the integrated count value pixel by pixel, before rounding it the final integer of the number of annual rings. All the pixels with integrated count values having the same integer (e.g. 3.12, 3.25, 3.38, 3.51.etc.) belong to the same annual ring, the integer part of the count giving the order number of the ring. Because the distance over one pixel in all directions except in x- and y- directions is more than one pixel, the integrated value should be scaled as in the Subsection 6.1.6.

After the integration process has been made along the lines from pith to all bark edge pixels, single annual rings can be tracked. However, the algorithm is rather intensive in terms of computing. Any inaccuracy in the frequency field is integrated. If the annual ring in one pixel is incorrectly measured, the next annual ring location will be incorrect. Thus this algorithm requires cross section surfaces with quite clear annual rings for acceptable results. However, it is possible to reduce the error caused by unprepared cross sections. The variation of the measured annual ring width within a single annual ring cannot be very high and the change in thickness cannot be abrupt. Thus the highly deviating values can be recognized as outliers and the values can be replaced e.g. with the mean value of the annual ring width measures for that single annual ring. The paths can be integrated from bark to pith in the reverse direction if the edge, the pith location and the bark thickness of the log cross section are known. The comparison of the same path integrated both from pith to bark and bark to pith reveals the errors. The step by step algorithm for the annual ring tracking is as follows:

Algorithm 7. Annual ring tracking

1-8. The full resolution frequency field is computed as described in steps 1-8 of the algorithm 1.

9-22 The estimate for the pith location c is computed as described in steps 1-14 of the algorithm 4.

23. The local frequencies of $\omega(x,y)$ at each pixel along the paths from pith c to all the edge pixels of the cross section surface are integrated.

24. The integrated values are scaled according to the slope of the path.

25. The integer part of the integrated local frequencies along each path reveals the annual ring number in current pixel location and thus tracks annual rings
26. The result is the annual ring number matrix *N(x,y)*, where annual ring number zero corresponds with background.

Figure 37 (a) shows the result of the annual ring tracking algorithm obtained from the cross section cut with chain saw and not prepared, the one presented in *Figure 36*. The order number of the annual rings is color coded. In the border area, the tracking is rather poor, because of the poor resolution of the image compared to the width of the annual rings. *Figure 37 (b)* presents the 10th annual ring from the *Figure 37 (a)*. Incipient cumulative error can be seen as a thicker annual ring region in the upper left sector of the annual ring. The reason for that can be seen as a small darker region in *Figure 36*. Close to this area another error can be seen, the rapid curve in the annual ring. This is a consequence of annual ring width measurement giving too low value at some of the annual rings closer to the pith.

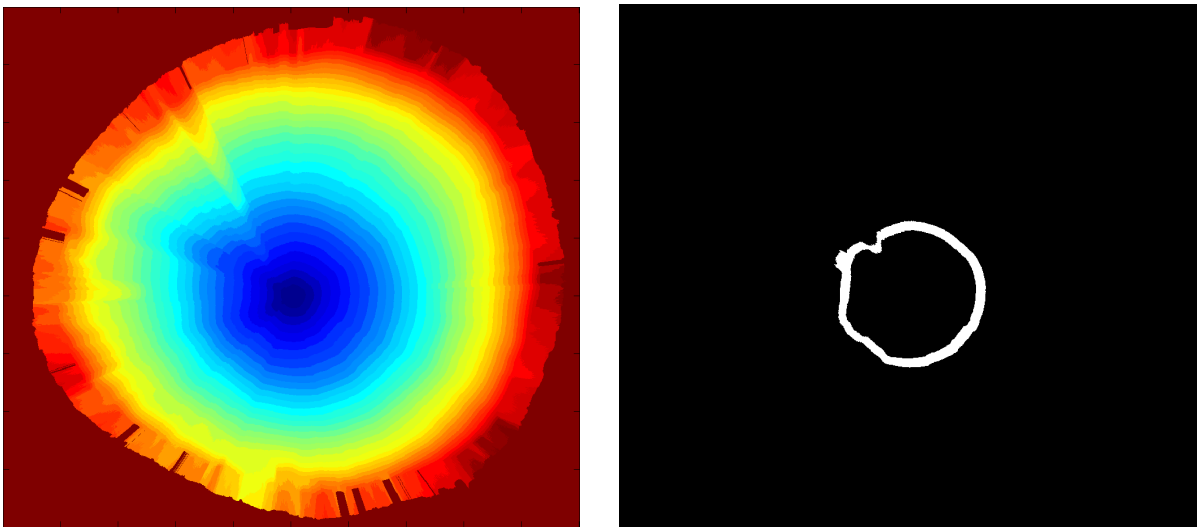

Figure 37. (a) Aall detected annual rings with different color shades. (b) The 10th annual ring from the image (a).

6.2 Methods based on geometry

This section discusses the methods that do not clearly belong either to the texture based methods or to the color based methods. They are here referred to as the geometry based analysis methods. The methods require quite a good segmentation of log cross-section from the background and thus are related to color based methods and deserve attention when arranging lighting. The first method transforms a cross section surface image of the log to

polar coordinates. The transformation allows parameterizing the shape of the cross section quite reliably, rapidly and simply. The second algorithm is for a rapid measurement of the thickness of the bark.

6.2.1. Shape of log end

First the log cross cut surface is segmented from the background by using appropriate lighting arrangement and a global threshold. The resulting mask is multiplied with one of the channels of the original image or a conversion image of the channels. The coordinate conversion from xy-coordinates to polar coordinates in the Cartesian coordinate system opens the log cross section image to a plane around the pith. The exact estimate of the location of the pith is a prerequisite, for such a representation. The conversion itself is quite straight forward. The conversion method takes pixels along the lines from the pith to the edge of the image and adds the lines into the result matrix as rows. The lines are taken at chosen intervals of angles around pith. The step by step presentation for algorithm is as follows:

Algorithm 8. Log end shape measurement.

1. A color or grayscale image *I(x,y)* of a wood cross section surface is taken.
2. An image channel or their conversion is thresholded to make a binary template *T(x,y)* assuming the value zero to correspond to the background and value one elsewhere. The saturation component of the HSI conversion is an appropriate selection in many cases, but the lighting arrangements affect the thresholding result.
3. Background is removed by multiplying the image *I(x,y)* with the binary mask *T(x,y)*.

4-17. The pith location estimate *c* is computed as described in steps 1-14 of the algorithm 4.

18. Pixel values along the lines from pith to the edge pixels of the image are taken and added into the result matrix as rows.
19. The paths have a different number of pixels. Thus locations in the result matrix without value are filled with zeros.

20. The first nonzero pixel in each row in the resulting matrix gives the profile describing log cross section shape.
21. Take the 1D FFT of the profile curve. Few first (e.g. five) FFT components describe the typical shape rather well.

Figure 38 (a) presents the original image in xy-coordinates, and *Figure 38 (b)* the green channel of the original image without background converted to the polar coordinates in Cartesian coordinate system. The blue line in *Figure 38 (a)* defines the zero angle and the blue arrow the direction of positive rotation. The blue line maps to the vertical axes of the converted image and the pith to the upper horizontal line.

The polar representation of a log cross section allows measuring the growth shapes and the shape of the cross section. However, the rings near the pith have only a few pixels in the original image. Thus the corresponding data in the polar matrix has been strongly interpolated: the real resolution in the low radius values of the polar matrix is rather poor. The highest non-zero y-coordinate value in each column in the converted image plots the edge curve. The edge curve of the result matrix provides the shape of the log cross section. If the edge curve is a straight line, the log cross section is round. However, if the log cross section is round but the pith is not exactly at the geometric center of the log cross section, the edge curve is a sinusoidal with the period of 2π. If we are only interested in the edge curve, but not in the annual ring conversions or the eccentricity of the log, the coordinate conversion can be made around the geometric centre. Then a round log cross section always corresponds to a straight line. The edge curve can be expressed as Fourier series. Normally, only a few first Fourier coefficients suffice to parameterize the shape of the log cross section well. Such Fourier coefficients are natural descriptors of log cross section shape: DC-component describes the mean diameter of log. After DC-component the first coefficient describes the eccentricity of the pith, the second coefficient describes the ellipticity of a log cross section etc. *Figure 38 (c),(d) and (e)* present the edge curve approximated with 6, 3 and 1 Fourier coefficients respectively.

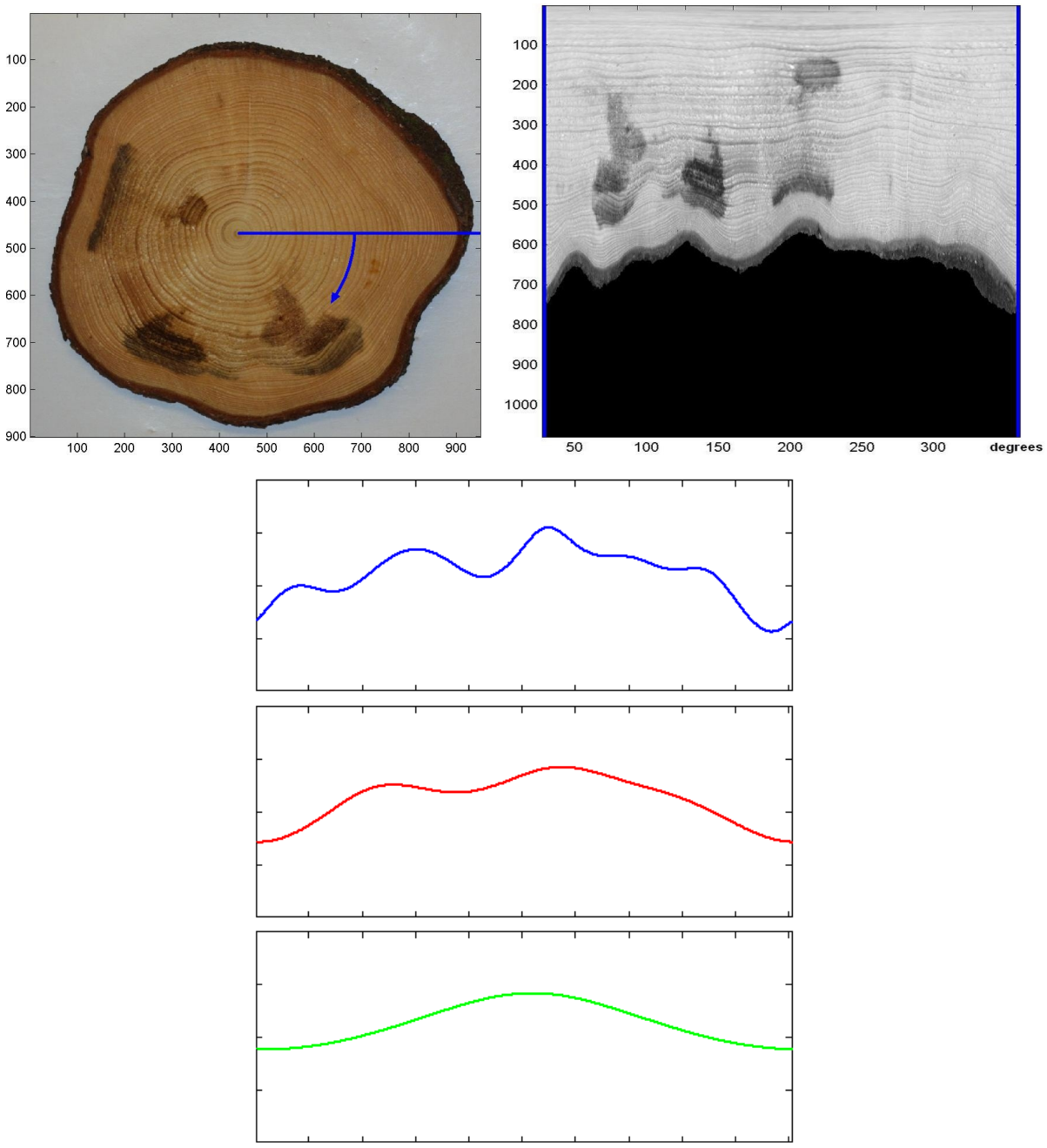

Figure 38. (a) The original image. The blue line defines the level of zero degree. (b) The green channel of Figure 38 (a) converted to the polar coordinates. Y-axis gives the radius in pixels. X-axis denotes the angle of the radius in degrees. (c), (d) and (e) The plotted edge curve approximated with 6 (blue), 3 (red) and 1 (green) Fourier coefficients respectively.

6.2.2 Measuring the thickness of bark

The method for measuring the thickness of the bark is based on 1D signal analysis, which was chosen as the approach because of the response time requirements in industrial applications.

The method specifies a number of lines through the pith or the geometric centre as the targets of the analysis. The angular interval between the lines determines the angular resolution and how many 1D signal samples must be processed. Along each line one of the color channels or their scalar combination, such as the mean or the first principal component of the channels, is analyzed. It is crucial for the performance of the algorithm to choose the target signal such that it has a high contrast between the background and the bark region and between the bark region and the sound wood. Typically, in Finnish conifers the color contrast between the bark and the sound wood material is quite high even if the cross section surface is rough as long as it is clean. The type of background defines the selection of the signal, but this is mostly affected by imaging arrangements. A light background is better for the conifers, because the bark is typically dark. The lighting conditions and the imaging arrangements are here similar to the global thresholding discussed more in detail in Subsection 6.3.1.

In this example the green channel was chosen, but because the lighting has wide spectrum and the background was even and light gray, any of the color channels, their mean or the saturation, and the intensity channels of the HSI conversion could have been chosen as well. The edge curve of the log cross section is determined in controlled circumstances after global thresholding as discussed more detailed in Subsection 6.3.1.

The thickness of the bark is determined in the intersections of the edge curve and the radial lines. The effect of global thresholding in the measurement can be removed by using tolerance of 10 pixels of background intensities. Thus 10 pixel intensities outside the edge curve are taken in the intensity curve. We need not to analyze the entire intensity curve along the line crossing the geometric center, but instead about 3 cm from the outer edge with tolerance pixels outside the edge curve is sufficient, because the bark in Finnish soft wood species is seldom thicker. The logs having thicker bark than 3 cm are handled as special cases in cutting and in the supply chain due to the size limitations of harvesters. The green channel signal along the path was differentiated to reveal sharp edges. The distance between the two highest absolute values of the differentiated variation in the 3 cm interval with tolerance is measured in pixels as the bark thickness. However, if the two highest values are extremely close (± 2 pixels) to one other, they are considered originating from the same edge (background - bark) and the third highest value is used instead to represent the inner edge

(bark – sound wood). The thickness of the bark in pixels is converted to that in millimeters according to scale calibration. The method requires that the variations in the color of the bark along the line studied are small. This requirement is typically well satisfied, in particular for Norway spruce. The log cross sections having very curved edges are somewhat problematic as the line crossing the geometric center may then be deviating largely from the normal to the bark surface, and therefore the estimate for the bark thickness will be too large. However, with the 2D-spectrum, we may calculate the orientation of the dominating frequency in the neighborhood of the point being analyzed in the bark area. Then the inspection line can be chosen along this orientation and it is exactly perpendicular to the bark. The step by step algorithm is the following:

Algorithm 9. Bark thickness measurement

1. A color or grayscale image $I(x,y)$ of wood cross section surface is taken
2. The scale calibration is made.
3. An image channel or their conversion is thresholded to make a binary template $T(x,y)$ assuming the value zero to correspond to the background and value one elsewhere. The saturation component of the HSI conversion is an appropriate selection in many cases, but the lighting arrangements affect the thresholding result.
4. The edge curve of the $T(x,y)$ is obtained.
5. The geometric center of log cross section surface g_1 is determined (*centroid* in Matlab).
6. A number of radial lines crossing the cross section surface through g_1 are set with a fixed angular interval.
7. Intensity values along the lines are differentiated.
8. Line segments of 3cm with tolerance in both ends of lines, where crossing the edge curve, are considered
9. The distance between two highest peaks of the differentiated signal in the 3 cm segments is evaluated
10. If the second highest peak is near (± 2 pixels) the first one, the third peak is considered to represent the inner edge.
11. The pixel values are converted in millimeters with scale calibration data. Each radial line gives two bark thickness estimates.

Figure 39 (a) presents the original image with 11 lines drawn through the geometric center. The values of the green color channel at pixels along the red line in *Figure 39 (a)* are presented as the red curve in *Figure 39 (b)*. The derivative of the green channel pixel values is denoted with the blue color under the intensity curve. Bark area causes a pair of sharp edges to the intensity signal. The early wood and latewood areas within the annual rings cause rapid variation in the intensity values. The green line segments under the intensity and derivative curves indicate the segment of 3 cm, to be analyzed for bark detection. In the rotten center area the mean of the intensity signal decreases and in the gray background it is clearly higher.

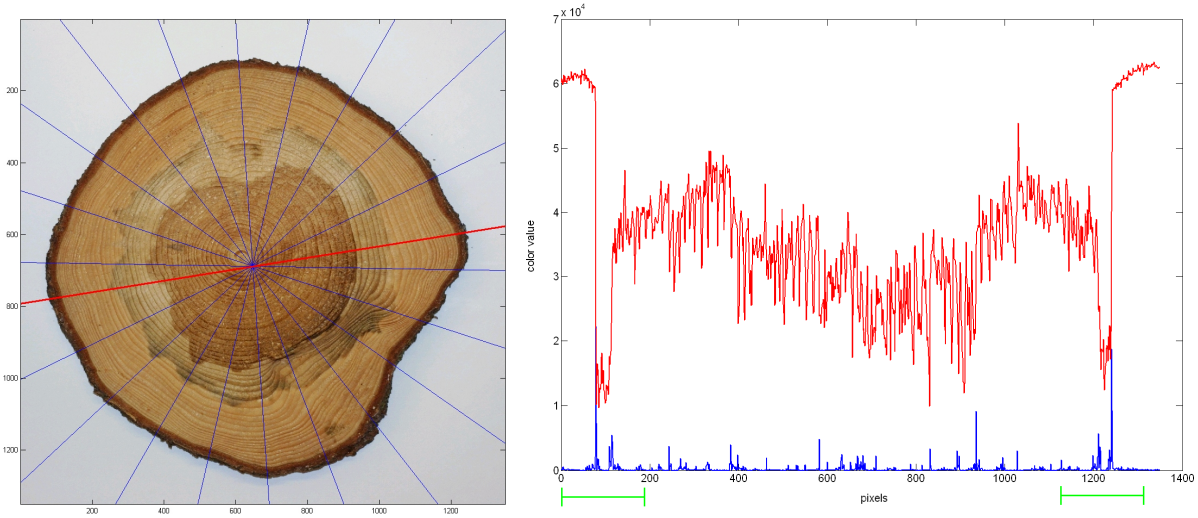

Figure 39. (a) The original image with lines along which the thickness of bark is measured. The intensities of green channel pixels along the red line in Figure 39 (a) are plotted in Figure 39 (b). The differentiated green channel signal is plotted as blue. Notice the sharp edges around the bark areas. Green line segments show the 3 cm intervals to be used in the estimation.

After differentiating the color channel signals along each of the lines, we get 22 thickness estimates for bark for the sample presented in *Figure 39 (b)*. According to an unpublished study on 530 samples of Norway spruce the thickness of bark typically vary ±1mm around the cross-section at the breast height. This enables us to exclude outliers, and to get a good estimate for the bark thickness. With the image size of 1300×1300 pixels on an area of 351×351 mm, the uncertainty of the bark thickness estimates is about ±0.6 mm if the inaccuracy of ±2 pixels in the locating the edges is supposed.

6.3 Color based methods

This Section discusses the wood property measurement with methods based on color analyses. These methods are not as robust as the methods based on texture analyses, and thus their feasibility is typically more restricted than that of the texture methods. Constant and/or special lighting and imaging arrangements are required. For instance, the wavelength band for lighting must be carefully selected according to the property of interest. During this study, the color analysis methods have been used rather as supporting methods. The Subsection 6.3.1 discusses the basic thresholding methods, how they are used during this study e.g. to segment a wood disc, a log cross section or a board cross section from the background. The segmentation of the bark and the rotten areas was also tested, but other than color based methods proved to be better in realistically varying imaging environments and for real-life samples in the wood supply chain.

The extraction of the early wood and the latewood regions is presented in Subsection 6.3.2-3. However, for analyses within an annual ring high quality images are required, and thus only highly prepared wood samples were used in the analysis. After the segmentation of the annual ring and their internal structure the latewood proportion within the wood sample was evaluated locally and globally.

The measurement of the color and area of rot is shortly discussed in subsection 6.3.4. The semiautomatic algorithm was developed to provide measurement data for the Finnish Forest Research Institute to model the propagation of rot inside the trunk of trees. The major part of the measurement task is the color calibration. In this method the user eventually determines the rotten areas.

6.3.1 Global thresholding methods in good measurement conditions

The wood sample was segmented from the background with global thresholding in many of the other analyses. This is much faster and more accurate than the other alternative, based on the 2D Fourier power spectrum.

The selection of the channel to be studied (i.e. RGB channel or their conversion) and the selection of the level of the threshold depend highly on the imaging arrangements. Typical object colors, the background color, the properties of the light and the locations of the light

spots are the most important parameters affecting the selection of the channel and the threshold. Automatic thresholding is a demanding task in a changing environment, but this is feasible by knowing points in the image that with certainty belong to the background in every image. In particular, in harvesters arranging a constant environment for thresholding is a challenging task, but could be based on special arrangements such as a powerful but short pulse flashlight and a camera at the opposite sides of and in an angle to the wood cross section. At sawmills it is quite straight forward to arrange imaging environment constant enough for thresholding.

In this study the RGB channels of the color image and their mean can be thresholded and the cross section of logs or boards can be segmented quite easily because of the well-controlled white or black background. However, the best results were achieved with the saturation component of the HSI representation that improves contrast between brightly colored objects and shades of gray. The original image was converted into the HSI color space and the saturation component was thresholded. When imaging samples of wood discs or board blocks, the background was arranged even and of shade of gray, including black and white.

The HSI conversion provided a working solution for segmentation with global thresholding also for cross section of full logs and boards. The log or the board end was spotlighted, thus reflecting the bright colors to the camera sensor whereas the background being further away, was darker and thus reflected less light. In this case, the thresholding was made on the saturation channel as well. However, the thresholding of the RGB image is also possible if the intensity difference between the log/board end and background is high enough.

The global thresholding procedure was applied also for segmenting the bark and the rotten areas in the images of the log cross sections. However, this procedure requires imaging environment to be very constant and the color of sound wood should not be too dark. The colors of the rotten areas are rather variable. Thus, either incipient rot is not detected or else slightly darker regions without rot are considered as rot, depending on whether the thresholding level is low or high, respectively. The bark and rotten areas were segmented in a set of images obtained under a fixed imaging environment and with a fixed threshold level. Every image was color calibratied. The algorithm detected bark and severe rot rather well for samples taken from a single tree trunk and typically for samples taken from the same stand of trees so that the samples have similar moisture content that affects the color of wood. The

thresholded regions were enhanced, so that the small regions in which rot was not detected but which were enclosed by detected areas were turned into detected ones. The outermost detected region was considered as the bark region and the inner ones as rot. However, the method classifies most other defects than rot and dirt also as rot.

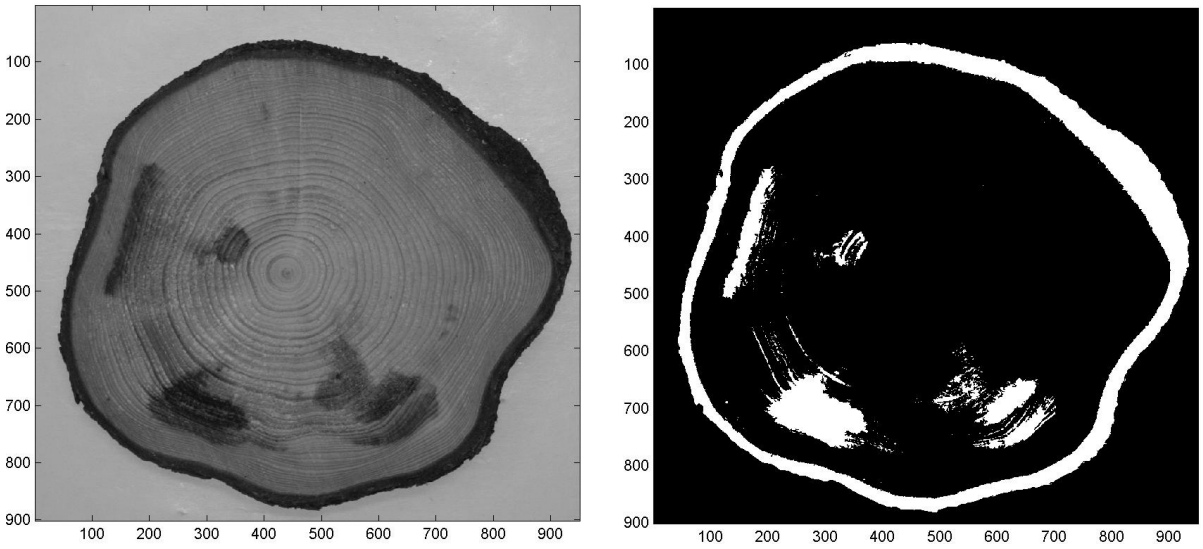

Figure 40. The segmentation of bark and severe rot with the global thresholding method.

The pixels in the bark region and rotten regions are counted and converted to real geometric measures with scale calibration. Thus the overall areas of the bark region and the rotten regions, of high interest in industrial applications, are measured. The left side of *Figure 40 (a)* shows a wood disc sample with root rot. *Figure 40 (b)* shows the bark and rotten regions after segmentation with a global fixed threshold. As seen in *Figure 40 (b*), the bark area can be segmented more accurately than the rotten areas due to more constant color. However, the method presented here works under fixed conditions or semiautomatically, as currently we do not have a universal solution for selecting the threshold automatically. The algorithms discussed in subsections 6.1.3 and 6.2.2 works better than the global thresholding for the detection of rot and the measurement of the bark in varying conditions.

6.3.2 Segmentation of early wood and latewood regions

Color variations within an image cause problems when identifying individual annual rings. The softwood species in the coniferous forest zone species produce one annual ring on the outer surface per year. An annual ring has two parts, the lighter area of early wood and the darker one of latewood.

The color of an early wood area in one part of the image may be so dark that color based methods easily confuse it with latewood color at another location. Furthermore, the color of latewood may vary between and within annual rings. If annual rings have an abnormally high proportion of wood material in a small compact area resembling latewood rather than early wood, the area is called compression wood. However, the color of compression wood typically slightly differs from that of latewood. Because of all these reasons simple global thresholding methods are not applicable for segmenting early wood and latewood.

The boundary between the latewood of previous year and the early wood of the following year is sharp, but within an annual ring the transition from early wood to latewood is rather smooth. To determine exactly the position of the boundary between early wood and latewood according to the formal definition based on the cell wall and the cell lumen widths, the single cells have to be visible and measurable. This can be achieved only by imaging the sample with a microscope, which covers only an extremely small area of the cross section surface.

When developing the analysis method for separating the early wood and the latewood, the board cross sections were prepared to get high quality images on annual rings. After cutting the logs or sawing the boards the surfaces were sandpapered and watered for better color contrast. In what follows, all the image examples are taken from the prepared board end images, but analyses made for similarly prepared log end images give results of similar quality. Our preliminary tests suggest that sharp chainsaw cutting surfaces watered provide images with adequate quality for this analysis. Thus the production scale applications of the method appear feasible. The rough log and board cross section surfaces after poorly maintained saw webs definitely continue to be problematic for the analysis, but continuously improved saw cut quality at least in sawmills supports the practical implementation of the method.

In this section, we describe how to solve the color variation problems with a local thresholding in a moving window and principal component analysis (PCA) for prepared board cross section images. The size of moving window is chosen so that at each location of the window both the early wood and the late wood regions within a single annual ring are present. Within the moving window, the first principal component evaluated from RGB

channels was chosen for analysis rather than the original color channels or their average. This maximizes the contrast between the early wood and latewood. The other two PCA components were neglected. If all RGB components correlate fully and make equal contribution to the PCA result, the algorithm is reduced to studying the mean of the RGB components. Thus the method is the most powerful when the spectrum of lighting has little power in some of the RGB color channels. Latewood intensity variations between and within annual rings can be noticed in the first PCA score image shown in *Figure 41 (a).*

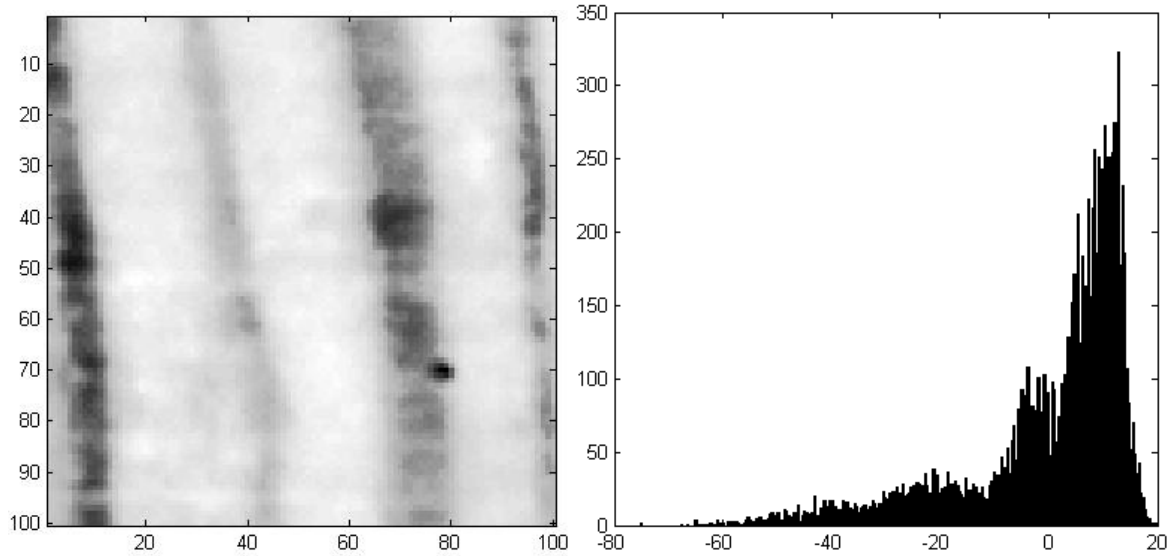

Figure 41. (a) The first score image of PCA and (b) Its histogram. The x-axis of the histogram describes intensity values after PCA. The y-axis tells the amount of pixels in the window representing each intensity value.

In the case of *Figure 41 (a)* thresholding is possible, whereas for the full original image or its PCA score image it would not give a satisfying result. *Figure 41 (b)* presents the histogram of *Figure 41 (a).* There are not only two peaks for high and low valued pixels, but there is also a large portion of intermediate intensities. We have chosen the threshold in a rather simple way: the histogram was thresholded with the mean of upper and lower 25% percentiles. The intensities of the lower percentile are supposed to belong to the latewood in high probability, and the intensities of the higher percentile to the early wood respectively.

The thresholds vary from window to window. The method attempts to segment clear annual rings from the current window by increasing color contrast although there are latewood areas with light colors. The method assumes that there is several color regions within the window whose color shades can be separated in two classes. Thus the method attempts to threshold almost even colored surfaces as well.

When the length of the move step of the window both in the x- and in the y-direction is chosen equal to or smaller than the size of the moving window, an entire binary image of individual annual rings can be constructed with the PCA score images. If the step is equal to the window size, corner shaped anomalies shown in *Figure 42 (a)* appear in the resulting binary image. The smaller the move step and the larger the overlap of adjacent windows are, the less and the smaller the corner anomalies and the better the resulting binary image will be. In the following, the results and the images are presented with maximum resolution, where the innermost pixels of the current window – the number of them equals with window step in x- and y-direction - are chosen for the resulting matrix after thresholding the first principal component.

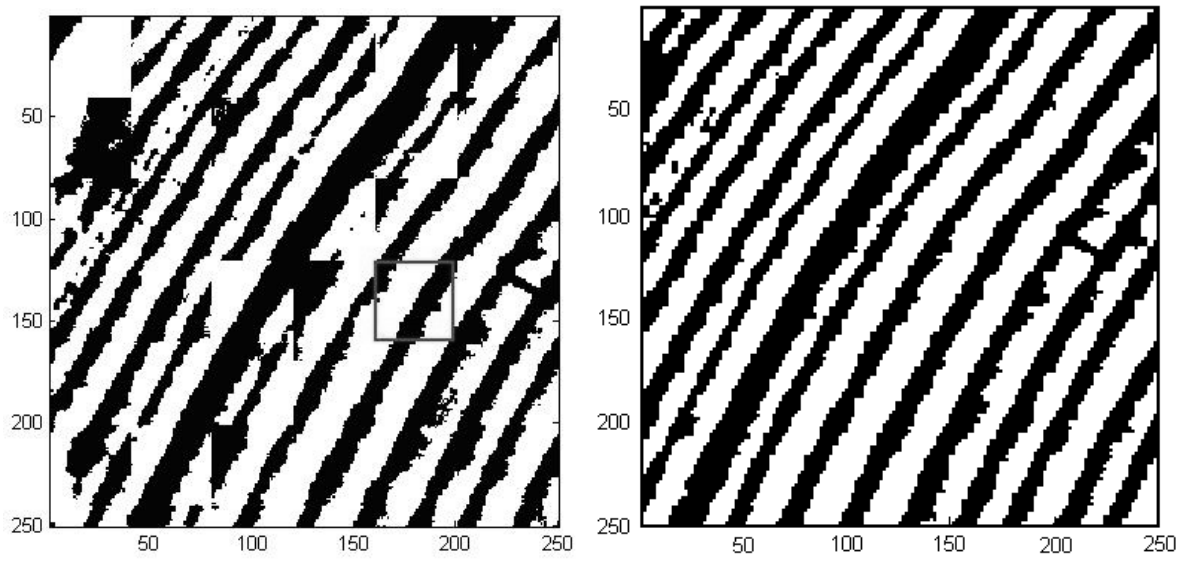

Figure 42 (a). Zoomed area of the result matrix. The corner shaped anomalies occurring near considerable varying colors in the original image. The anomalies cover some annual rings partially. The moving window can be seen as the square. Image (b) shows the window with corrected corner anomalies.

The corner anomalies arise as follows. In the example the window of size 40×40 pixels is chosen for a board cross section image, and the move step of the window is chosen equal to as the linear size of the moving window, i.e. 40 pixels. Therefore the original image is divided to 40×40 pixel sized disjoint windows and the PCA is carried out for all the windows. The result matrix is formed by combining all the blocks of thresholded first component score windows. *Figure 42 (a)* shows a window, which is a zoomed area of the binary result matrix, demonstrating corner anomalies. Comparing the window area with the upper left corner area of original image below in *Figure 43*, we notice in this region a

latewood stripe considerably darker compared with the adjacent stripes. This exceptional stripe distorts the shape of the local histogram and hence the threshold and causes the anomalies into the result matrix.. Anomalies may be either black or white corner shaped layers. In some cases corner anomalies may cover adjacent annual rings so that the rings cannot be discerned at all.

The problem was overcome as follows. The size of the moving window was maintained at 40×40 pixels and the threshold was evaluated as explained above. Now instead of placing the entire 40×40 pixel sized first component score image into the result matrix, only the center part of the score image was placed. The size of center part is optional, but it determines the length of the move step: e.g. center part of size 10×10 pixels requires that the move step of the window is 10 pixels. The size of the center part determines the maximum size of corner shaped anomalies as well. Thus, the smaller the center part is, the better is the result, however at the expense of computation time. The computation time increases in square of the inverse of the move step. The reason to choose the large window but preserving only the center part of result instead of choosing small window with the size of the chosen center part is that the moving window must be large enough to cover the widest annual rings.

The result matrix is enhanced with morphological image analysis routines. All disjoint areas, smaller than 20 pixels, were removed. After correction and enhancing the corner shaped anomalies can be fully removed as seen in *Figure 42 (b)*. For the image, the move step is only two pixels to obtain the highest correction level. However, the procedure slows down considerably because of the shorter moving step of the moving window. The step by step algorithm for separating annual rings is as follows:

Algorithm 10. Earlywood and late wood segmentation

1. A color image $I(x,y)$ of wood cross section surface is taken.
2. An image channel or their conversion is thresholded to make a binary template $T(x,y)$ assuming value zero to correspond to the background and value one elsewhere. The saturation component of HSI conversion is an appropriate selection in many cases, but the lighting arrangements affect strongly in the thresholding result.

3. The moving window *W* of size *M*×*N* is chosen.
4. The size *U*×*V* of the center part *C* in moving window *W* is chosen. Parameters *U* and *V* (smaller than *M* and *N*) determine the moving window steps in vertical and horizontal direction.
5. In each moving window location where *T(x,y)* equals with one the first principal componenet for the RGB components of the window *W* is calculated to enhance local image contrast.
6. The first principal component of each window is chosen for further analysis and its score image of size *M*×*N* is thresholded with the mean of the upper and lower 25% percentiles of the histogram.
7. The center part of size *U*×*V* is taken from the thresholded score image and added in resulting binary image *B(x,y)* in the location corresponding the original image location in *I(x,y)*.
8. All small disjoint areas i.e. holes and spots are removed in *B(x,y)*.

*Figure 43 p*resents the original RGB image of a prepared board cross section surface. The variations of the shades of brown within the image are clearly noticeable. In particular, the upper left corner has a very dark and thick latewood region in a single annual ring. There are large color variations between the early wood areas at different annual rings in the center area as well. Despite these difficulties, a rather good binary image, *Figure 44*, presenting the estimated areas of the early wood and the latewood within the individual annual rings is obtained with the method presented. The move step of the window was 2 pixels for the highest resolution possible with an even size of window and correspondingly the center part area was 2×2 pixels from each 40×40 pixel sized window for the PCA analysis. The resulting image is quite clear as manifested in *Figure 44*. Even the narrowest of the annual rings can be discerned in the binary result matrix. Probably the narrowest annual ring is actually “a fake annual ring” due to a cold period during spring so that the tree has produced two early wood and latewood rings in one year. However, the wood material of the darker part is similar to the normal latewood having smaller cells and thicker cell wall. Obviously, the fake annual rings may cause problems in counting the annual rings of tree for age assessment.

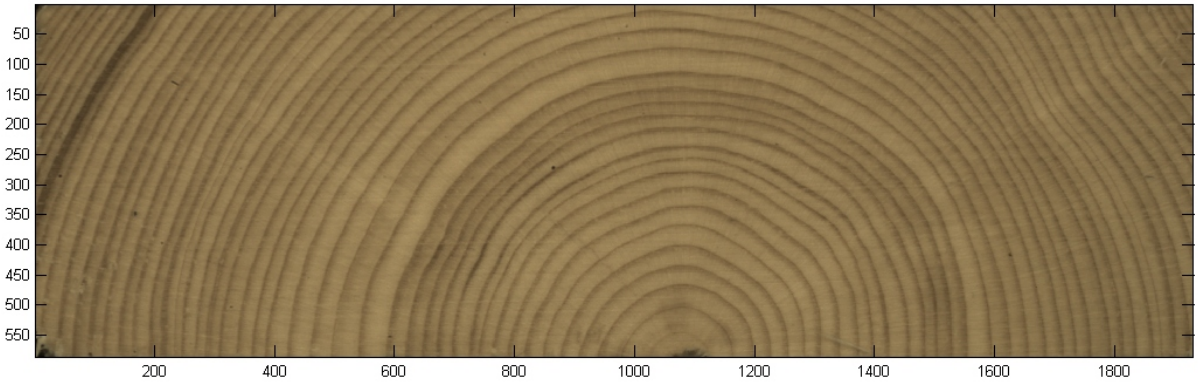

Figure 43. The original prepared board cross section image.

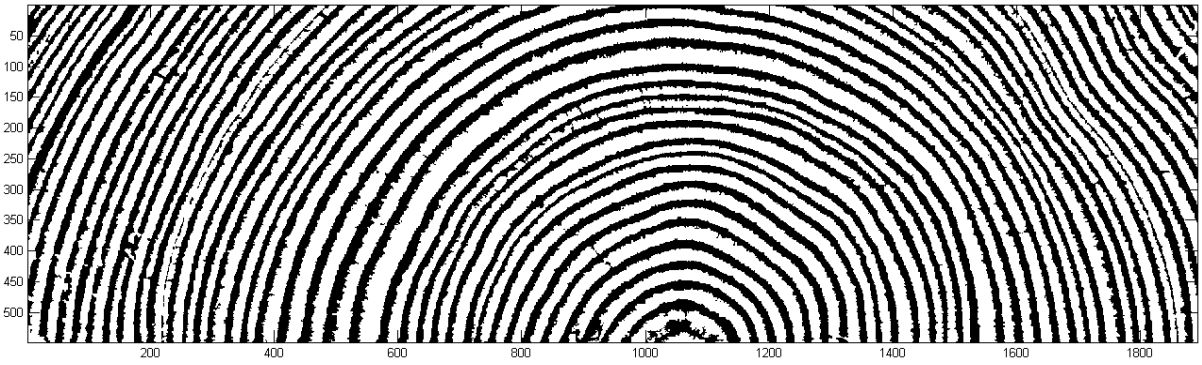

Figure 44. The resulting binary image after combining the PCA score blocks and enhancing procedure. The moving window size is 40x40 pixels, the center area size 2x2 pixels. Early wood areas are marked as white and latewood areas as black. Individual annual rings are clear despite varying color levels in the original image in Figure 43.

Figure 45 shows the result of the early wood and latewood separation more in detail for the annual rings in a zoomed region of another board cross section image. The result corresponds quite well to human visual evaluation. The horizontal color defect in the mid-region of the original image does not disturb the separation considerably. The smooth right hand side edges of the darker latewood stripes can be also noticed.

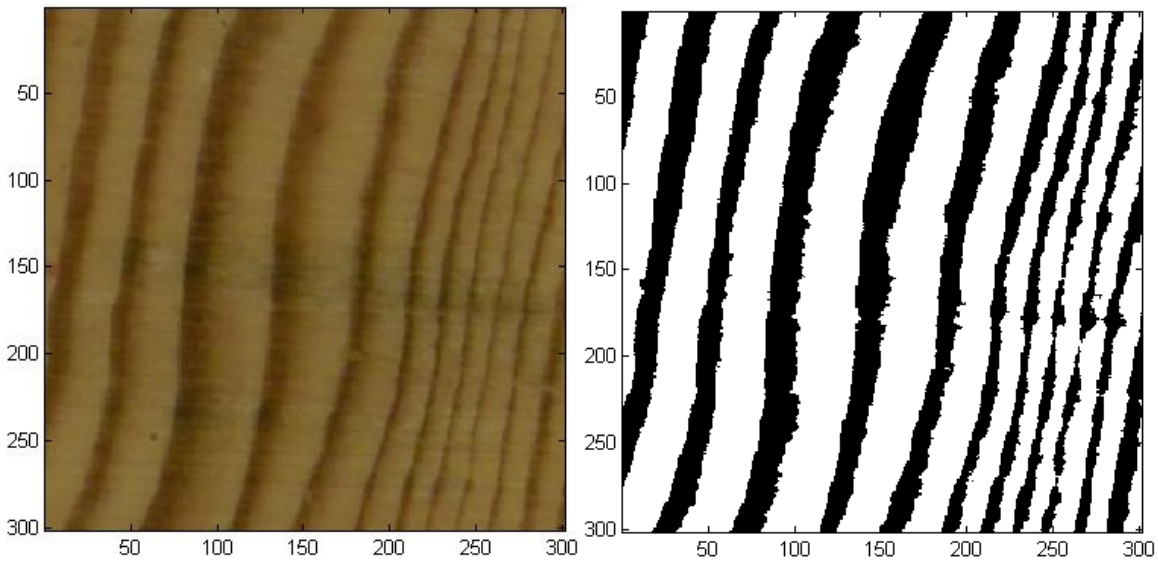

Figure 45. (a) The zoomed area of a sample surface. Note the smooth right edge of the darker latewood stripes and the horizontal dark color defect crossing the image (b) The result of early wood and latewood segmentation

6.3.3 Global and local latewood proportion analyses

The latewood proportion both globally and locally, is considered informative about timber strength in particular when measured from logs. Latewood region is denser than early wood region and thus latewood has better strength and stiffness properties [8][71]. With this information about latewood proportion, the sawing of logs can be optimized.

The moving window was found a useful tool for obtaining the estimate for the latewood proportion. Again the widest annual rings require a window size of 40×40 pixels or larger for images such as the one in *Figure 43*.

After constructing the binary image with early wood and latewood separated, the global estimate for percentage proportions of early wood and latewood within the entire log or board end is obtained simply by counting proportions of white and black pixels in the resulting binary image, such as in *Figure 44*. If the analysis is done for images taken from both undefected and prepared cross sections of a log or a board, the latewood proportion inside the log or the board can be estimated.

The length of the move step of the window is application specific. For global assessment it may be sufficient to know latewood proportion of a log or board from sample locations within the cross section surface only and the binary image revealing separate annual rings is

not always needed. Then the moving step both in x- and in y-directions may be chosen considerably larger than the window size (40 pixels in the example images). In such a case there are only a few samples (i.e. windows) taken from the log or board cross section image, but this is usually sufficient for obtaining a quick global estimate for the latewood proportion. The corner shaped anomalies within the sample window can be avoided using the same procedure as discussed in the previous section, but it is applied only within each sample window. Thus, the step of the moving window can be large to take only a few samples from the cross section images, but the step of the moving window should be small when moving the center area within each sample window to avoid the corner anomalies. The step by step algorithm for estimating global latewood proportion is following.

Algorithm 11a. Global latewood proportion

1. If binary image of annual rings *B(x,y)* exist the latewood proportion is the simply number of black pixels within the wood cross section surface in *B(x,y)*, i.e. the locations where *T(x,y)* equals with one.

If more rapid estimate for latewood proportion is required, but not the binarized annual rings, the algorithm follows the algorithm 10, with exception of moving window step:

Algorithm 11b. Global latewood proportion

1-3 Steps are as steps 1-3 in the algorithm 10.
4. The moving window step *s* for sampling is chosen. The size of sample windows equals with moving window.
5. The size $U \times V$ of the center part *C* in moving window *W* is chosen. Parameters *U* and *V* (smaller than *M* and *N*) determine the moving window steps within the sample window in vertical and horizontal direction until *C* moves outside the window.

6-7 Steps are as steps 5-6 in the algorithm 10.
8. The center part of size $U \times V$ is taken from the thresholded score image and added in the result binary image *B(x',y')*.
9. All small disjoint areas i.e. holes and spots were removed in *B(x',y')*.

10. The latewood proportion is the number of black pixels divided with the total number of pixels in the cross section surface area in *B(x',y')*.

note: *B(x',y')* is smaller than original image *I(x,y)* and now there are no continuous annual rings in *B(x',y')*.

The method of evaluating the latewood proportion locally within the cross section surface was developed based on the mean filtering. The latewood proportion field was estimated by counting the percentage proportions of black and white pixels within the moving window location. It can be made simultaneously when calculating the thresholded score blocks of the first principal component for the entire binary image of separated annual rings. These percentage values are inserted into the result matrix into corresponding locations as explained above.

Figure 46 presents the local latewood proportion as a field calculated simultaneously with the binary image in *Figure 44*. The move step of the window has been only two pixels as chosen in the previous section to obtain the best resolution for the binary image, however with the high cost of computation time. The darker a point in the image is, the higher the proportion of latewood in the neighborhood of that point.

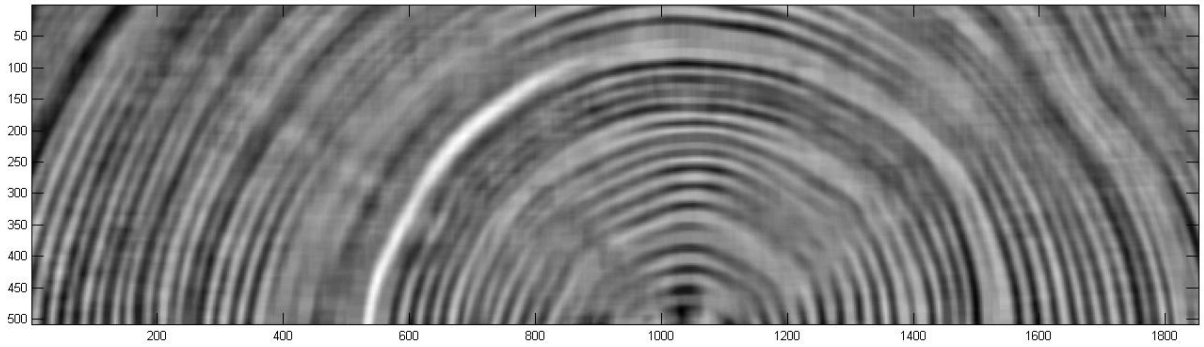

Figure 46. The local latewood proportion field presented as an image. The areas of high proportions of latewood denoted as dark. The ghost effect of annual rings is remarkable.

In *Figure 46*, the "ghost effect" of annual rings can be noticed within the local latewood proportion field as a short wavelength variation. *Figure 47* shows the origin of the ghost effect that depends on the frequency of the variation and the window size. The figure shows two extreme cases for a window, in which the black stripes represent latewood regions and white stripes represent early wood regions. In *Figure 47 (a)*, 1/3 of the pixels are white, thus

their evaluated proportion is 33.3%. In *Figure 47 (b)*, 2/3 of the pixels in the window are white, thus their proportion is 66.6%. When the window moves across the pattern, the proportion of white pixels varies between those values. For the window covering only one stripe, black or white, the proportion of black and white pixel within the window varies between 0% and 100%. Thus the variation decreases if the window size increases and frequency stays constant.

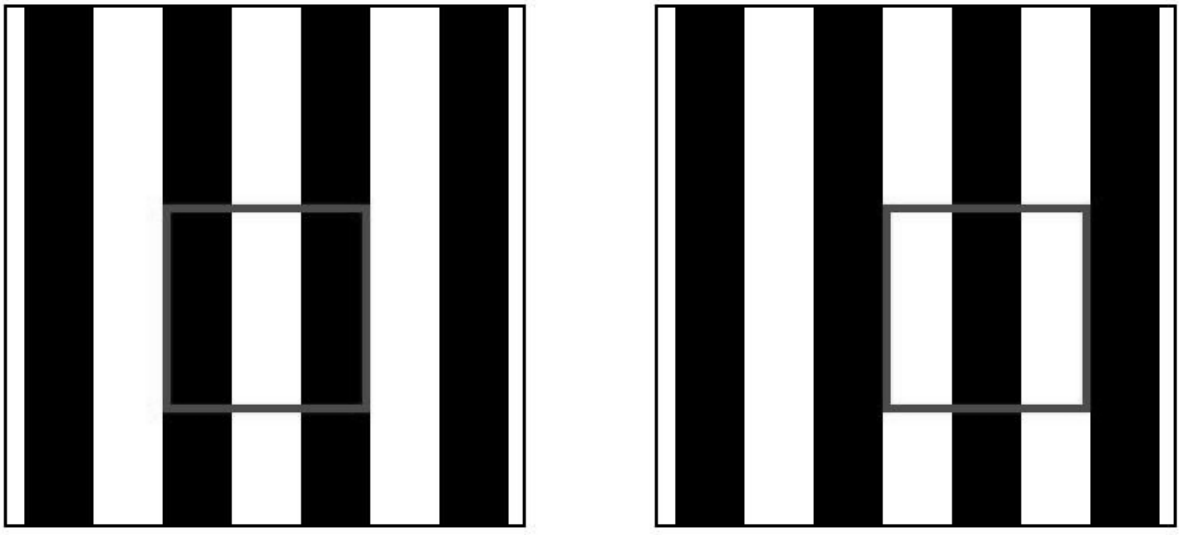

Figure 47. The visualization of the origin of the ghost effect. The proportion of black and white pixels varies according to the window location. If the window would cover the equal number of black and white stripes the variation do not exist.

We removed this variation with low pass filtering in frequency domain [47][133]. The latewood proportion image was expanded into a square. Values outside the latewood proportion field were filled with the mean value of the field. The square was Fourier transformed by using FFT. The cutoff frequency of the low-pass filter should be at most the inverse of the width of the widest annual rings and all the variations above this frequency were removed. Our cutoff frequency is 1/40 pixels i.e. the inverse of the vertical or horizontal window size. The low pass filtering was simply a sharp cutting edge in the frequency domain. Then the filtered Fourier transform was inverted to the spatial domain. The step by step algorithm for local latewood proportion is as follows:

Algorithm 12. Local latewood proportion.

1-7. Binary image of separated annual rings is created as described in steps 1-7 in subsection 6.3.2

9. During the previous procedure the proportion of black pixels in the center part *C* are counted in each location of the moving window. Alternatively: after the previous procedure the moving window is moved across the binary image *B(x',y')* and the proportion of black pixels in each location of the moving window is counted. Value is inserted in local latewood proportion matrix *L(x'y')* in location that corresponds the center of *W*.
10. *L(x'y')* is low pass filtered to remove the ghost effect.

Figure 48 shows the final result after filtering with cutoff frequency 1/40 pixels. When comparing *Figure 46* and *Figure 48*, the dark and light areas in corresponding locations can be noticed, but the high frequency variation caused by the annual rings almost vanishes and the high resolution of latewood proportion is retained. The resolution can be easily reduced by decreasing the cutoff frequency if not so precise local early latewood information is needed.

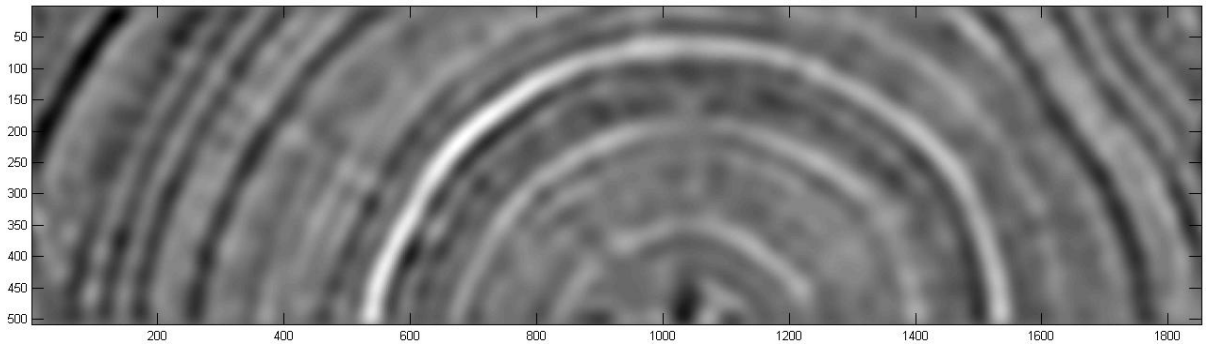

Figure 48., The local areas of high proportions of latewood are presented as dark points. After the spectral filtering of the image of latewood proportion field, the ghost effect of annual rings is removed.

6.3.4 Measuring the color of rot.

The Finnish Forest Research Institute has been modeling the propagation of rot inside the single trees. For this purpose wood disc samples were cut from several heights of rotten trunks in order to develop a model by which the amount and the severity of the rot at any

height can be estimated on the basis of the amount and severity of rot measured at a single height. A subtask in this modeling effort was to measure the color and area of rotten regions in the wood disc samples with the algorithms developed in this thesis work. The samples were photographed and the images were color calibrated. As high fidelity measurement was required for modeling purposes, the segmentation of the rotten regions was semiautomatic: the user determines the boundaries of rotten areas. The automatic rot detection methods discussed earlier, both the 2D-spectrum based texture analysis and the global thresholding based color analysis, cannot detect the rot boundaries reliably enough, in particular in the case of mild rot. Therefore the rotten areas were determined from the images with mouse. The images were thresholded using the user defined rot area boundaries. After color calibration the mean colors and the areas of the rots and the areas of the sound wood were measured. The measures from the set of trunks provide the identification data for the modeling. The results of the rot modeling research will be presented by Finnish Forest Research Institute.

Figure 49 (a) shows a fully rotten wood disc cut from 50 cm height above the ground. Rot is not very severe because the rot color is quite light and the annual rings are visible although the rot covers the entire disc. *Figure 49 (b)* presents a wood disc cut from the same trunk at the height of 390 cm. The mild rot is mostly visible as a darker ring. This mild rot is not problematic in pulp and paper making. However, in sawmill industry such mild rots are still color defects and these are avoided.

Figure 49. (a) A rotten wood disc cut from the bottom of the trunk. (b) The disc with mild rot cut upper from the same trunk.

7 Sources of Uncertainty in Imaging and Application Environment

An image based measurement system has several sources of uncertainty and errors. The uncertainty may originate from the imaging devices, i.e. cameras or optics, from the imaging arrangements or from the imaging environment. This Chapter reviews the sources of uncertainty with the emphasis on the uncertainty caused by the camera and its optics. Some of the sources of uncertainty were already discussed when calibration was considered, such as the image distortion. Thus only uncertainties and errors remaining after the calibration are discussed. In addition to the optical distortion, mechanisms that may locally blur the images or distort the color content are discussed. As Section 7.3 discusses, most of the sources of uncertainty are quite small and do not considerably affect the measurement results with methods presented in this thesis. However, one has to be aware of them and take them into account during the analyses and when making conclusions based on the results.

7.1 Sources of uncertainty due to imaging devices

Imaging devices, such as cameras, objectives and their lenses, cause always uncertainty in the image. The distortion caused by the lens system and the optics are called aberrations. The chromatic aberration causes color distortion in the image. The monochromatic aberration blurs or distorts the images. The blurring monochromatic aberration – spherical aberration, coma and astigmatism – are difficult to correct afterwards. Distorting monochromatic aberration – tangential and radial distortion and field curvature – can be corrected afterwards. They have to be taken into account in the image based measurements, because the distortions change the correct pixel locations and thus affect the measurement results. The distorting aberration is corrected with the camera calibration discussed in Chapter 4. The uncertainty of correction of distortion is discussed here. After that the effect and the uncertainty of scale calibration and color calibration are discussed. The blurring monochromatic aberration, such as spherical aberration, coma and astigmatism will be discussed briefly. Other visible blurring effects, such as blurring due to sampling and CCD-sensor implementation, are also discussed. [54][158]

Most of the sources of uncertainty, such as slight blurring, are negligible in everyday use of cameras. A small deviation of pixels from their correct location cannot be noticed without careful and detailed inspection of the image. In the measurement applications based on images, the distortion of an image and inaccuracy in locations of pixel produce distorted or increasingly uncertain measurement results. Similarly blurring of the edges makes the measurement more complicated. It is not always unambiguous with blurred edge, what is the correct pixel location of an edge of the object.

7.1.1 Image distortion and sources of uncertainty in camera calibration

Images taken with conventional camera systems have always some distortion, such as tangential and radial distortion. In addition, the field curvature distorts images. The image plane is slightly curved and a planar object will be imaged approximately as a plane only in the paraxial region, i.e. near the optical axis. Field curvature is typically disturbing at wide imaging angles and in the border areas of the image. The field curvature can be corrected using an appropriate combination of positive and negative lenses, but such correction has little effect on other forms of aberrations.

The imaging errors caused by radial and tangential distortion can be corrected with the camera calibration. The camera calibration corrects the field curvature also if the correction element is not in the objective. For instance, in Canon D30 Camera equipped with 3.11 megapixel CMOS-sensor and with a normal objective, the imaged positions deviate about three pixels from the correct ones in the corner areas. This represents about 3*0.37 mm/pixel = 1.1 millimeters error before camera calibration when imaged from a distance of 130 cm, the typical imaging distance in this study. The printing accuracy of the calibration target defines the quality of the camera calibration. The calibration targets can be printed on paper and attached to a rigid plate, but the best calibration results are obtained when the pattern is printed directly on a metal surface. Camera calibration provides the camera parameters such that by using those all the images taken with the same imaging system can be corrected.

When the pixel values in inaccurate locations are moved to their correct locations during the calibration process, there will be gaps in the image. Those missing pixel values are interpolated on the basis of the values of surrounding pixels. Obviously, the interpolation

causes blurring of sharp color edges. Correspondingly, the interpolation does not cause problems at similarly colored areas.

To obtain the best calibration results, the calibration target has to be absolutely planar: thus bending e.g. due to temperature variations must be controlled. All dimensions of the calibration target have to be accurate, which sets high requirements for the printing of the calibration target. The requirement for printing accuracy depends on the camera and imaging distance, but with the cameras and distances used in this study, the calibration target distances must be known with accuracy better than 0.1 mm, because the square corners are located at the sub-pixel level in the calibration software.

7.1.2 Sources of uncertainty in scale calibration

The scale calibration during this study was carried out using the calibration targets. The scale calibration targets are in each image and thus typically in the border areas around the object to be measured so that they do not disturb the imaging of the object to be measured, whereas the camera calibration targets cover field of view. Obviously, the camera calibration should be made before the scale calibration. The scale calibration is particularly sensitive to distortions due to the location of the calibration targets. The requirements for the printing accuracy of the calibration target are high in both cases. The automatically recognized known points in the scale calibration target should be as far apart as possible to minimize the scale conversion uncertainty caused by the inaccurate locations of the points. With our checkerboard pattern of 10.0 mm × 10.0 mm squares, locating the two nearest corners of a square with the accuracy of 0.5 pixels and counting the pixels between them, we obtain a result that one centimeter corresponds e.g. 37 pixels with ±1 pixel tolerance (±0.5 pixels in both locations). If we instead locate the corners of the row of 10 squares with same accuracy, we obtain that 100.0 mm distance between those points covers e.g. 372 pixels and thus we get the result that one centimeter distance corresponds 37.2 pixels with tolerance of ±0.1 pixels.

If the correspondence between the object distance and its size in pixels is known, the scale calibration can also be made using the distance measurement. In this case the scale calibration uncertainty is typically dominated by the uncertainty of the distance measurement devices, for instance lasers. Typical uncertainty of the consumer distance measurement

lasers is approximately ±1 mm. Furthermore, the unevenness and out of perpendicularity may increase uncertainty in scale calibration, but these can be reduced by using several distance measurements. However, it is noteworthy that the poor camera calibration does not disturb the scale calibration made with the object distance measurement, which is contrary to what happens in scale calibration with the calibration target.

7.1.3 Sources of uncertainty in color calibration

High requirements are set for the quality of the color calibration target. If the color calibration target is printed with conventional printers, the white color (typically paper color) is not absolutely white, nor is the printed black color the absolute black. Printed color shades are not exact. Excellent color calibration plates are produced commercially and their use is strongly recommended. It is possible to measure the exact colors within the object with the color calibration target having colors standardized in this manner. If the colors of the calibration target are under non-uniform light the calibration is distorted.

In the study, the measurement of absolute colors was not an essential part of the color calibration: only getting the colors comparable between different images. The relationship between the colors and the detected intensity values was identified with a few gray shade regions printed on a paper calibration target. One of the images was fixed to be basis and the colors in other images were adapted to the first one. The printing properties of the laser printer and the uneven lighting caused that the calibration function deviated slightly from linear.

7.1.4 Chromatic aberration

The different wavelengths of light refract in objectives differently in the boundary between the lens glass and air. This phenomenon is known as the chromatic aberration or color aberration [54]. The chromatic aberration may change the colors at the edges between areas of different color. Wavelengths emitted from a given point are not projected exactly to same location at the imaging sensor. The longer the focal length, the larger is the color aberration. In particular, at high contrast edges in the image, the aberration is notable. Chromatic aberration can be reduced with achromatic lenses, in which materials with differing dispersion are assembled together. There are special designs of lenses decreasing the

chromatic aberration as well, but it is difficult to remove chromatic aberration completely. *Figure 50 (a)* illustrates the principle of chromatic aberration: different colors have different foci and are thus diffracted to different locations on the array sensor. *Figure 50 (b)* shows that diffraction can be reduced using achromatic lenses. *Figure 50 (c)* shows that special design of lenses can also decrease the color aberration.

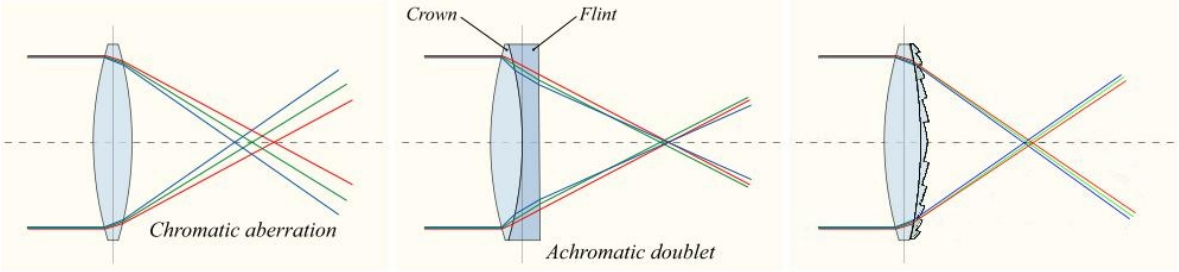

Figure 50. (a) The principle of chromatic aberration. (b) The correction with the achromatic lens. (c) The diffractive optical element.

Figure 51. The zoomed corner area of a calibration target with checkerboard pattern. The chromatic aberration can be noticed clearly at the vertical edges of squares. The upper edge is reddish and lower edge greenish. The edge blurring derives mainly from sampling and Bayer-interpolation and covers 3-4 pixels between the black and white regions.

Figure 51 shows a color image of the zoomed corner of the calibration target with checkerboard pattern. The image has been taken with a wide angle lens. The color aberration is clearly visible. The upper vertical edge between the white and black square seems to be reddish, whereas the lower vertical edge below the previous edge and between the black and white square seems to be greenish. The same effect is noticeable also with horizontal edges.

7.1.5 Edge blurring due to Bayer-interpolation.

In the CCD and CMOS sensors the red, green and blue sensors are tiled to a Bayer-matrix structure. The spatial resolution of the color channels is poorer than the sensor resolution. Thus all color channel images have gaps filled with values interpolated by using the values of the surrounding pixels. Although the theoretic black and white square edge were just at the edge between two pixels, the interpolation of Bayer matrix data blurs the edges between different color regions.

Each camera manufacturer has a proprietary Bayer interpolation algorithm to fill the gaps of the color channels. In particular, at the edge of the color regions, the interpolated values tend to be incorrect and thus the combination of the channels may produce unwanted colors. This effect may be noticed at the edge as a slight color variation when the edges are not parallel to pixel rows or columns. However, they may be present and mixed with color aberration.

7.1.6 Edge blurring due to sampling

The array sensor of a digital camera digitizes the field of view through the objective. The pixels receive the emitted light from the objects. The sampling of a continuous view causes the edge blurring because the color edge hardly ever happens to be exactly at the edge between two pixels. When imaging for instance the checkerboard type calibration target, the edge between the black and the white squares is always blurred in the image. In the theoretical situation with perfect light, perfect colors and appropriate exposure, an 8-bit sensor detects the intensity value of 256 for the white region and 0 for the black one. At the edge between the black and the white squares, there will be a blurred pixel. The gray level of the blurred pixel depends on how much of the white region and the black region the view for the pixel covers. The darker the gray level of the blurred pixel, the nearer the edge is to the

adjacent black pixel. However, this is possible to use in locating the edge at the sub-pixel level, if the real edge is known to be sharp.

In addition to color errors, *Figure 51* demonstrates clearly the blurring of the edge. When inspecting the image, 3-4 blurred pixels can be noticed at the edges between black and white squares. The visible edge blurring is mainly derived from sampling and Bayer interpolation discussed in previous sections.

7.1.7 Blurring monochromatic aberration

In addition to the forms of aberration discussed above, the optical lens systems have blurring aberrations even when the light is monochromatic. However, this is mostly corrected by the additional lens elements of high quality objectives. Thus the uncertainty is typically small and hidden under more significant effects such as the sampling and Bayer interpolation.

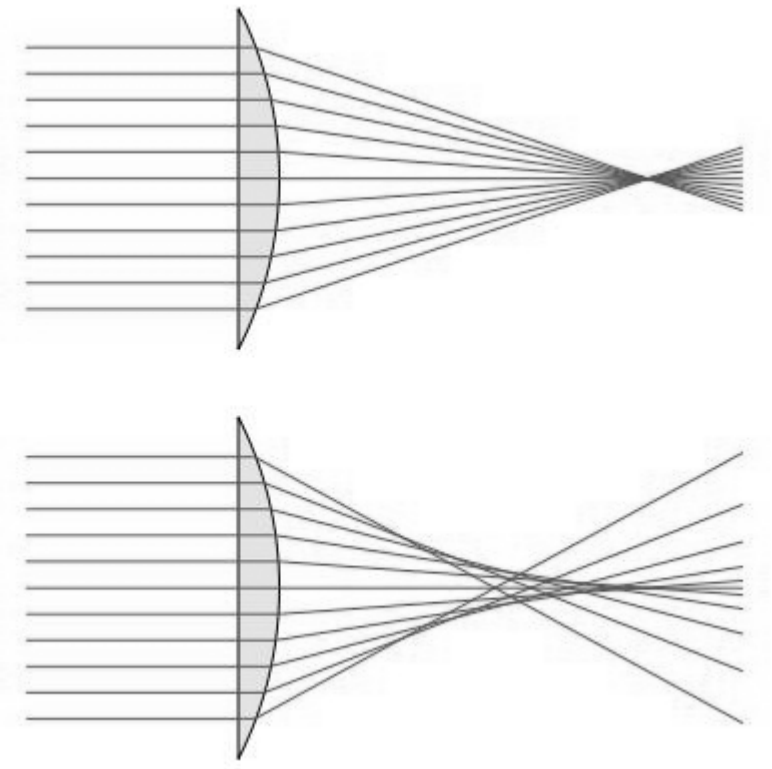

Figure 52. (a) A perfect lens focuses all the light rays on the same focal point in the top image. (b) Spherical aberration causes that light rays intersects the optical axis in different locations and focal point is not exact.

Spherical aberration is a phenomenon, in which the light refracted from the border areas of a curved lens intersects the optical axis in a location different from that of the light refracted from the center area of the lens [54]. This means that the rays of light have a different focal point. Spherical aberration causes blur in the image. It can be corrected with an appropriate combination of the positive and the negative lenses that have an appropriate combination of refraction indices. *Figure 52 (a)* shows the perfect lens without spherical aberration. All the incoming light rays have the same focal point. A lens suffering from the spherical aberration is shown in *Figure 52 (b)*: the closer the lens is to the focal point the further away from the optical axis the incident ray is.

Even when the spherical aberration is corrected, the rays refracted from the border areas will intersect the optical axis in a different location, if the object is not on the optical axis. This is known as the coma or the comatic aberration and it can be noticed as blur in the border areas of images [54]. *Figure 53* shows the principle of the coma. The object point is assumed to be at infinite distance, and thus incoming rays are parallel. The rays of the point light source coming through the lens center are projected correctly to the single point. The coma effect produces increasing circle artifacts adjacent to the correct location. The coma effect exists in all lens systems, but it is best known in astronomy, because it is a notable error source in telescopes and makes discerning stars close to each other impossible.

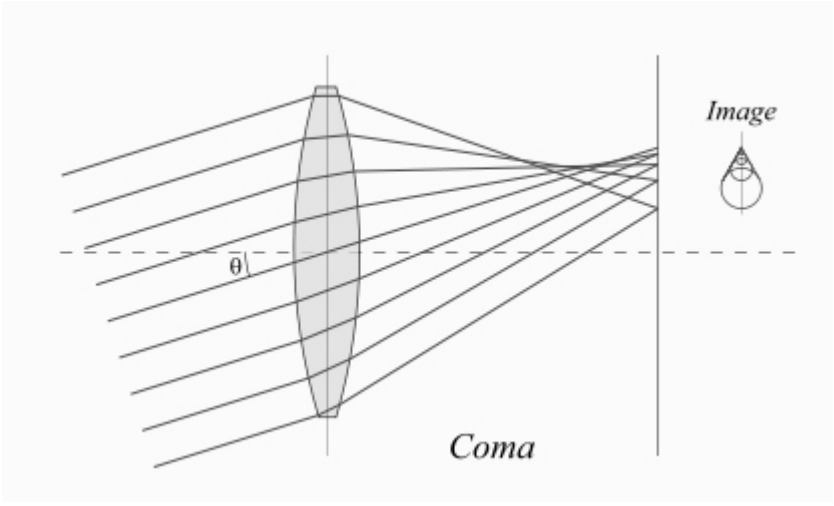

Figure 53. The coma effect on a single point produces the growing circles

Astigmatism is a monochromatic aberration that occurs when an optical system has different focal points for rays that propagate in two perpendicular planes [54]. It is caused by the imperfect grinding of the lens surfaces. Astigmatism is quite common in human eyes.

Astigmatism can be minimized with an appropriate lens combination. *Figure 54* shows the principle of the astigmatism. The light rays propagating from the object point P in two perpendicular planes have their focal point in different locations. T_1 shows the focal point of vertical rays and S_1 the focal point of horizontal rays correspondingly. The optical axis is marked between Q and Q_1.

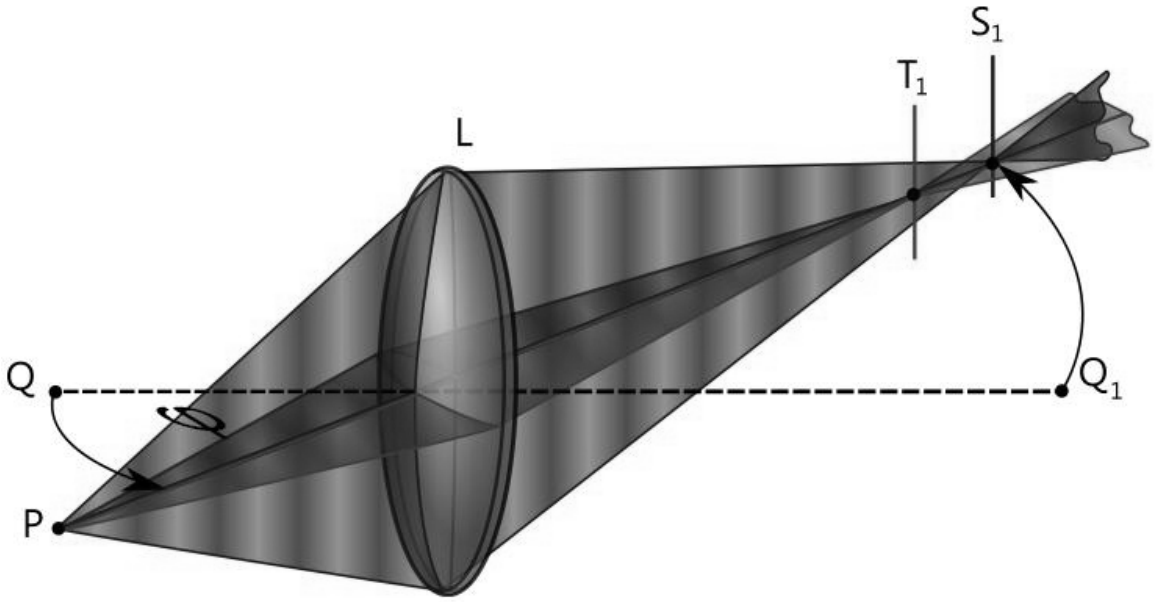

Figure 54. When light rays propagating through the lens system in two perpendicular planes (blue and red) have different focal points, astigmatism exists.

As a summary, most of the types of aberration discussed can be corrected or minimized using correction elements in lenses. Thus the high quality objectives for cameras may consist of tens of lens elements ground to match one another.

7.1.8 Other camera based sources of uncertainty

Vignetting is the phenomenon in which he camera optics causes the gradual fading out of the image at points near it is periphery. Although the lighting was even, the vignetting may be noticed in image corners. However, the effect of vignetting is removed as a part of correcting the effect of uneven lighting by imaging a white planar surface.

In addition to lenses, the cameras itself may cause errors in the images. Imaging sensors are sensitive components and several types of error disturbing images may occur. Even the new camera sensor arrays have some inactive pixels. The missing information is interpolated

based on the data of the surrounding pixels. In a CCD array, the charge may overflow or penetrate from a pixel to an adjacent pixel with various mechanisms under suitable conditions [63]. The background noise may blur the images with any type of sensor. The noise level depends e.g. on the properties of the sensor and the imaging temperature. However, the background noise is the most harmful in dark imaging conditions when the signal to noise ratio is low.

The exposure time, determined with the camera shutter, is the duration of photon collection to pixel charge wells. The aperture value determines the size of the hole through which the light gets to the camera sensor. By increasing the aperture (decreasing the numerical aperture value) increases the number of photons observed at the sensor array, when the exposure time is kept constant. However a larger aperture may blur regions in the image because of a shallower depth of field. A long exposure time may cause problems in online applications, because the processing time may be very short and the object may be moving rapidly. Time for imaging and image processing may be some tenths of seconds. For instance in the sawmill environment, the speed may be three objects per second.

Obviously, the inaccurate focusing blurs the edges of the image. Both underexposure and overexposure deteriorate the image quality. If one of the three image color components is overexposured only in a small region, it distorts the image colors in the region. The overexposure of a small region on the single color channel is quite difficult to notice with naked eyes. However, it is easy to recognize the overexposure computationally.

7.2 Other sources of uncertainty

This section describes uncertainty caused by the imaging arrangements, such as the camera positioning, the location of the calibration targets and the unevenness of the cross section surface of the wood. The uncertainties due to the algorithms, such as locating the peak in the power spectrum or the choice of the thresholding level are discussed.

7.2.1 Sources of uncertainty caused by imaging arrangements

The imaging arrangements affect the image quality and thereby also the measurement results. The cross section surface was assumed to be planar and perpendicular to the optical

axis of the imaging system. However, it is impossible to meet this requirement exactly, and thus the image suffers always from a perspective distortion. The perspective distortion can be corrected computationally, which, however, requires additional information, e.g. in case of this study based on targets in scale calibration. In photogrammetry, the aerial images are typically tilted, and thus have a perspective distortion that must be corrected. Conventionally, stereo imaging is used to correct the errors of perspective distortion in the construction of maps from tilted aerial photographs [158]. In stereo imaging the distance to the image points can be measured using a second image taken with another camera or with the same camera moved a known distance. As an alternative the distance to the object can be measured actively with e.g. a laser distance measurement device. If the object is planar (such as the log cross section surface should be), only three distance measurements are needed to identify the surface position. The calibration target with checker board pattern located in the image can be used for detecting the orientation in the close range measurements. Thus the scale is known across the image and the correction parameters are known.

The thickness of the wood discs imaged may vary. Typically, the calibration target is attached to the background board and hence it is not in the same plane with the wood disc surface imaged. In the case of imaging the cross section surfaces of logs, the positioning of the calibration target may be problematic. Thus an error occurs in measurement results if the distance between the camera and the cross cut surface is different from that between the camera and the calibration target. The effect of the error was evaluated by imaging the calibration target at two distances, 100 cm and 98 cm using the Nikon D70 camera. The setting simulates the situation we have the 2 cm thick wood disc or the calibration target is 2 cm away from the correct position of the face of the full log end. The scale of 6.29 pixels per millimeter for the closer calibration target was measured whereas the corresponding scale measure for the calibration target 2 cm further was 6.17 pixels per millimeter. This means that the error for the single pixel was 0.0032 mm, but obviously the error analysis is valid only for this camera and distance. For an object covering the full camera view, the measurement error is approximately 9.7 mm. Thus this is the maximal error due to the 2 cm distance difference between object surface and calibration target. The relative error is a bias of about 2%.

It may be happen that the trunk is not cut properly and the cross section surface is not perpendicular to the log center axis. The oblique cross section surface produces errors in the

measurements, the reason being the perspective distortion discussed above. The evaluation of the effect of the small distance difference in the previous section is valid here as well. If the log was cut so that one edge of the cross cut surface is 2 cm closer than the opposite edge, and the log cross section covers the field of view it means again 2% relative scale error for the edge pixel that is away from the correct distance, when using the Nikon D70 camera with 100 cm distance from the object.

7.2.2 Sources of uncertainty due to algorithms

Obviously, the implementation of the algorithms affects the accuracy of the measurement results. The algorithms may recognize the features of the images incorrectly and assess their dimensions inaccurately. The problems may originate from various reasons. The quality achievable in cross section surface preparation - sawing or sandpapering devices - sets additional requirements for the algorithms. Typically the saw marks are parallel, possibly bending streaks and in some cases the algorithms may confuse them with the stripes in the annual rings. The marks originated from wood processing devices are visible in the 2D Fourier power spectrum and may produce additional peaks in the spectrum. The high spectrum peak originating from severe saw marks may be chosen as the dominating frequency instead of the spectrum peak corresponding to the annual ring pattern.

The size of the moving window affects the uncertainty in measurement results. A large window may give more accurate results. However, such results may no longer describe the local behavior of the annual ring pattern with spatial resolution required. If the moving window is too small, at some locations the moving window may not cover a single annual ring, and thus the peak of the spectrum is not produced correctly according to the annual ring width and orientation.

Most of the algorithms discussed in the thesis were based on the local 2D Fourier power spectrum evaluated with the moving window. The properties of the annual rings were estimated on the basis of the location of the dominating peak in the spectrum. Thus any inaccuracy in the location of the peak limits the accuracy of the measurement results. In the 2D Fourier power spectra the angular resolution of the low frequencies is poorer than that of the high frequencies. However, accuracy when locating the spectrum peak can be increased when detecting the peak location in the sub-pixel level as discussed in Chapter 5.

The algorithms that recognize defective regions within the log or board are not able to recognize the defect types. Thus stains and dirt on the cross section may be considered as defects.

Thresholding is a typical method of segmenting the image with color and intensity information. A small change in threshold may change the area of the rotten part notably, in particular in the mildly rotten areas. The correct threshold level is difficult to determine, even visually. Similarly, the measurement result obtained with the algorithm measuring the latewood proportion depends highly on the threshold level. The algorithm does not have exact threshold level, but it varies from window to window according to data within the current moving window. Indeed, it is nearly impossible to set the exactly correct threshold level without analyzing individual wood cells, their cell wall thicknesses and the size of the lumen. However, the methods developed are quite well in accordance with human visual assessment.

7.3 Effect of sources of uncertainty on wood quality measurements

The sources of uncertainty discussed above affect the measurement results. This section discusses the most important uncertainty sources of the algorithms and analyses developed.

In this thesis the imaging conditions were arranged so that the lighting has a wide spectrum and high power. Thus the color intensities were quite high, the signal-to-noise ratio was good, and the effect of the sensor noise was negligible in the measurements. After camera calibration the lens distortions, such as tangential and radial distortion and field curvature, were corrected and their effect on measurement results was evaluated to be negligible. The high quality objectives with several correction lenses were used, making the effect of optical monochromatic aberration negligible.

The local annual ring width measurement with the 2D power spectrum was based on the locating of the highest peak in the spectrum. Thus the resolution of the power spectrum and the accuracy when locating the peak have a large effect on the accuracy of the results. In addition, the accuracy of scale calibration is relevant for the accuracy of the ring width measurement, because the pixel results need to be converted to millimeters. The accuracy of

the locations of the corners of the squares in scale calibration is reduced by the edge blurring between the black and white squares. This edge blurring originates from sampling, Bayer-interpolation, camera calibration interpolation and color aberration. The edge between black and white color regions may be spread over 5-6 pixels. However, the effect of the blurred edges in scale calibration can be reduced, if the distance between the points for which the calibration is based on is maximized. The small difference in distances of the cross cut section surface and the calibration target to the camera caused an error less than 2% in the measurement results in the real world distances. The manual positioning of the camera and the possible unevenness of the wood cross section surface caused both the uncertainty of a few percent.

The annual ring orientation measurement, the pith locating algorithm, the defect detection, the identification of the inner/outer side of a board, the estimation of the board curvature and the algorithm for counting annual rings were all based on the 2D Fourier power spectrum. Thus the accuracy in the location of the dominating peak in the spectrum is a perquisite for accurate measurement results. However, in spite of several incorrect locations of spectrum peaks in different image locations, the algorithms are able to produce the correct result. As none of these algorithms require scale calibration the edge blurring mechanisms do not cause uncertainties or errors.

The algorithm for tracking the annual rings is also based on the 2D power spectrum. Thus an accurate location of the dominating peak in the spectrum is a perquisite also for this algorithm. In this algorithm, any inaccuracies in the peak location may cause large deviations in several annual rings as the algorithm integrates such errors. This algorithm does not depend on scale calibration and the edge blurring is irrelevant.

The evaluation of the shape of the log cross section with respect to the pith is mainly dependent on the accuracy of the estimate of the pith location. If only the outer shape of the log is required the conversion to polar coordinates is made using the geometric center, and the accuracy of the pith location is irrelevant. The blurring of the edges does not disturb considerably segmenting the log cross section from the background.

The bark thickness measurement is influenced by several sources of uncertainty. Sampling, Bayer interpolation and chromatic aberration blur both of the bark edges and affect the scale

calibration needed. The positioning of the camera and the distance difference between the calibration target and the log cross section surface affect the measurement result through the scale calibration.

The uncertainty in the thresholding level for the PCA score image causes the uncertainty for the algorithms separating and measuring the proportion of latewood. However, the late wood boundaries obtained correspond rather well to the, human evaluation although no detailed statistical analyses could be made because of the workload in human segmentation.

For semiautomatic rot color measurement, the inaccuracy of the color calibration is the main source of uncertainty. Vignetting and unevenness of the lighting cause problems unless they are not corrected by analyzing the intensity profile by imaging a white board. Obviously, the edges of rot determined by human affect the color measurement.

8 Discussion

This Chapter discusses the achievements of this study and their applicability in industry. The feasibility of the methods and the algorithms in industrially relevant application environments is discussed. Further studies on the measurement setup, the methods and the algorithms are proposed so that commercial products can be developed. The general requirements for real-life applications and ongoing application development are reviewed shortly. The application possibilities of the methods related or different areas are envisioned at the end of the Chapter.

8.1 Main achievements

In this thesis, a set of analysis methods for wood cross section images have been innovated and developed. Furthermore, a review of the geometry and quality properties relevant in forest industry, a review of existing wood measurement methods and applications were presented, and the scientific research for the wood measurement was discussed. Based on this analysis the technology gaps were identified for the motivation of this study. The reliability and uncertainties of the image based measurements were discussed. The methods developed can be utilized in the analyses of wood quality and geometry properties and these algorithms fill some of the gaps indentified in the technology review. The methods presented are not yet ready for full-scale applications, but they provide an algorithmic basis for further development of industrial applications. The major advantage of the camera based methods is that they are rather inexpensive in comparison with many competing technologies.

The methods based on power spectrum are quite robust. The algorithms named as Thickness field of annual rings, Orientation field of annual rings Defect detection, Locating the pith, Board side and curvature detection and Counting of annual rings work well for unprepared and partly defected cross section images, when annual rings are mostly visible. The robustness of Annual ring tracking algorithm was reduced due to the integration of errors. The methods based on geometry, Log end shape measurement and Bark thickness

measurement, work rather well for unprepared cross section surfaces of wood when the cross section surface can be segmented from the background. Thus the imaging environment has a considerable effect on the measurement. Early wood and latewood segmentation and latewood proportion analyses required a prepared cross section surface, but the methods work well after preparation. Bark area measurement with the global thresholding may be feasible, but the color analysis and the global thresholding based method for rot area measurement seems to be difficult to develop.

The methods developed were tested with many images taken with various devices and under various lighting. Three systems cameras and a scanner were used for the log and board cross cut surface imaging. Most of the images were taken from samples such as wood discs and blocks, but full logs and boards were also tested. The flash light, tungsten light, conventional bulbs and normal room lighting were used for illumination. Images were taken in distances varying from about 0.5 – 2 meters. Images were taken from cross section surfaces prepared with sandpaper, but unprepared surfaces sawn with sharp chainsaw as well.

The accuracy of the measurement results is rather complicated to evaluate due to time-consuming manual reference measurements. Thus data has not been extensively analyzed with statistical methods. For instance, the method for evaluating the local annual ring widths actually measured the dominating annual ring width in a small local region, and these measures were achieved throughout the cross section surface. The reference measurements for ring width and bark thickness were obtained manually with a ruler and thus the reference was both sparse and subject to considerable uncertainty itself. The accuracy of the orientation measurement, the pith location, the inner/outer board detection and the defect detection is easy to assess roughly by visual inspection of the original wood samples or images and the analysis results obtained. The accuracy of the annual ring counting algorithm was compared with a human counting from the image or from the original sample. Analysis results of the methods were presented and conversed with experts in the Finnish Forest Research Institute, and the results were considered to be promising.

However, the performance of the measurement of average thickness of annual rings was tested in research made by VTT [51]. They compared several measurement techniques to estimate the strength of timber. The author of this thesis measured the mean thickness of the annual rings in both ends of 100 pine and 100 spruce boards with the method described in

Subsection 6.1.1. VTT compared the measurement results against their own strength measurements. The R^2 values for estimating the modulus of elasticity (MOE) and modulus of rupture (MOR) were between 0.35…0,53. R^2 values were slightly better for spruce than for pine, and slightly better for MOE than MOR. The R^2 values were in the same range as those obtained with the manual density measurement, the acoustic measurements of logs and close to X-ray measurements of logs. The best R^2 values were obtained with X-ray measurement of boards, in the range 0.7…0.8. When the measurement of annual ring width was combined with knot analysis, the R^2 values were between 0.52…0.60.

8.2 Opportunities to fill the technology gaps with image based methods

The goal for studying image based wood measurement methods was to provide knowledge that can be utilized in machine vision based application development for the forest industry. Plenty of information about wood properties, including even internal properties, can already be obtained, but the existing devices, such as X-ray based, are large and require careful shielding, are expensive, and consume considerably power. Not all the existing measurement devices can be replaced with systems based on color cameras, but such systems are able to provide information that has been more difficult or more expensive to obtain. Cameras, imaging sensors and computers for image processing are quite inexpensive. Thus the camera based solutions may produce add value to wood products with relatively small investments.

However, industrial applications of the methods developed require good quality cross section surface images of logs and boards in the real industrial environment. Sawing causes considerable marks in particular on the log cross section surface, and these marks may blur the annual ring pattern. To obtain the quality measurements with the image analysis algorithms discussed in the thesis, the overall annual ring pattern is required to be visible, but this does not mean that each individual annual ring must completely visible. The 2D Fourier power spectrum based methods are insensitive to missing ring segments. The analysis methods may succeed even if the annual ring pattern is visible only here and there, because the texture methods analyze the local annual ring pattern, not the individual annual rings. At present the sharpness of the chainsaw chain has not been optimized for image based measurements. Cutting marks can be reduced considerably and wetting can be used for improving the contrast in the images. With the high economic potential of measurements,

cross section surfaces of logs and boards will be improved to be better suited for image based measurement solutions. Thus the measurement setup should be thought to incorporate the properties of cutting equipment.

The image based measurement methods developed can be applied through the wood supply chain, from forests to mills. The present harvester head measurements are limited to dimension measurements of logs based on mechanical systems such as feed rollers, and quality assessment is made only by the human harvester operator. Detailed and reliable quality measurements in forest have the potential of changing the supply chain radically and increasing value of wood. The advantage of the image based harvester measurements is that the cross section surface of the log is typically fresh and it is not contaminated by dirt, mud and decay that are often caused in transportation and storing. The evaluation of the annual ring width, the number of annual rings, the diameter under/on bark, the eccentricity etc. can be used in sorting the bucked logs into the piles according to the quality in the forest stand. A much finer grading according to quality than the present one would be possible.

Today the sawing optimization is almost entirely based on the outer shape of the log. Only the largest sawmills have X-ray based devices for the detection of internal defects. In some cases, the X-ray device can be used to detect heartwood and sapwood regions of the log. In the sawmills, the image based measurements for the thickness of bark, for the number, the widths, and distribution of annual rings in the log, latewood content, the log eccentricity and the ellipticity, the presence of visible defects such as rot, color defects and cracks can serve as the basis for optimizing both the geometry and the end product quality in sawing of logs. If the log is not round and has different annual ring widths on opposite sides, this can be taken into account so that boards of constant quality are obtained. After the sawing, the analysis methods presented for the cross section surface images of wood can be utilized. The annual ring widths and latewood content are known to be informative about the board strength. The local variation of the widths of annual rings and latewood content can be used to indicate the uniformity of quality of the board. The bending properties of board and whether the board is sawn from the heartwood or sapwood region of the log can be analyzed with the curvature of annual rings and the estimated pith location.

In the pulp mills state-of-the-art measurement stations measure the volume of the sample set of the incoming wood with devices based on lasers and cameras. Quality continues to be

measured by a human observer. Therefore intelligent quality measurement devices have a vast potential. The measurement of the width of the annual rings would increase further the economic potential of quality information. If images of high enough quality are available, the latewood proportion can be evaluated. A high content of latewood within logs is supposed to reduce the brightness of logs. Furthermore, transportation and storing of pulp wood logs reduce the brightness of pulp wood and thus more bleaching agents are needed in pulping or paper making. If the latewood ratio cannot be measured directly, the mean color in the cross cut surface of a single pulp log or the mean color of the cross sections of all the pulp wood logs in a pile can be evaluated as indirect information about the ratio.

In the plywood industry, machine vision systems based on cross section surface analyses can be used when positioning the log according to the roundness before peeling. The system can also sort out eccentric logs. Pith location and annual ring information can be utilized in peeling the logs according to annual ring locations, and thus a ply obtained would supposedly contain less transitions from early wood to latewood and vice versa. The plies were more uniform than today and the strength of the plywood boards might be increased. The density of a ply can be controlled during turning when the widths of annual rings and the latewood content are measured.

8.3 Future opportunities in method development

The methods developed during this research are only a basis for the further development of method and applications. Improvements to the algorithms presented and entirely new algorithms are desirable for image based wood measurements. However, novel algorithms tend to require more computation capacity. Here we will discuss how the algorithms presented in the thesis can be improved further and how image based wood measurements methods can be utilized more effectively.

The defect detection algorithm based orientation and frequency analysis needs to be enhanced to defect identification algorithm. The shape of the defected area and its position relative to the pith are parameters that could be taken into account in defect identification. Knots are typically located radially relative to the pith whereas the orientation of severe rot, dirt or stain is ambiguous. It is characteristic to mild rot, dirt and stain, that the orientation of annual rings exists at the center of the defect, but at the borders the result of orientation

analysis changes rapidly. Cracks and splits cause typically very rapid changes to the the result of the orientation analysis, but the region is much narrower than for knots. The resolution for evaluating the width of the defect can be improved with an additional small moving window within the original moving window. The color of the defect is useful information for defect identification. The color based measurement of rot area and its severity can be used in predicting the rot propagation inside the trunk, and thus the bucking can be optimized further. This has a high economic potential, but requires rot area estimates in fractions of seconds

The present counting algorithm of annual ring appears quite accurate when compared to human visual inspection. However it can be improved by counting along a path that is normal to the rings at all locations. The average absolute curvature of the resulting path may serve as a new wood property measure indicating irregularities in the growth of the tree. If the paths from pith to bark are strongly curved in the same direction at several locations of the log cross section surface, the direction of spirality of the logs is obtained.

The algorithm for tracking the annual rings is rather vulnerable to small defects on the cross section surface. Any error in annual ring width is integrated and thus errors in early annual rings will cause errors at in all the later annual rings. The robustness of the method can be improved either by running the counting both from pith to bark and from bark to pith or by constraining the field of adjacent ring widths to be smooth.

The compression wood in softwoods appears as a dark and thick latewood region within some annual rings. However, compression wood is typically a compact area and never covers the entire cross section surface. The algorithm for detecting the early wood and the latewood may be developed further into detection of compression wood. Compact regions with a high proportion of latewood would then be recognized as compression wood. The average color of the region could be used as an additional piece of information. The color of the compression wood region could be compared with the color of an adjacent region or the color of the region opposite with respect to the pith.

8.4 Challenges in development of industrial applications

The research in this thesis aims to be a basis for the algorithm development in industrial applications. In addition to improving the image analysis algorithms, the application environment should be improved. This Section describes which problems occur when applying the methods in real-life application environment, and some ideas how to solve them. Ongoing application projects based on the results of this thesis are shortly discussed, although these are not contributions of this thesis.

Dust, steam, fog, temperature variation, direct sun light, uncontrolled artificial light and mechanical vibrations reduce the quality of images. Their effect is the worst in outdoor environment, in particular in forests, but dust, steam and vibrations are the limiting factors also in many sawmill applications.

The lighting becomes of high importance in the application development phase. In an indoor environment, such as at sawmills, the lighting is quite easily kept constant, but in outdoor environment it is much more challenging. The forestry machines work under all forms and intensities of natural light, during winter and summer. The image based analysis methods work only if the analysis methods are robust to variation in lighting. Powerful artificial lighting dominating the brightest of natural light, the sunlight, is one alternative. Lasers and power LEDs provide artificial lighting powerful enough for many applications. If the lighting power is high, the illumination time has to be very short to avoid the risk for human eyes. Thus high speed cameras are typically required. If the lighting pulse is extremely short it helps also to avoid blurring caused by mechanical vibrations, which are common in moving machines, such as harvesters.

The location of the log or board cross sections and the distance between the machine vision camera and a single log or board cross section surface are fairly simple to keep sufficiently constant on conveyor belts of sawmills. However, variation in the log or board location makes the measurement more problematic. In the extreme case, the log is not in the image at all, which of course must be recognized. When the log end appears in the image, the distance from the camera to the object may be unknown. If the location cannot be fixed with mechanical arrangements, the problem can be solved with stereo imaging or with the combination of a camera and a laser device. Structured laser light, e.g. parallel lines or a

grid, can be produced, observed and the distances of the object edges calculated. Active laser distance measurement devices can be used. One point laser measurement devices are inexpensive, but they produce only one distance measure at a time. Sweeping lasers are more expensive.

If the log or board moves longitudinally in the harvester head or on the conveyor belt, the camera cannot be located in front of the log or board end surface, but it needs to be located at an angle. Thus perspective errors occur. Because of the perspective error the resolution of the image varies across the image. When the camera angle with respect to the cross section surface is known, the perspective error can be corrected with a mathematical transformation. Though the imaging at an angle increases computational load, this camera location is advantageous when segmenting the log or board cross section surface from the background. A heavy lighting spot can be located on the side opposite to the camera so that the camera sees only the spotlighted cross section surface, but not the spotlighted side of the log. The side of the log closer to the camera remains in the shadow and contrast between the spotlighted cross section surface and the shadowed log side is very high.

The log or board cross section surfaces can be improved for better images. An automatic washing with brushing would remove dirt, mud and waste particles. In addition to a simple washing, watering improves the contrast. A better contrast can be achieved with appropriate staining as well. The chainsaw of a harvester and the saw blades at sawmills could be improved to reduce sawing marks. Such image improvement systems will be developed and installed, if the economic value of information obtained is high enough and the measurements with improvements can be carried out in fractions of a seconds, so that the production speed needs not to be decreased.

The pixel resolution of the cameras improves rapidly. In some applications the entire cross section needs not be imaged. For instance, if only a slice from the pith to bark or a sector of the log covers the image, the camera can be closer to the cross section surface and the resolution for single annual rings increases. Thus e.g. the early wood and the latewood areas within annual rings can be measured more accurately.

Many algorithms discussed in this thesis are computationally heavy, but the image resolution can be reduced in many algorithms without jeopardizing the relevance of the results. If the

resolution of the image cannot be reduced, the resolution of the result can be reduced instead, so that annual rings are analyzed at sample areas and the results generalized to the whole cross section. This can be made using a moving window with large moving step (i.e. multiple times the moving window dimensions).

The telecentric optics, free from perspective distortion, may offer an interesting improvement for image based measurement, because the scale calibration and the problems of varying object distance can be avoided. However, the diameter of the telecentric lens must be the same as the dimensions of the object to be imaged. Large telecentric lenses with the field of view over 400 mm have been manufactured, but their price is very high.

.

In the laboratory, the imaging circumstances can be set up as optimal, but in industrial applications the requirements are more difficult to satisfy. Indoor applications, such as those sawmills, are easier than outdoor ones. However, the conditions at sawmills are much harsher than in laboratory. Cameras and lighting devices must be shielded and vibrations must be dampened. Sawdust and small wood particles are present and may harm the imaging devices. At plywood and at pulp and paper mills air humidity and the moistening of logs may cause problems to the machine vision systems. At pulp mills some measurements, such as sampling measurements and pile measurements on the truck are made outdoors. Thus cameras and other devices have to be resistant to variations in temperature and in lighting conditions. If the imaging distance is several meters, rain, fog and snowfall may blur the images.

Of course, the hardest environment for machine vision based measurements is in the forest. Harvester head has to stand heavy stress and hits, and thus imaging components have to be durable too. The lighting and temperature vary from a winter midnight to a sunny summer day. Chainsaw waste, sawing dust, snow and even mud are sometimes present complicating the measurements.

During the research work presented in this thesis application projects have been started. The annual ring width measurement has been speeded up to meet the sawmill requirements. The 2D power spectrum was calculated in a few sample windows, annual ring width was evaluated in about 100 locations within the board cross section surface, and the mean annual

ring width for all boards was evaluated. After the application project the analysis time for one board was less than 0.2 seconds.

An application project was launched to develop machine vision based harvester measurements. A part of the research is to develop the log cross section surface measurements. The preliminary results of the ongoing project manifested that the effect of sunlight can be overcome with the extremely short high power laser pulse for exposure. As a result imaging conditions are kept practically constant regardless of the time of day. Furthermore the movement, shaking and trembling of the object is frozen with the short exposure time and no image blurring occurs. The perspective error caused by the non-perpendicular mounting of the camera has been corrected reliably if the cross section surface itself is planar.

8.5 Ideas for future research

The algorithms discussed in the thesis are developed for the images taken with the conventional visible light range cameras. However, similar analysis algorithms can be applied for images taken with other imaging systems, such as UV, infrared, microwaves, X-ray or NMR based imaging devices. These imaging systems emphasize wood properties different from those observed with cameras operating on the visible light range.

In addition to harvesters, sawmills and pulp and paper mills the camera based methods could be used in other stages of wood supply chain, such as the measurements of wood piles at road side, in timber trucks, rail cars and grab loader vehicles. The annual ring level analyses may problematic due to longer imaging distance, but diameters of logs, the mean color of logs and the presence of defects could be evaluated.

The applications assessing the quality of the faces of sawn board, rather than ends, have been available for many years. These systems are based on color analyses, but the texture based analyses of this thesis may offer improvements under difficult lighting conditions. The methods discussed in this thesis can be used similarly for the conventional problems, for instance in detecting knots and rot. The grain orientation and the grain width can be

measured. The boards can then be classified according to the grain properties, and boards visually similar offered to consumers.

The bark images of the standing trees and logs provide the information about wood species. Image based wood species recognition systems have been studied [72][141]. The quality properties of wood can be evaluated on the basis of side images. The bark of pine appears different in the butt log and in the top log. It may be possible to detect and measure the knottiness, wounds and scars of a tree or a log based on side images.

The analysis algorithms developed for the log cross sections can possibly be used also for root and branch analysis in forest research. Although the annual rings are not so visible, it may be possible to evaluate them. The pith location and the bark thicknesses can be evaluated and automatic area measurements seem to be possible for root cross sections.

9 Conclusion

This work discusses the application of the image analysis methods for the cross section surface images of wood pieces, such as disc samples, logs or boards. The analysis and measurement methods have been developed in the laboratory environment for measurement of wood properties, which are visually detectable at the cross section surface. The main attention has been in the analysis of annual rings. These algorithms are based on texture analysis methods that are found to be robust.

The most important texture analysis method applied in this study is the 2D Fourier power spectrum. The power spectrum serves as the basis for most of the wood property measurement algorithms presented in the thesis. Dominating annual ring width and orientation throughout the log cross section surface can be evaluated with texture analysis methods even in unprepared and defective cross section surfaces. Furthermore, the width and the orientation of annual rings has been utilized in defect detection, locating the pith, counting and the tracking of the annual rings.

Some color and geometry based methods were also developed, but they are less robust. Methods for evaluating the shape of the log cross section and the bark thickness require high contrast between the log cross section and the background. Bark analysis methods requires contrast also between the bark and the wood and a rather constant color of bark.

The thesis discusses well-known color analysis methods such as global thresholding for segmenting the object from the background. Single annual rings are thresholded and the latewood proportion is evaluated using color based algorithms. The thesis reviews the calibration methods required: the camera calibration for the distortion correction, the color calibration to get colors in all images comparable, and the scale calibration to transform the measured pixel values into real world measures. The possible error sources in an image based measurements are discussed. The errors and uncertainties may originate, for instance,

from camera optics and hardware components, algorithm implementation, and imaging environment such as lighting, temperature or vibrations.

The thesis discusses generally the importance of the measurements for the forestry and its impact on Finnish economy. The most important wood properties are presented. The extensive review of industrial and forestry oriented researches utilizing different physical phenomena describes the state of art in wood measurement research. The commercial machine vision based solutions for the industrial wood measurement are presented. The results of this research are evaluated in relation to the present-day image based wood measurement applications and as the conclusion the opportunities for new image based measurements are revealed. It is expected that many of the methods outlined in this thesis will be turned into industrial applications. Indeed, such development work has been carried out alongside this thesis work.

References

[1] Anonymous. *Quality of Life and Management of Living Resources. Compression Wood in Conifers – the Characterisation of its Formation and its Relevance to Timber Quality*. Final Report of Research programme QLK5-CT-2001-00177, funded by European Union – Framework Programme FP5. 8th April, 2005.

[2] Anonymous. *Key to the Finnish forest industry*. Publication of Finnish Forest Industries Federation. 127 pages. Helsinki, Finland. 2006

[3] Arnerup Fredrik. *Infrared Imaging of Scots Pine Cross Sections: Automatic Heartwood Size Measurements.* Master's thesis. The Royal Institute of Technology, Sweden. 17th May, 2002.

[4] von Arx, Georg and Diez Hansjörg. *A tool for the Analysis of Annual Root Rings in Perennal Forbs.* Application Note of Media Cybernetics Inc. 2006.

[5] Autolog. The webpage of the company. www.autolog.com. Referenced 14.8.2008.

[6] Baden Fuller Arthur John. *Microwaves – An introduction to microwave theory and techniques.* Second Edition. Pergamon Press. 1979. ISBN 0-08-024228-6.

[7] Ballard D.H. *Generalizing the Hough Transform to Detect Arbitrary Shapes.* Pattern Recognition. Volume 13, Number 2, Pages 111-122. 1981.

[8] Barnett John R. and Jeronimidis George (edited by). *Wood Quality and its Biological Basis.* Blackwell Publishing, Oxford, United Kingdom, 2003. ISBN 1-84127-319-8.

[9] Bishop Christopher M. *Pattern Recognition and Machine Learning.* Springer Science+Business Media, New York, NY, USA, 2006. ISBN 0-387-31073-8.

[10] Bouguet Jean-Yves. Camera Calibration Toolbox for MATLAB. Webpage. newbologna.vision.caltech.edu/bouguetj/calib_doc/ Referenced 26.11.2008.

[11] Brown Duane C. *Close-Range Camera Calibration.* Proceedings of the Symposium on Close-Range Photogrammetry in Urbana, Illinois, USA. January, 1971. Pages 855-866.

[12] Bucur Voichita. *Nondestructive Characterization and Imaging of Wood.* Springler-Verlag Berlin Heidselberg, 2003. ISBN 3-540-43840-8. p.333.

[13] Canny John. *A Computational Approach to Edge Detection.* IEEE Transaction on Pattern Analysis and Machine Intelligence. Volume 8, Number 6, pages 679-698. November, 1986.

[14] Cerda Mauricio, Hitschfeld-Kahler Nancy and Mery Domingo. *Robust Tree-Ring Detection.* Lecture Notes in Computer Science, Volume 4872/2007: Advances in Image and Video Technology. Pages 575-585. December 2007.

[15] Chang Sun Joseph, Olson James R. and Wang Paul C. *NMR imaging of internal features in wood.* Forest Products Journal. Volume 39, Number 6, pages 43-49. June, 1989.

[16] Childers Donald G. (edited by) *Modern Spectrum Analysis.* A volume in the IEEE Press Selected Reprint Series. IEEE Press. New York, USA, 1978.

[17] Cho Tai-Hoon, Conners Richard W. and Araman Philip A. *A Computer Vision System for Analyzing Images of Rough Hardwood Lumber.* Proceedings of IEEE 10th International Conference on Pattern Recognition. Volume 1, p 726 – 728. 16-21 June 1990.

[18] Cho Tai-Hoon, Conners Richard W. and Araman Philip A. *A computer vision system for automated grading of rough hardwood lumber using a knowledge-based approach.* Proceedings of IEEE International Conference on Systems, Man and Cybernetics. Pages 345-350. Los Angeles, California, USA. 4-7 November 1990.

[19] Ciccotelli Joseph and Portala Jean-François. *Applications of artificial vision in wood industry.* Industrial Metrology. Volume 2, Numbers 3-4, Pages 185-194. May, 1992.

[20] Clarke T.A and Fryer J.G. *The Development of Camera Calibration Methods and Models.* Photogrammetric Record, Volume 16, Number 91, pages 61-66. April 1998.

[21] Coates Eyler Robert, Chang Sun Joseph and Liao T. Warren. *A quick defect detection algorithm for magnetic resonance images of hardwood logs.* Forest Product Journal. Volume 48, Number 10, pages 68-74. October 1998.

[22] Comact Inc. The webpage of the company. www.comact.com. Referenced 14.8.2008.

[23] Conner W. Steven, Schowengerdt Robert A, Munro Martin & Hughes Malcolm K. *Design of a Computer Vision Based Tree Ring Dating System.* Proceedings of the IEEE Southwest Symposium on Image Analysis and Interpretation, pages 256-261. Tucson, Arizona, USA. 5-7 April, 1998.

[24] Conner W. Steven, *A Computer Vision Based Tree Ring Analysis and Dating system.* Master of Science thesis, University of Arizona, USA, 1999.

[25] Conner W. Steven, Munro Martin, Hughes Malcolm K. *Engineering design of an image acquisition and analysis system for dendrochronology.* Optical Engineering, Volume 39, Issue 2, pages 453-463. February 2000.

[26] Conners Richard W., McMillin Charles W., Lin Kingyao and Vasquez-Espinosa Ramon E. *Identifying and locating surface defects in wood: Part of an automated lumber processing system.* IEEE Transactions on Pattern Analysis and Machine Intelligence Volume 5, number 6, pages 573-583. November, 1983.

[27] Conners Richard W., Cho Tai-Hoon, Ng Chong T., Drayer Thomas H., Tront, Joe G., Araman, Philip A., and Brisbon, Robert L. *A Machine Vision System for Automatically Grading Hardwood Lumber.* Proceedings of the First International Conference on Automated Lumber Processing Systems and Laser Machining of Wood. pp. 53-57. East Lansing, Michigan, USA. 11-12 September, 1990.

[28] Conners Richard W., Cho Tai-Hoon, Ng Chong T. and Drayer Thomas H. *A Multisensory Machine Vision System for Hardwood Defect Detection.* Proceedings of Process Control/Production Management of Wood Products: Technology for the 90's. Pages 99-111. Athens, Georgia, USA. October 31 - November 1, 1990.

[29] Contreras Ignacio, Guesalga Andres, Fernandez M. Paulina, Guarini Marcelo and Irarrazaval Pablo. *MRI fast tree log scanning with helical undersampled projection acquisitions.* Magnetic Resonance Imaging. Volume 20, Issue 10, Pages 781-787. December, 2002.

[30] Cooper Jerome, Steele Philip, Mitchell Brian, Boden Craig and Lionheart William. *Detecting Juvenile and Knot Wood in Southern Pine Logs with Electrical Impedance Tomography.* Proceedings of ScanTech 2007, the 12th International Conference on Scanning Technology and Process Optimization in the Wood Industry, pages 16-26. Atlanta, Georgia, USA, June 19, 2007.

[31] Cooper Jerome E., Steele Philip H., Mitchell Brian K., Boden Craig and Lionheart William R.B. *Detection Juvenile Wood in Southern Pine Logs with Brush Electrodes.* Proceedings of the 9th EIT conference 2008. June 16-18, 2008. Dartmouth College, New Hampshire, USA.

[32] Cown D.J. and Clement B.C. *A wood densitometer using direct scanning with X-rays.* Wood Science and Technology. Volume 17, Number 2, Pages 91-99. June, 1983.

[33] Desch H.E. and Dinwoodie J.M. *TIMBER: Its Structure, Properties and Utilization.* Sixth edition. MacMillan Education. 1981. ISBN 0-333-25751-0.

[34] Dralle A/S. The webpage of the company. www.dralle.dk. Referenced 15.8.2008.

[35] Él'piner Isaak Efimovich. *Ultrasound - Physical Chemical and Biological Effects.* Consultants Bureau Enterprises Inc. New York, USA. 1964.

[36] Enarvi Seppo. *Image-based Detection of Defective Logs.* Master's thesis. Helsinki University of Technology. August 16, 2006.

[37] Eskelinen Pekka and Eskelinen Harri. *A K-band Microwave Measuring System for the Analysis of Tree Stems.* Silva Fennica Volume 34, Number 1, Pages. 37-45. 2000.

[38] Evans Robert and Ilic Jugo. *Rapid prediction of wood stiffness from microfibril angle and density.* Forest Products Journal. Volume 51, Number 3, Pages 53-57. March, 2001.

[39] Finnish Forest Industries Federation, webpage. www.forestindustries.fi Referenced 30.01.2008.

[40] FinScan. The webpage of the company. www.finscan.fi. Referenced 14.8.2008.

[41] Fisher N.I. *Statistical analysis of circular data.* Cambridge University Press, Great Britain.1993. ISBN 0-521-35018-2.

[42] Foveon. The webpage of the company. www.foveon.com. Referenced 30.9.2008.

[43] Fuentealba Cecilia, Simon Christophe, Choffel Denise, Charpentier Patrick and Masson Daniel. *The k-Nearest Neighbor Method for Automatic Identification of Wood Products.* Proceedings of the 14th International Conference on Electronics Communications and Computers (CONIELECOMP'04). 16-18 February 2004.

[44] Fuentealba Cecilia, Simon Christophe, Choffel Denise, Charpentier Patrick and Masson Daniel. *Wood products identification by internal characteristics readings.* ICIT '04 IEEE International Conference on Industrial Technology, 2004. Volume 2. Pages 763-368. 8-10 December 2004.

[45] Gjerdrum P. and Høibø O. *Heartwood detection in Scots pine by means of heat-sensitive infrared images.* Holz als Roh- und Werkstoff. Volume 62, Number 2, Pages 131-136. April, 2004.

[46] Gonzalez Rafael C. and Winz Paul. *Digital Image Processing.* Addison-Wesley Publishing Company. Reading, Massachusetts, USA. 1977.

[47] Gonzales Rafael C. and Woods Richard E. *Digital Image Processing.* Second edition. Prentice Hall. Upper Saddle River, New Jersey. 2002. ISBN 0-201-18075-8.

[48] Gonzalez Rafael C., Woods Richard E. and Eddins Steven L. *Digital Image Processing Using MATLAB®.* Pearson Prentice Hall. Upper Saddle River, New Jersey, USA. 2004. ISBN 0-13-008519-7.

[49] Gopalan Giribalan. *An Interactive Image Analysis System for Dendrochronology.* Master's thesis. University of Arizona, USA. 2000.

[50] Han Wei and Birkeland Rolf. *Ultrasonic Scanning of logs.* Industrial Metrology. Volume 2, Numbers 3-4, Pages 253-281. May 1992.

[51] Hanhijärvi Antti, Ranta-Maunus Alpo and Turk Goran. *Potential strength grading of timber with combined measurement techniques. Report of the Combigrade-project – phase 1.* VTT publications 568. Otamedia Oy, Espoo, Finland. 2005.

[52] Hanning Tobias, Kickingereder Reiner, Casasent David. *Determining the average annual ring width on the front side of lumber.* Proceedings of SPIE, Volume 5144, Optical Measurement Systems for Industrial Inspection III. Pp. 707-716, May 2003.

[53] He Jing. *A Comparison of Artificial Neural Network Classifiers for Analysis of CT Images for the Inspection of Hardwood Logs.* Master's thesis. Virginia Polytechnic Institute and State University. September, 1997.

[54] Hecht Eugene. *Optics.* Fourth edition. Addison-Wesley. San Francisco, California, USA. 2002. ISBN 0-8053-8566-5

[55] Heikkilä Janne and Silvén Olli. *A Four-step Camera Calibration Procedure with Implicit Image Correction.* Proceedings of IEEE Computer Society Conference on Computer Vision and Pattern Recognition, pages 1106-1112. San Juan, Puerto Rico. 17-19 June, 1997. ISBN: 0-8186-7822-4.

[56] Hopkins Forrest F., Morgan Ira L., Ellinger Hunter D., Klinksiek Rudy V., Meyer Glenn A. and Thompson J. Neils. *Industrial Tomography Applications.* IEEE Transactions on Nuclear Science. Volume 28, Issue 2, Pages 1717-1720. April, 1981.

[57] Hu Chuanshuang, Tanaka Chiaki and Ohtani Tadashi. *On-line determination of the grain angle using ellipse analysis of the laser light scattering pattern image.* Journal of Wood Science. Volume 50, Number 4, pages 321-326. August 2004.

[58] Hu Chuanshuang, Tanaka Chiaki, Ohtani Tadashi and Okai Reynolds. *An improved automatic control of natural wood routing using ellipse analysis technology to measure grain direction.* Forest Product Journal. Volume 55, Number 4, Pages 46-51. April, 2005.

[59] Inx-Systems. The webpage of the company. www.inx.fi/systemsenglanti.html. Referenced 14.8.2008.

[60] Jackson J. Edward. *A User's Guide to Principal Component Analysis.* John Wiley & Sons, Inc. 571 pages. Printed in United States of America, 1991. ISBN 0-471-62267-2.

[61] James William L., Yen You-Shin and King Ray J. *A Microwave Method for Measuring Moisture Content, Density, and Grain Angle of Wood.* Research Note FPL-0250. United States Department of Agriculture, Forest Service, Forest Products Laboratory. March 1985.

[62] James William L. *Electric Moisture Meters for Wood.* United States Department of Agriculture, Forest Service, Forest Products Laboratory. General Technical Report FPL-GTR-6. June, 1988.

[63] Janesick James R. *Scientific Charge-Coupled Devices.* SPIE Press. Washington, USA, 2001. ISBN 0-8194-3698-4.

[64] Jolliffe Ian T. *Principal Component Analysis*. Springer-Verlag New York inc. 271 pages. New York, USA, 1986. ISBN 0-387-96269-7.

[65] Kaestner Anders P. and Bååth Lars B. *Microwave Polarimetry Tomography of Wood*. IEEE Sensors Journal. Volume 5, Issue 2, Pages 209-215. April, 2005.

[66] Kak Avinash C. and Slaney Malcolm. *Principles of Computerized Tomographic Imaging*. IEEE Press. New York, USA, 1988. ISBN 0-87942-198-3.

[67] Kärkkäinen Matti. *Puutieteen perusteet.* Hämeenlinna. Karisto Oy, 2003. ISBN 952-5118-51-7. Written in Finnish.

[68] Kauppinen Hannu, Rautio Hannu and Silvén Olli. *Non-segmenting defect detection and SOM based classification for surface inspection using color vision.* SPIE 3826, Conference on Polarization and Color Techniques in Industrial Inspection, pages 270-280. Munich Germany, June 17-18, 1999.

[69] Kellner Michael A., Hanning Tobias, Farr Holger. *Real-time analysis of the grain on wooden planks.* Proceedings of SPIE, Volume 4664, Machine Vision Applications in Industrial Inspection. Pp. 135-144. March 2002.

[70] Klinkhachorn P., Franklin J.P., McMillin C.W., Conners E.W. and Huber H.A. *Automated computer grading of hardwood lumber*. Forest Product Journal, Volume 38, Issue 3, pp 67-69. 1988.

[71] Kollmann Franz F.P. and Côté Wilfred A. Jr. *Principles of Wood Science and Technology. Volume I: Solid Wood.* Springer-Verlag Berlin Heidelberg New York Tokyo. 1984. ISBN 3-540-04297-0.

[72] Kosonen Sampsa. *Tree Species Recognition with Machine Vision Using Color and Texture Analysis.* Master's thesis. Helsinki University of Technology. Espoo, Finland. 2007.

[73] Laggoune Hayet, Sarifuddin Madenda and Guesdon Vincent. *Tree Ring Analysis.* Proceedings of the Canadian Conference on Electrical and Computer Engineering. Pages 1574-1577. 1-4 May, 2005.

[74] Lampinen Jouko, Smolander Seppo, Silvén Olli and Kauppinen Hannu. *Wood Defect Recognition: A Comparative Study*. Proceedings of Workshop on Machine Vision in Advanced Production, Oulu, Finland. 1- 3 June 1994.

[75] Lampinen Jouko and Smolander Seppo. *Wood defect recognition with self-organizing feature selection.* Proceedings of SPIE Conference on Intelligent Robots and Computer Vision XIII: Algorithms and Computer Vision. Boston, Massachusetts. 31 October – 2 November 1994.

[76] Lindeberg Tony. *On Scale Selection for Differential Operators.* Proceedings of the eighth Scandinavian conference on image analysis. Pages 857-866. Tromsø, Norway, May 1993.

[77] Lisker Oy. The webpage of the company. www.lisker.fi. Referenced 14.8.2008.

[78] LMI technologies. The webpage of the company. www.sensorsthatsee.com. Referenced 18.8.2008.

[79] Longuetaud Fleur, Leban Jean-Michel, Mothe Frédéric, Kerrien Erwan and Berger Marie-Odile. *Automatic detection of pith on CT images of spruce logs.* Computers and Electronics in Agriculture. Volume 44, Issue 2, pages 107-119. August 2004.

[80] Longuetaud Fleur, Mothe Frédéric and Leban Jean-Michel. *Automatic detection of the heartwood/sapwood boundary within Norway spruce (Picea abies (L.) Karst.) logs by means of CT images.* Computers and Electronics in Agriculture. Volume 58, Issue 2, Pages 100-111. September 2007.

[81] Luhmann Thomas, Robson Stuart, Kyle Stephen and Harley Ian. *Close Range Photogrammetry: Principles Methods and Applications.* Whittles publishing. Dunbeath, Scotland, United Kingdom. 2006. ISBN 1-870325-50-8.

[82] Lundqvist Sven-Olof and Evans Robert. *Illustration of wood and fiber measurements with SilviScan.* STFI Report ART 15, 2004. Published at the Seminar "New Possibilities for R&D" at the inauguration of SilviScan-3 at STFI Packforsk, February 2, 2004.

[83] Luxscan Technologies. The webpage of the company. www.luxscan.lu. Referenced 14.8.2008.

[84] Marjanen Kalle, Ojala Petteri and Ritala Risto. *Measurement of annual ring width of log ends in forest machinery.* Proceedings of SPIE, Electronic Imaging 2008. Volume 6812-12. San Jose, California, USA. 27-31 January, 2008.

[85] Martin P., Collet R., Barthelemy, G. and Roussy G. *Evaluation of Wood Characteristics: Internal Scanning of the Material by Microwaves.* Wood Science and Technology. Volume 21 Number 4, p. 361-371. December 1987.

[86] Matthews Peter and Beech Brian. *Method and apparatus detecting timber defects.* U.S. Patent 3976384. 24th August, 1976.

[87] McDonald Kent A. *Lumber defect detection by ultrasonics.* Research Paper FPL 311. Forest Products Laboratory, Forest Service, U.S. Department of Agriculture, Madison, Wisconsin. 1978.

[88] McMillin Charles W. *Application of Automatic Image Analysis to Wood Science*. Wood Science. Volume 14, number 3, pages 97-105. January, 1982.

[89] McMillin Charles W., Conners Richard W. and Huber Henry A. *ALPS – A potential new automated lumber processing system.* Forest Products Journal. Volume 34, Number 1, Pages 13-20. January, 1984.

[90] Mecano. The webpage of the company. www.mecanogroup.com. Referenced 18.8.2008.

[91] METLA, Finnish Forest Research Institute. Webpage. www.metla.fi/suomen-metsat/index-en.htm Referenced 18.10.2007.

[92] METLA, Finnish Forest Research Institute, MetINFO information service, webpage. www.metla.fi/metinfo. Referenced 19.04.2009. Written in Finnish.

[93] Metsäteho. *Wood Measuring Methods Used in Finland 2007.* Webpage. www.metsateho.fi/uploads/Tuloskalvosarja_2008_08b_Wood_measuring_methods_2007_tm.pdf. Referenced 09.10.2008.

[94] Microtec. The webpage of the company. www.microtec.eu. Referenced 14.8.2008.

[95] Microtec. *GOLDENEYE, Quality scanner from the technology leader MiCROTEC.* A commercial brochure.

[96] Mikropuu Oy. The webpage of the company. www.mikropuu.fi. Referenced 19.8.2008.

[97] Morales Sebastián, Guesalaga Andrés, Fernández M. Pauline, Guarini Marcelo and Irarrázaval Pablo. *Computer reconstruction of pine growth rings using MRI.* Magnetic Resonance Imaging. Volume 22, Issue 3, Pages 403-412. April 2004.

[98] Nabney I.T. *NETLAB Algorithms for Signal Processing.* Springer-Verlag London Berlin Heidelberg. 420 pages. Printed in Great Britan, 2004. ISBN 1-82533-440-1.

[99] Newnes-McGehee. The webpage of the company. www.newnes-mcgehee.com. Referenced 20.3.2009.

[100] Niskanen Matti, Kauppinen Hannu and Silvén Olli. *Color and texture based wood inspection with non-supervised clustering.* Proceedings of 12th Scandinavian Conference on Image Analysis, pages 336-342. Bergen, Norway. June 11-14, 2001.

[101] Norell, Kristin. *Finding the Pith in Rough Cross-Sections of Logs in Saw Mill Environments.* Proceedings SSBA 2006: Symposium in Image Analysis, Gerogsson, Fredrik; Börlin, Niclas (ed.). Pages 132-135. Umeå, Sweden 2006.

[102] Norell Kristin, Lindblad Joakim and Svensson Stina. *Grey Weighted Polar Distance Transform for Outlining Circular and Approximately Circular Objects.* Proceedings of ICIAP 2007, International Conference on Image Analysis and Processing. Pages 647-652. 10-14 September, 2007.

[103] Norell Kristin and Borgefors Gunilla. *Estimation of pith position in untreated log ends in sawmill environments.* Computer and Electronics in Agriculture. Volume 63, Issue 2, pages 155-167. October, 2008.

[104] Nyström Jan and Hagman Olle. *Real-time spectral classification of compression wood in Picea abies.* Journal of Wood Science. Volume 45, Number 1, Pages 30-37. January, 1999.

[105] Nyström Jan. *Automatic Measurement of fiber orientation in softwoods by using the tracheid effect.* Computers and Electronics in Agriculture. Volume 41, Issues 1-3, Pages 91-99. December 2003.

[106] Österberg Petri, Ihalainen Heimo and Ritala Risto. *Method for Analyzing and Classifying Wood Quality through Local 2D-Spectrum of Digital Log end Images.* Proceedings of International Conference on Advanced Optical Diagnostics in Fluids, Solids and Combustion, VSJ-SPIE '04. Tokyo, Japan.4-6 December, 2004.

[107] Österberg Petri, Ihalainen Heimo and Ritala Risto. *Processing Log End Images for Analysis of Wood Quality and Tree Growth.* Proceedings of 5th IUFRO WP 5.01.04 Work Shop on "Connection between Forest Resources and Wood Quality: Modelling Approaches and Simulation Software". Waiheke Island, Auckland, New Zealand. 20-27 November 2005.

[108] Österberg Petri, Ihalainen Heimo and Ritala Risto. *Measurement of Wood Quality Parameters from Annual Rings using Color Analysis with Digital Images.* IMEKO XVIII World Congress and IV Brazilian Congress of Metrology. Metrology for a sustainable development. Rio de Janeiro, Brazil. 17-22 September 2006.

[109] Österberg Petri, Ihalainen Heimo and Ritala Risto. *Robust Methods for Determining Quality Properties of Wood Using Digital Log End Images.* SCANTECH 2007, The 12th International Conference on Scanning Technology and Process Optimization in the Wood Industry. Atlanta, Georgia, USA.19 June 2007.

[110] Otsu Nobuyuki. *A Threshold Selection Method from Gray-Level Histograms.* IEEE Transactions on Systems, Man, and Cybernetics. Volume SMC-9, Number 1, pages 62-66. January, 1979.

[111] Palviainen Marjo. *Logging residues and ground vegetation in nutrient dynamics of a clear-cut boreal forest.* Doctoral thesis. University of Joensuu, Finland. November 2005.

[112] Peltola Aarre. (Editor-in-Chief). *Statistical Yearbook of Forestry 2007*. Publications of METLA, Finnish Forest Research Institute. Available also in the internet in www.metla.fi/julkaisut/metsatilastollinenvsk/index-en.htm.

[113] Polge H. *Fifteen Years of Wood Radiation Densitometry*. Wood Science and Technology. Volume 12, Number 3, Pages 187-196. September, 1978.

[114] Pont David, Brownlie Rod K. and Grace Jennifer C. *Disc Image-Processing Software for Three-Dimensional Mapping of Stem Ring Width and Compression Wood*. New Zealand Journal of Forestry Science. Volume 37, Number 2, Pages 169-185. March 2007.

[115] Quin jr. Franklin, Steele Philip H. and Shmulsky Rubin. *Locating knots in wood with an infrared detector system.* Forest Products Journal. Volume 48, Number 10, Pages 80-84. October, 1998.

[116] Rauschkolb Mark R. *Algorithms for Automatic Tree Ring Identification and Measurement.* Master's thesis. Mississippi State University. January 1994.

[117] Regent Instruments Inc. The webpage of the company. www.regentinstruments.com. Referenced 19.8.2008.

[118] Rema Control. The webpage of the company. www.rema.se. Referenced 29.8.2008.

[119] Rice R.W, Steele P.H. and Kumar Lalit. *Detecting knots and voids in lumber with dielectric sensors.* Industrial Metrology. Volume 2, Numbers 3-4, Pages 309-315. May, 1992.

[120] Rinntech. The webpage of the company. www.rinntech.com. Referenced 19.8.2008.

[121] Ross Robert J., Willits Susan W., Segen William von, Black Terry, Brashaw Brian K. and Pellerin Roy F. *A stress-wave-based approach to nondestructive evaluation of logs for assessing potential veneer quality using small-diameter ponderosa pine.* Proceedings of the Eleventh International Symposium on Nondestructive Testing of Wood. Madison, Wisconsin, USA. September 9-11, 1998.

[122] Ross Robert J., Willits Susan W., Segen William von, Black Terry, Brashaw Brian K. and Pellerin Roy F. *A stress wave based approach to NDE of logs for assessing potential veneer quality. Part 1. Small-diameter ponderosa pine.* Forest Products Journal Volume 49, Number 11/12, pages 60-62. November/December 1999.

[123] Sandoz J.L. *Grading of construction timber by ultrasound.* Wood Science and Technology. Volume 23, Number 1, Pages 95-108. February, 1989.

[124] Sarvas Risto. *Havupuut.* Second edition. Metsälehti kustannus. Karisto Oy Hämeenlinna, Finland, 2002. ISBN 952-5118-33-9. Written in Finnish.

[125] Savolainen T, Kaipio J.P., Karjalainen P.A and Vauhkonen M. *An electrical impedance tomography measurement system for experimental use.* Review of Scientific Instruments. Volume 67, Issue 10, Pages 3605-3609. October, 1996.

[126] Sepúlveda Paul. *Measurement of spiral grain with computed tomography.* Journal of Wood Science. Volume 47, Number 4, Pages 289-293. July, 2001.

[127] Sepúlveda Paul, Oja Johan and Grönlund Andreas. *Predicting spiral grain by computed tomography of Norway spruce.* Journal of Wood Science. Volume 48, Number 6, Pages 479-483. November 2002.

[128] Shen Jun, Zhou Jianqin and Vasquez Orlando. *Experimental Study of Optical Scattering and Fiber Orientation of Softwood and Hardwood with Different Surface Finishes.* Applied Spectroscopy. Volume 54, Number 12, Pages 1793-1804. December 2000.

[129] Silvėn Olli, Niskanen Matti and Kauppinen Hannu. *Wood inspection with non-supervised clustering.* Proceedings of the Third Workshop on Measuring of Wood Properties, Grades and Qualities in the Conversion Chains and Global Wood Chain Optimisation. Espoo, Finland. June 18-22, 2000.

[130] Simonaho Simo-Pekka, Palviainen Jari, Tolonen Yrjö and Silvennoinen Raimo. *Determination of wood grain direction from laser light scattering pattern.* Optics and Lasers in Engineering, Volume 41, Issue 1, pages 95-103. January, 2004.

[131] SKS Vision Systems. The webpage of the company. www.visionsystems.fi. Referenced 19.8.2008.

[132] Smith W. Rick. *A Prototype and Algorithms for Tree Ring Area Measurement.* Proceedings of the ACM 33rd Annual Southeast Regional Conference. Pages 254-259. Clemson, South Carolina, March 17.18, 1995.

[133] Sonka Milan, Hlavac Vaclav, Boyle Roger. *Image Processing, Analysis, and Machine Vision.* Second edition. PWS Publishing, Brooks/Cole Publishing Company. Pacific Grove, California, 1998. ISBN 0-534-95393-X.

[134] Sprecher Automation. The webpage of the company. www.sprecher-automation.com Referenced 14.8.2008.

[135] Steele Philip H., Kumar Lalit and Shmulsky Rubin. *Differentiation of knots, distorted grain, and clear wood by radio-frequency scanning.* Forest Products Journal. Volume 50, Issue 3, Pages 58-62. March 2000.

[136] Steele Philip H. and Cooper Jerome E. *Estimating lumber strength with radio frequency scanning.* Computers and Electronics in Agriculture. Volume 41, Issues 1-3, pages 77-83. December 2003.

[137] Steele Philip H. and Cooper Jerome E. *Moisture and density detector (MDD).* United States Patent 6784671. August 31, 2004.

[138] Steele Philip, Cooper Jerome and Lionheart William. Through-log density detector. United States Patent 6784672. August 31, 2004.

[139] Sturm Peter F. and Maybank Stephen J. *On Plane-Based Camera Calibration: A General Algorithm, Singularities, Applications.* Proceedings of IEEE Computer Society Conference on Computer Vision and Pattern Recognition, Volume 1, pages 430-437. Fort Collins, Colorado, USA. 23-25 June 1999. ISBN: 0-7695-0149-4.

[140] Sundholm Jan (edited). *Mechanical Pulping.* Papermaking Science and Technology book series, Book 5. Gummerus Printing, Jyväskylä, Finland, 1999. ISBN 952-5216-05-5.

[141] Suomela Tiina. *Puulajin tunnistus rungon värin ja tekstuurin perusteella.* Master's thesis, Tampere University of Technology. Tampere, Finland. 2004. Written in Finnish.

[142] Tanaka Toshinari and Ferenc Divós. *Wood inspection by thermography.* The 12th International Symposium on Nondestructive Testing of Wood. Sopron, Hungary. September, 2000.

[143] Taylor Fred W., Wagner Francis G. Jr., McMillin Charles W., Morgan Ira Lon and Hopkins Forrest F. *Locating knots by industrial tomography – A feasibility study.* Forest Products Journal. Volume 34, Number 5, Pages 42-46. May, 1984.

[144] Tiuri Martti and Heikkilä Sakari *Microwave Instrument for Accurate Moisture Measurement of Timber.* The proceedings of the 9th European Microwave Conference. Pp 702-705 October 1979.

[145] Tsai Roger Y. *A Versatile Camera Calibration Technique for High-Accuracy 3D Machine Vision Metrology Using Off-the-shelf TV Cameras and Lenses.* IEEE Journal of Robotics and Automation. Volume 3, Number 4. Pages 323-344. August 1987.

[146] Tsehaye A., Buchanan A.H. and Walker J.C.F. *Sorting of Logs using Acoustics.* Wood Science and Technology. Volume 34, Number 4. P. 337-344. November, 2000.

[147] Uusitalo Jori. *Metsäteknologian perusteet.* Karisto Oy, Hämeenlinna, Finland, 2003. ISBN 952-5118-58-4. Written in Finnish.

[148] Vaz C. Carvalho P. Duarte F and Dourado A. *A vision-based system for automatic growing ring detection and measurement.* Computer and Industrial Engineering, Volume 46, Number 2, pages 347-354. April 2004.

[149] Ventek. The webpage of the company. www.ventek-inc.com. Referenced 18.8.2008.

[150] Viitanen Jouko and Mattila Pentti. *Menetelmä ja mittalaite puunkäsittelyn yhteydessä.* Finnish patent FI 102716 B. 15th February 1999.

[151] Wagner Francis G., Taylor Fred W., Ladd Douglas S., McMillin Charles W. and Roder Fredrick L. *Ultrafast CT scanning of an oak log for internal defects.* Forest Products Journal. Volume 39, Number 11/12, Pages 62-64. November/December 1989.

[152] Waid J.S. and Woodman M.J. *A Non-Destructive Method of detecting Diseases in Wood.* Nature. Volume 180, Number 4575, page 47. July 6, 1957.

[153] Wang Xinli. *Log Classification by single X-ray scans using texture features from growth rings.* Proceedings of the 3rd Asian Conference on Computer Vision - ACCV'98. Volume 1352/1997, pages 129-136. January 8-10, 1998.

[154] Watson Gerald L. and Latshaw Don. *Veneer Inspection System.* United States Patent 3694658. 26th September, 1972.

[155] Welch Peter D. *The use of fast Fourier transform for the estimation of power spectra: A method based on time averaging over short, modified periodograms.* IEEE transactions on audio and electroacoustics. Volume 15, Number 2, pages 70-73. June, 1967.

[156] Weszka J.S., Nagel R.N. and Rosenfeld A. *A Threshold Selection Technique.* IEEE Transactions on Computers. Volume C-23, Number 12, pages 1322-1326. December 1974.

[157] White Neil and Waterfall Roger. *EIT for the condition monitoring of wood poles carrying overhead power lines.* IEE Colloquium on Advances in Electrical Tomography. Digest No: 1196/143, Pages 13/1-13/3. June 19, 1996.

[158] Wolf Paul R. *Elements of Photogrammetry.* McGraw-Hill Book Company. ISBN 0-07-071337-5. USA, 1974.

[159] WoodEye. The webpage of the Innovativ Vision AB. www.woodeye.se. Referenced 14.8.2008.

[160] Wyckhuyse A. and Maldague X. *A Study of Wood Inspection by Infrared Thermography, Part I: Wood Pole Inspection by Infrared Thermography.* Research in Nondestructive Evaluation. Volume 13, Number 1. Pages 1-12. September 2001.

[161] Wyckhuyse A. and Maldague X. *A Study of Wood Inspection by Infrared Thermography, Part II: Thermography for Wood Defects Detection.* Research in Nondestructive Evaluation. Volume 13, Number 1. Pages 13-22. September 2001.

[162] Wyckhuyse A. and Maldague X. *Wood inspection by infrared thermography.* Proceedings of the IV International Workshop-Advances in Signal Processing for Nondestructive Evaluation of Materials. Pages 201-206, 2002.

[163] Zhang Zhengyou. *Flexible Camera Calibration by Viewing a Plane from Unknown Orientations.* The Proceedings of the 7th IEEE International Conference on Computer Vision, Volume 1, pages 666-673. Kerkyra, Greece. 20-27 September 1999.

[164] Zhou James and Shen Jun. *Improved phase demodulation for grain orientation measurement.* Optics and Lasers in Engineering. Volume 45, Number 1, pages 160-169. January, 2007.

[165] Zhu Dongping, Conners Richard and Araman Phil. *CT Image Sequence Processing For Wood Defect Recognition.* Proceedings of 23rd Southeast Symposium on System Theory. Pages 75-79. 10-12 March, 1991.

[166] Zhu Dongping, Conners Richard W. and Araman Phil. *3D-signal processing in a computer vision system.* IEEE International Conference on System Engineering, pages 457-460. Fairborn, Ohio, USA. 1-3 August 1991.

[167] Zhu, Dongping, Conners Richard W, Schmoldt Daniel L. and Araman Philip A. *CT Image Sequence Analysis for Object Recognition – A Rule-Based 3-D Computer Vision System.* IEEE International Conference on Systems, Man and Cybernetics. Volume 1, pages 173-178. Charlottesville, Virginia, USA. 13-16 October, 1991.

[168] Zhu Dongping, Conners Richard W, Lamb Frederick and Araman Philip. *A Computer Vision System for Locating and Identifying Internal Log Defects Using CT Imagery.* Proceedings of the 4th International Conference on Scanning Technology in the Wood Industry, pages 1-13. San Francisco, California, USA. 28-29 October, 1991.